Uniwersytet im. Adama Mickiewicza w Poznaniu
Wydział Chemii

ROZPRAWA DOKTORSKA

mgr Michał Cegłowski

Funkcjonalizacja polimerów i nanomateriałów węglowych z zastosowaniem niskocząsteczkowych receptorów molekularnych

Functionalization of polymers and carbon nanomaterials with low molecular weight receptors

w formie spójnego tematycznie cyklu artykułów opublikowanych w czasopismach naukowych

Promotor: prof. dr hab. Grzegorz Schroeder
Promotor pomocniczy: dr Maciej Zalas

Poznań 2015

SPIS TREŚCI

WSTĘP

Celem naukowym rozprawy doktorskiej pod tytułem „Funkcjonalizacja polimerów i nanomateriałów węglowych z zastosowaniem niskocząsteczkowych receptorów molekularnych" było opracowanie metod syntezy i otrzymanie nowych, funkcjonalnych polimerów i materiałów węglowych zawierających receptory molekularne. Układy były tak zaprojektowane, aby wykazywały zdolność selektywnego wiązania wybranych jonów i cząsteczek. Celem pracy była nie tylko synteza tych układów, ale również ustalenie mechanizmu oddziaływań cząsteczek gościa z cząsteczkami receptorów osadzonych na nanorurkach węglowych lub wbudowanych w polimer.

Badania przeprowadziłem dla trzech różnych materiałów: wielościennych nanorurek węglowych (CNT), poli(metylowodorosiloksanu) (PMHS, ang. *polymethylhydrosiloxane*) oraz poli(eteru metylowo-winylowego-*alt*-bezwodnika maleinowego) (poly(MVE-*alt*-MA), ang. *poly(methyl vinyl ether-alt-maleic anhydride)*), na których osadzane były receptory molekularne. Struktury materiałów poddanych funkcjonalizacji przedstawiono na rysunku 1.

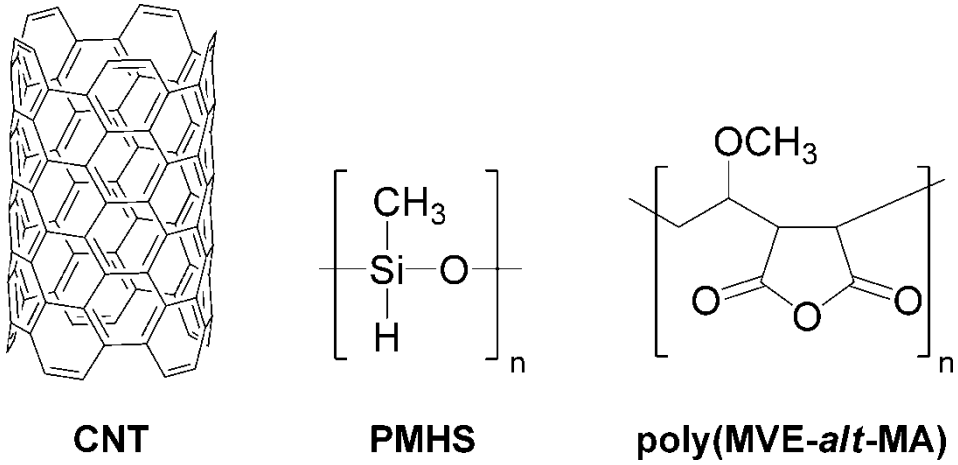

Rysunek 1. Struktury materiałów poddanych funkcjonalizacji.

Funkcjonalizacja nanorurek węglowych miała na celu otrzymanie nowych matryc węglowych stosowanych w technice MALDI-MS (ang. *matrix-assisted laser desorption/ionization mass spectrometry*) oraz sprawdzenie ich przydatności jako matryc w rejestracji widm masowych związków o niskiej masie cząsteczkowej. Ponadto celem badań było sprawdzenie wpływu funkcjonalizacji na proces jonizacji analitu.

Kolejnymi materiałami poddanym funkcjonalizacji były polimery. Funkcjonalizacja PMHS miała na celu otrzymanie polimerów krzemoorganicznych zawierających w swoich łańcuchach bocznych pochodne pirazolu, które zdolne są do tworzenia trwałych kompleksów z kationami metali grup przejściowych. Ponadto celem pracy było wyznaczenie stałych

trwałości kompleksów, zbadanie mechanizmu wiązania jonów oraz wyznaczenie selektywności w stosunku do określonych jonów.

Opracowanie metody syntezy polimeru zdolnego do tworzenia kompleksów z cukrami i diolami było kolejnym zadaniem realizowanym w trakcie wykonywania pracy. W tym celu poly(MVE-*alt*-MA) poddałem funkcjonalizacji za pomocą kwasu 3-aminofenyloboronowego oraz wyznaczyłem stałe trwałości kompleksów między uzyskanym polimerem oraz wybranymi cukrami i diolami w celu ustalenia selektywności.

Polimer poly(MVE-*alt*-MA) poddałem także procesowi funkcjonalizacji za pomocą zasady Schiffa uzyskanej w wyniku reakcji 2-acetylopirydyny oraz hydrazydu kwasu 4-aminobenzoesowego. Następnie sprawdziłem zdolności sorpcyjne uzyskanego materiału w stosunku do kationów miedzi(II), kadmu(II), chromu(III), niklu(II) oraz kobaltu(II). W tym celu wyznaczyłem izotermy adsorpcji, kinetykę adsorpcji, wpływ temperatury oraz pH na proces adsorpcji

ŻYCIORYS NAUKOWY

Urodziłem się 25 czerwca 1987 roku w Poznaniu. W 2006 r. ukończyłem I Liceum Ogólnokształcące im. Karola Marcinkowskiego w Poznaniu. W tym samym roku rozpocząłem studia magisterskie na kierunku Chemia Podstawowa na Wydziale Chemii Uniwersytetu im. Adama Mickiewicza w Poznaniu. W latach 2008 i 2010 otrzymałem Stypendium Ministra Nauki i Szkolnictwa Wyższego za osiągnięcia w nauce. W roku 2010 otrzymałem stypendium w ramach Programu Best From The Best, przyznawane przez firmę Volkswagen.

W maju 2011 roku uzyskałem tytuł magistra chemii, broniąc pracę pt. „Funkcjonalizacja nanorurek węglowych". Promotorem mojej pracy był prof. dr hab. Grzegorz Schroeder. W 2012 roku otrzymałem wyróżnienie do Nagrody im. Janiny Janikowej w konkursie PTChem na najlepszą pracę magisterską.

W 2011 roku rozpocząłem studia doktoranckie w Zakładzie Chemii Supramolekularnej Wydziału Chemii Uniwersytetu im. Adama Mickiewicza w Poznaniu. Również w roku 2011 rozpocząłem studia podyplomowe „Bezpieczeństwo w użytkowaniu i zarządzaniu substancjami chemicznymi" na Wydziale Chemii Uniwersytetu Łódzkiego, które ukończyłem w roku 2012 z wynikiem bardzo dobrym.

W czerwcu 2012 roku uzyskałem kompetencje jako „Auditor wewnętrzny REACH" po zdaniu egzaminu organizowanego przez TÜV NORD Polska.

Od roku 2012 jestem wykonawcą w grancie „Nieorganiczno-organiczne materiały hybrydowe o aktywności biologicznej", o numerze rejestracyjnym 2011/03/B/ST5/01573, przyznanym przez Narodowe Centrum Nauki.

W roku 2013 zostałem kierownikiem grantu „Polimery funkcjonalizowane receptorami molekularnymi", o numerze rejestracyjnym 2012/05/N/ST5/01274, przyznanym przez Narodowe Centrum Nauki. W roku 2013 otrzymałem również Stypendium Fundacji UAM.

Od 1 października 2013 do 1 maja 2014 odbywałem staż w Katedrze Biochemii i Neurobiologii na Wydziale Inżynierii Materiałowej i Ceramiki Akademii Górniczo-Hutniczej im. Stanisława Staszica w Krakowie pod kierunkiem prof. dr hab. Jerzego Silberringa, podczas którego zajmowałem się opracowaniem nowej techniki analitycznej TLC-MS wykorzystującą jonizacją za pomocą źródła DBDI.

Jestem współautorem szesnastu publikacji w czasopismach z listy filadelfijskiej oraz jedenastu rozdziałów w monografiach naukowych. Brałem udział w dwunastu konferencjach międzynarodowych oraz siedmiu krajowych.

LISTA PUBLIKACJI

PUBLIKACJE WCHODZĄCE W SKŁAD ROZPRAWY DOKTORSKIEJ

Publikacje w czasopismach z listy filadelfijskiej

1) Michał Cegłowski, Grzegorz Schroeder, "Laser desorption/ionization mass spectrometric analysis of surfactants on functionalized carbon nanotubes", Rapid Communications in Mass Spectrometry 2013;27(1):258-64 (IF = 2,642; punkty MNiSW = 30).

2) Michał Cegłowski, Szymon Jasiecki and Grzegorz Schroeder, "Laser desorption/ionization mass spectrometric analysis of folic acid, vancomycin and Triton® X-100 on variously functionalized carbon nanotubes", Rapid Communications in Mass Spectrometry 2013;27(23):2631-8 (IF = 2,642; punkty MNiSW = 30).

3) Michał Cegłowski, Błażej Gierczyk, Grzegorz Schroeder, "Poly(methyl vinyl ether-alt-maleic anhydride) Functionalized with 3-Aminophenylboronic Acid: A New Boronic Acid Polymer for Sensing Diols in Neutral Water", Journal of Applied Polymer Science 2014; 131(18):9358-64 (IF = 1,640; punkty MNiSW = 25).

4) Michał Cegłowski, Grzegorz Schroeder, "Removal of heavy metal ions with the use of chelating polymers obtained by grafting pyridine–pyrazole ligands onto polymethylhydrosiloxane", Chemical Engineering Journal 2015; 259(0):885-893 (IF = 4,058; punkty MNiSW = 40).

5) Michał Cegłowski, Grzegorz Schroeder, "Preparation of Porous Resin with Schiff Base Chelating Groups for Removal of Heavy Metal Ions from Aqueous Solutions", Chemical Engineering Journal 2015, 263:402-411 (IF = 4,058; punkty MNiSW = 40).

Rozdziały w monografiach

1) Michał Cegłowski, Grzegorz Schroeder, „Synthesis of pyrazole-based bidentate and tridentate supramolecular ligands", W: V.I. Rybachenko (red.), From molecules to functional architecture. Supramolecular interactions, East Publisher House, Donetsk 2012, s. 213-228, ISBN 978-966-317-155-5.

2) Michał Cegłowski and Grzegorz Schroeder, „Functional polymers forming complexes with metal ions", W: V. I. Rybachenko (red.), New trends in supramolecular chemistry, East Publisher House, Donetsk 2014, s. 185-204, ISBN 978-966-317-208-8.

POZOSTAŁE PUBLIKACJE

Publikacje w czasopismach z listy filadelfijskiej

1) Rafał Frański, Małgorzata Zembald, Maciej Zalas, Błażej Gierczyk, Michał Cegłowski, Grzgorz Schroeder, "Formation of the [M+Cu+4Cl]+ Ion Under Laser Desorption Ionization Conditions as a Result of Cl Addition to a C≡C Bond (M - Methyl Or Ethyl Ester of 3,5-Bis(2,2′-Bipyridin-4-Ylethynyl)Benzoic Acid)" Rapid Communications in Mass Spectrometry 2014, 28 (24): 2759-2762.

2) Marek Smoluch, Michal Ceglowski, Joanna Kurczewska, Michal Babij, Teodor Gotszalk, Jerzy Silberring, and Grzegorz Schroeder, "Molecular Scavengers as Carriers of Analytes for Mass Spectrometry Identification", Analytical Chemistry 2014; 86(22):11226–11229.

3) Michał Cegłowski, Marek Smoluch, Michał Babij, Teodor Gotszalk, Jerzy Silberring, Grzegorz Schroeder, "Dielectric Barrier Discharge Ionization in Characterization of Organic Compounds Separated on Thin-Layer Chromatography Plates", PLoS One 2014; 9(8):e106088.

4) Rafał Frański, Marta Kowalska, Joanna Czerniel, Maciej Zalas, Błażej Gierczyk, Michał Cegłowski, Grzegorz Schroeder, "Copper complexes formed by 3,5-bis(2,2′-bipyridin-4-ylethynyl)benzoic acid and its methyl and ethyl esters as studied by electrospray ionization mass spectrometry", Central European Journal of Chemistry 2013;11(12):2066-75.

5) Błażej Gierczyk, Grzegorz Schroeder, Michał Cegłowski, "Polyoxaethylene polypodands - Powerful reduction catalysts in solid-liquid and liquid-liquid phase transfer systems", Journal of Physical Organic Chemistry 2013;26(4):306-14.

6) Błażej Gierczyk, Michał Cegłowski, Marcin Kaźmierczak, Maciej Zalas, "Multinuclear magnetic resonance studies of 2-aryl-1,3,4-thiadiazoles", Magnetic Resonance in Chemistry 2012;50(9):637-41.

7) Maciej Zalas, Błażej Gierczyk, Michał Cegłowski, Grzegorz Schroeder, "Synthesis of new dendritic antenna-like polypyridine ligands", Chemical Papers 2012;66(8):733-40.

8) Michał Cegłowski, Urszula Narkiewicz, Iwona Pełech and Grzegorz Schroeder, „Functionalization of gold-coated carbon nanotubes with self-assembled monolayers of thiolates", Journal of Materials Science 2012;47(7):3463-7

9) Błażej Gierczyk, Grzegorz Schroeder, Michał Cegłowski, „New polymeric metal ion scavengers with polyamine podand moieties", Reactive and Functional Polymers 2011;71(4):463-79.

10) Urszula Narkiewicz, Iwona Pełech, Marcin Podsiadły, Michał Cegłowski, Grzegorz Schroeder, Joanna Kurczewska, „Preparation and characterization of magnetic carbon nanomaterials bearing APTS-silica on their surface", Journal of Materials Science 2010;45(4):1100-6.

11) Joanna Kurczewska, Błażej Gierczyk, Michał Cegłowski, Grzegorz Schroeder, „Inorganic magnetic support for sodium cation scavenging", Thin Solid Films 2009;517(21):6076-80.

Rozdziały w monografiach

1) Michał Cegłowski, Grzegorz Schroeder, „Toksykologia nanomateriałów", W: G. Schroeder (red.), Kosmetyki – bioaktywne składniki, Cursiva 2012, s. 7-24, ISBN 978-83-62108-17-6.

2) Michał Cegłowski, Grzegorz Schroeder, „Związki metali jako barwniki w kosmetykach", W: G. Schroeder (red.), Kosmetyki – chemia dla ciała, Cursiva 2011, s. 197-217, ISBN 978-83-62108-11-4.

3) Michał Cegłowski, Grzegorz Schroeder, „Chemiczna funkcjonalizacja nanorurek węglowych", W: G. Schroeder (red.), Chemiczna funkcjonalizacja powierzchni dla potrzeb nanotechnologii, Cursiva 2011, s. 9-61, ISBN 978-83-62108-07-7.

4) Michał Cegłowski, Grzegorz Schroeder, „Nanorurki węglowe", W: G. Schroeder (red.), Nanotechnologia, kosmetyki, chemia supramolekularna, Cursiva 2010, s. 215-238, ISBN 978-83-62108-04-6.

5) Michał Cegłowski, Grzegorz Schroeder, „Funkcjonalizacja powierzchni", W: G. Schroeder (red.), Receptory molekularne – właściwości i zastosowanie, Cursiva 2009, s. 71-89, ISBN 978-83-62108-02-2.

6) Michał Cegłowski, Grzegorz Schroeder, „Metody syntezy katenanów oraz rotaksanów", W: G. Schroeder (red.), Wybrane aspekty chemii supramolekularnej, BETAGRAF P.U.H., Poznań 2009, s. 11-39, ISBN 978-83-89936-22-6.

7) Michał Cegłowski, Grzegorz Schroeder, „Polimery supramolekularne”, W: G. Schroeder (red.), Materiały supramolekularne, BETAGRAF P.U.H., Poznań 2008, s. 153-175, ISBN 978-83-89936-21-9.

8) Michał Cegłowski, Grzegorz Schroeder, „Efekty stabilizujące układy gość – gospodarz”, W: G. Schroeder (red.), Receptory supramolekularne, BETAGRAF P.U.H., Poznań 2007, s. 11-25, ISBN 978-83-89936-19-4.

9) Michał Cegłowski, Grzegorz Schroeder, „Strategia syntezy niektórych związków makrocyklicznych”, W: G. Schroeder (red.), Syntetyczne receptory molekularne, BETAGRAF P.U.H., Poznań 2007, s. 17-48, ISBN 83-89936-18-6.

KONFERENCJE NAUKOWE

Międzynarodowe konferencje naukowe

1) Michał Cegłowski, Grzegorz Schroeder: „Preparation of resin with Schiff base chelating groups for removal of heavy metal ions from aqueous solutions" XVII International Symposium „Advances in the Chemistry of Heteroorganic Compounds", 21 listopada 2014, Łódź.

2) Michał Cegłowski, Marek Smoluch, Jerzy Silberring, Grzegorz Schroeder: „FAPA ion source for direct analysis of compounds from TLC plates" 4th Conference of Polish Mass Spectrometry Society, 26-29 maja 2014, Trzebnica.

3) Michał Cegłowski, Marek Smoluch, Jerzy Silberring, Grzegorz Schroeder, „Mass spectrometric analysis of pyrazole derivatives from TLC plates using FAPA ion source" 32nd Informal Meeting on Mass Spectrometry, 11-14 maja 2014, Balatonszárszó, Węgry.

4) Michał Cegłowski, Grzegorz Schroeder, „Characterization and diol binding properties of poly(MVE-*alt*-MA) functionalized with 3-aminophenylboronic acid", XVI International Symposium „Advances in the Chemistry of Heteroorganic Compounds", 15 listopada 2013, Łódź.

5) Michał Cegłowski, Grzegorz Schroeder, „Characterization and diol binding properties of poly(MVE-*alt*-MA) functionalized with 3-aminophenylboronic acid", 11th International Congress of Young Chemists "YoungChem2013", 9-13 października 2013, Poznań.

6) Michał Cegłowski, Grzegorz Schroeder, „Water soluble boronic acid functionalized poly(MVE-*alt*-MA) as sensor for biologically relevant compounds", EuroBoron 6 – European Conference on Boron Chemistry, 8-13 września 2013, Radziejowice.

7) Michał Cegłowski, Grzegorz Schroeder, „Synthesis, characterization and sorption properties of polysiloxanes functionalized with pyrazole derivatives", Central European School on Physical Organic Chemistry, 27-31 maja 2013, Przesieka.

8) Wojciech Ostrowski, Michał Cegłowski, Rafał Frański, „Demethoxycurcumin-metal complexes – tautomerism and comparison with curcumin-metal complexes, as studied by ESIMS/MS"; 31st Informal Meeting on Mass Spectrometry, 5-8 maja 2013, Palermo, Włochy.

9) Michał Cegłowski, Wojciech Ostrowski, Grzegorz Schroeder, „Laser desorption/ionization mass spectrometric analysis of folic acid, vancomycin and triton® X-

100 on variously functionalized carbon nanotubes", 31st Informal Meeting on Mass Spectrometry, 5-8 maja 2013, Palermo, Włochy.

10) Michał Cegłowski, Grzegorz Schroeder, „Polymers functionalized with molecular receptors", 10th International Congress of Young Chemists „YoungChem2012", 10-14 października 2012, Gdańsk.

11) Michał Cegłowski, Grzegorz Schroeder, "Matrices for MALDI mass spectrometry based on covalently functionalized carbon nanotubes", 30th Informal Meeting on Mass Spectrometry, 29 kwietnia – 3 maja 2012, Ołomuniec, Czechy.

12) Szymon Jasiecki, Michał Cegłowski, Grzegorz Schroeder, „Functionalized carbon nanotubes as the matrices for MALDI mass spectrometry", Joint Conference of the Polish Mass Spectrometry Society and the German Mass Spectrometry Society, 4-7 marca 2012, Poznań.

13) Urszula Narkiewicz, Iwona Pełech, Joanna Kurczewska, Michał Cegłowski and Grzegorz Schroeder, „Magnetic nanocarbons", NanoMats 2009, 10-13 sierpnia 2009, Stambuł, Turcja.

Krajowe konferencje naukowe

1) Michał Cegłowski, Grzegorz Schroeder, „Receptory molekularne i kompleksy metali podstawnikami polimerów", 56 Zjazd Naukowy PTChem i SITPchem, 16-20 września 2013, Siedlce.

2) Michał Cegłowski, Grzegorz Schroeder, "Polimery krzemoorganiczne funkcjonalizowane pochodnymi pirazolu", 55 zjazd PTChem i SITPChem, 16-20 września 2012, Białystok.

3) Michał Cegłowski, „Funkcjonalizacja nanorurek węglowych", Kwasy boronowe w chemii supramolekularnej, 15-17 kwietnia 2011, Radziejowice.

4) Michał Cegłowski, Grzegorz Schroeder, „Funkcjonalizacja nanorurek węglowych z wykorzystaniem metalizacji", 53 Zjazd PTChem i SITPChem, 14-18 września 2010, Gliwice.

5) Grzegorz Schroeder, Błażej Gierczyk, Bogusława Łęska, Radosław Pankiewicz, Michał Cegłowski, Dawid Lewandowski, „Synteza i właściwości podandów polioksaetylenowych". 50 Zjazd PTChem i SITPChem oraz 11 ICCE, 9-12 września 2007, Toruń.

6) Błażej Gierczyk, Bogusława Łęska, Radosław Pankiewicz, Grzegorz Schroeder, Michał Cegłowski, Dawid Lewandowski, „Zastosowanie nowych, nieorganicznych estrów

surfaktantu niejonowego - Triton-X w katalizie przeniesienia międzyfazowego", I Krajowa Konferencja Nanotechnologii, 25-28 kwietnia 2007, Wrocław.

7) Michał Cegłowski, Błażej Gierczyk, Grzegorz Schroeder, „Badania UV-VIS i ESI-MS pochodnych fluoresceiny, rodaminy B i oranżu metylowego", Ogólnopolskie Sympozjum naukowego Koła Chemików UAM, 27-29 października 2006, Jeziory k/Poznania.

FUNKCJONALIZACJA NANORUREK WĘGLOWYCH

Technika MALDI-MS, do zarejestrowania widma, wymaga zastosowania mieszaniny analitu oraz odpowiedniej matrycy, np. kwasu sinapowego lub 2,3-dihydroksybenzoesowego. Wymóg ten jest jednocześnie ograniczeniem tej metody, gdyż uzyskanie dobrej jakości widma masowego analitu o niskiej masie cząsteczkowej jest niezwykle trudne ze względu na liczne sygnały o wysokiej intensywności pochodzące od zastosowanej matrycy. W celu ominięcia tego problemu, zamiast konwencjonalnych matryc organicznych, stosuje się substancje nieorganiczne, które są źródłem nielicznych sygnałów o małej intensywności w obszarze niskich mas cząsteczkowych. Pośród zastosowanych w tym celu substancji nieorganicznych znalazły się nanorurki węglowe, które zostały użyte jako matryce, w analizie MALDI-MS, do otrzymania widm masowych związków o niskich masach cząsteczkowych, takich jak peptydy [1]. Rozwinięciem tej metody jest zastosowanie utlenionych nanorurek węglowych, które posiadają na swojej powierzchni grupy karboksylowe. Okazało się, że nanorurki węglowe z tak zmodyfikowaną powierzchnią lepiej spełniają swoje zadanie jako matryce, gdyż grupy karboksylowe stają się dodatkowym źródłem jonów. Co więcej, proces utlenienia usuwa z ich powierzchni amorficzny węgiel, który jest głównym źródłem zanieczyszczeń obserwowanych na widmie masowym [2, 3]. Problemem badawczym, jaki rozwiązałem i opisałem w publikacji pt. „*Laser desorption/ionization mass spectrometric analysis of surfactants on functionalized carbon nanotubes*" było sprawdzenie, czy funkcjonalizacja nanorurek węglowych za pomocą kwasu sinapowego, związanego w sposób kowalencyjny oraz niekowalencyjny, doprowadzi do uzyskania efektywnych matryc w technice MALDI-MS. W tym celu wielościenne nanorurki węglowe posiadające w swojej strukturze grupy karboksylowe, wprowadzone na skutek częściowego utlenienia, poddałem reakcji z chlorkiem tionylu. Tak utworzony materiał zmodyfikowałem w dwojaki sposób: poprzez bezpośrednią reakcję z kwasem sinapowym oraz poprzez reakcję z nadmiarem etylenodiaminy, a następnie dodanie do tak uzyskanego materiału kwasu sinapowego. Pierwsza z opisanych metod pozwoliła mi na otrzymanie nanorurek węglowych sfunkcjonalizowanych kwasem sinapowym związanym w sposób kowalencyjny, natomiast dzięki drugiej otrzymałem nanorurki węglowe sfunkcjonalizowane kwasem sinapowym związanym w sposób niekowalencyjny (poprzez utworzenie pary jonowej). Schemat przeprowadzonych reakcji przedstawiono na rysunku 2. Oba uzyskane materiały (oznaczone odpowiednio jako CNT-SA oraz [CNT-NH_3^+][SA]) scharakteryzowałem za pomocą spektroskopii w podczerwieni.

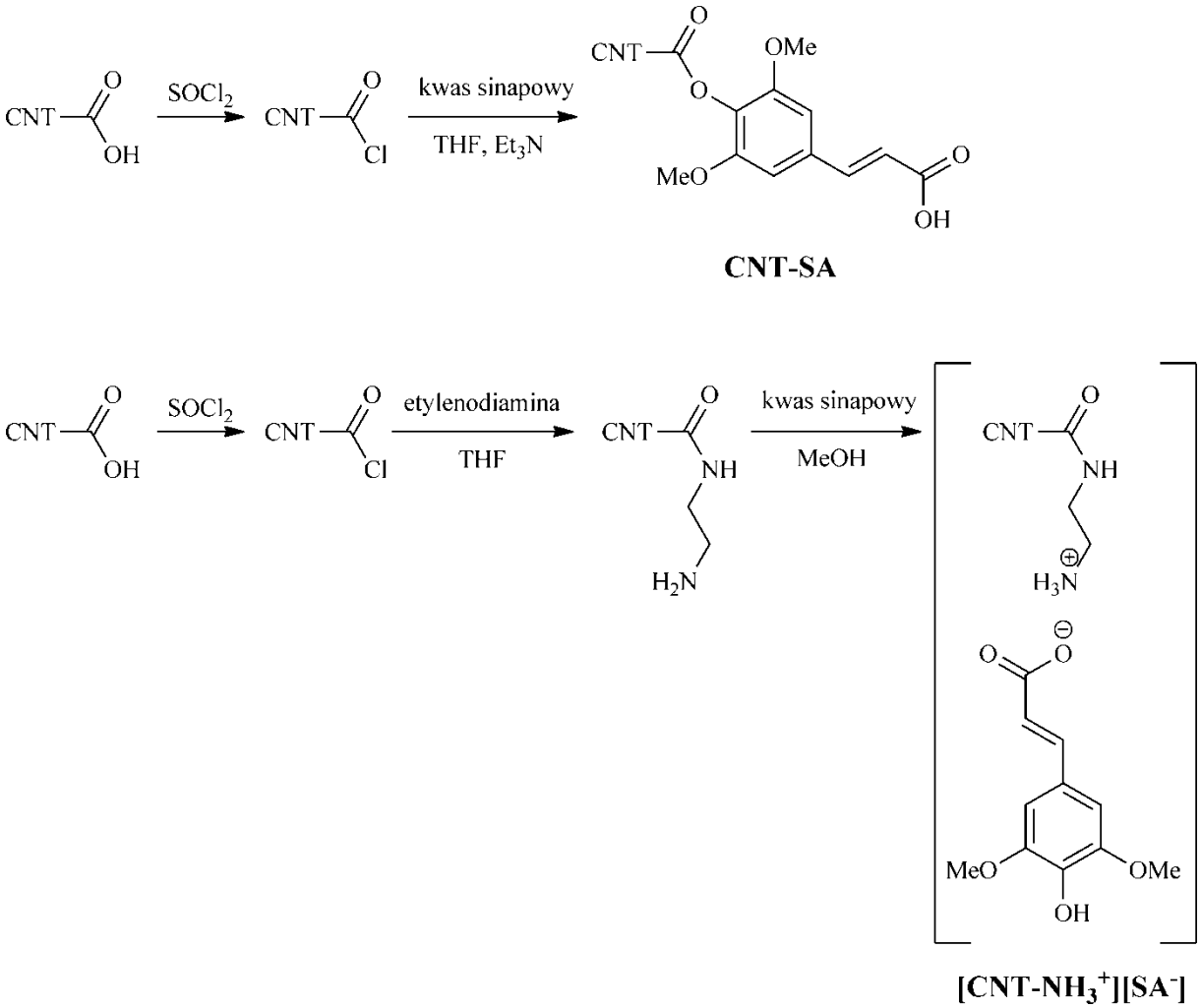

Rysunek 2. Schemat otrzymywania nanorurek węglowych sfunkcjonalizowanych kwasem sinapowym w sposób kowalencyjny (CNT-SA) oraz niekowalencyjny ([CNT-NH_3^+][SA]).

Jako anality wybrałem surfaktanty niejonowe zawierające ugrupowania polioksaetylenowe. Dwa z zastosowanych analitów stanowiły etery cetylowe glikolu polietylenowego o różnej długości łańcucha polioksaetylenowego (mające komercyjne nazwy Brij® 52 oraz Brij® 56), natomiast trzecim analitem był eter monometylowy glikolu polioksaetylenowego o masie cząsteczkowej średniej liczbowo (ang. *number average molecular weight*) wynoszącej 750 g/mol. Porównując widma masowe zarejestrowane techniką MALDI-MS wymienionych analitów z zastosowaniem CNT-SA oraz [CNT-NH_3^+][SA] jako matryc zauważyłem, że całkowita intensywność widm, uzyskanych z zastosowaniem CNT-SA, jest większa niż w przypadku [CNT-NH_3^+][SA]. Tę obserwację wytłumaczyłem obecnością wolnych grup karboksylowych znajdujących się na powierzchni CNT-SA. Z uwagi na fakt, iż synteza była wykonywana w naczyniach szklanych, a rozpuszczalniki wykorzystywane podczas syntezy były przechowywane w szklanych butelkach, grupy karboksylowe mogły przekształcić się w

aniony karboksylanowe występujące w postaci soli sodowej lub potasowej. Tak utworzone ugrupowania są bardzo wydajne w przenoszeniu jonów sodu i potasu bezpośrednio do analitów, co skutkuje zwiększeniem całkowitej intensywności zarejestrowanych widm. Sygnały pochodzące od zanieczyszczeń, powstałych najprawdopodobniej w wyniku rozkładu matrycy, miały niższą intensywność na widmach masowych zarejestrowanych z zastosowaniem [CNT-NH_3^+][SA]. Fakt ten wytłumaczyłem inną dystrybucją energii lasera zaabsorbowaną przez próbkę. W przypadku [CNT-NH_3^+][SA] część energii zostaje zużyta na zerwanie wiązania jonowego, przez co mniejsza jej ilość oddziałuje na strukturę nanorurek węglowych. Podsumowując, wykazałem że sfunkcjonalizowane kwasem sinapowym nanorurki węglowe mogą być z powodzeniem wykorzystywane jako matryce w analizie MALDI-MS, a sposób funkcjonalizacji (kowalencyjny lub niekowalencyjny) ma wpływ na jakość uzyskanego widma.

Aplikacyjne zastosowanie nowej generacji funkcjonalizowanych nanorurek węglowych przedstawiłem w pracy pt. „*Laser desorption/ionization mass spectrometric analysis of folic acid, vancomycin and Triton® X-100 on variously functionalized carbon nanotubes*". Problemem badawczym, jaki podjąłem w tej pracy, było sprawdzenie efektywności sfunkcjonalizowanych w różny sposób nanorurek węglowych jako matryc w analizie MALDI-MS. W tym celu przebadałem pięć materiałów: niezmodyfikowane nanorurki węglowe (CNT), nanorurki węglowe z grupami hydroksylowymi (CNT-OH) lub karboksylowymi (CNT-COOH) oraz nanorurki węglowe sfunkcjonalizowane kowalencyjnie za pomocą kwasu sinapowego (CNT-SA) lub galusowego (CNT-GA). Proces funkcjonalizacji za pomocą kwasu galusowego przeprowadziłem analogicznie jak w przypadku kwasu sinapowego. Jako anality zastosowałem trzy różne substancje: kwas foliowy, antybiotyk – wankomycynę oraz surfaktant niejonowy Triton® X-100. Dodatkowo widmo każdego z analitów zarejestrowałem, w celach porównawczych, z czystym kwasem sinapowym jako matrycą. Zarejestrowane widma masowe wykazały wyraźnie, że wszystkie zastosowane matryce, oparte na bazie nanorurek węglowych, efektywnie adsorbują energię lasera i przenoszą ją na analit, powodując jego jonizację. Całkowita intensywność widm masowych uzyskanych z zastosowaniem CNT oraz CNT-OH była o około jeden rząd wielkości niższa, niż w przypadku pozostałych materiałów węglowych. Obserwację tę wyjaśniłem faktem, iż pozostałe funkcjonalizowane nanorurki węglowe mają w swojej strukturze aniony karboksylanowe występujące w postaci soli sodowej, które mogą być źródłem kationów sodu. Zbliżoną intensywność w przypadku CNT-COOH, CNT-SA oraz CNT-GA wyjaśniłem postulując, że funkcjonalizacja kwasem sinapowym, czy galusowym nie zmienia właściwości

nanorurek węglowych w procesie przenoszenia zaabsorbowanej energii lasera na analit. Różnice w całkowitej intensywności widm między tymi trzema materiałami najprawdopodobniej oznaczają, że dany analit ma większe powinowactwo do powierzchni nanorurki węglowej sfunkcjonalizowanej w określony sposób, a co za tym idzie możliwe jest dobranie najbardziej efektywnych par matryca nanorurkowa – analit. Porównanie z klasyczną matrycą MALDI-MS, czyli kwasem sinapowym, wykazało że matryca ta praktycznie nie nadawała się do zarejestrowania widma kwasu foliowego, gdyż sygnały pochodzące od tego analitu miały dużo niższą intensywność niż sygnały pochodzące od matrycy. Co więcej, widma masowe wankomycyny oraz Tritonu® X-100 otrzymane z zastosowaniem kwasu sinapowego były gorsze jakościowo, niż widma tych analitów zarejestrowane z zastosowaniem matryc na bazie nanorurek węglowych. Oznacza to, że otrzymane przeze mnie matryce nadają się lepiej do analizy MALDI-MS związków o niskich masach cząsteczkowych, niż najczęściej stosowane, „tradycyjne" matryce organiczne.

FUNKCJONALIZACJA POLIMERÓW

Kwasy boronowe zdolne są do tworzenia kompleksów z diolami w wyniku równowagowej reakcji prowadzącej do uzyskania odpowiedniego estru. Ze względu na te unikalne właściwości, polimery zawierające w swojej strukturze receptory boronowe cieszą się olbrzymim zainteresowaniem badaczy. Polimery należące do tej grupy związków znalazły liczne potencjalne zastosowania, między innymi jako nośniki leków [4, 5] oraz sensory wykrywające substancje aktywne biologicznie [6]. Problemem badawczym, jaki podjąłem w pracy pt. "*Poly(methyl vinyl ether-alt-maleic anhydride) Functionalized with 3-Aminophenylboronic Acid: A New Boronic Acid Polymer for Sensing Diols in Neutral Water*", była synteza rozpuszczalnego w wodzie polimeru zawierającego w swojej strukturze receptory boronowe, który byłby zdolny do tworzenia selektywnych oddziaływań z cukrami oraz diolami. W celu otrzymania odpowiedniego polimeru przeprowadziłem reakcję między poli(eterem metylowo-winylowym-*alt*-bezwodnikiem maleinowym) (poly(MVE-*alt*-MA), ang. *poly(methyl vinyl ether-alt-maleic anhydride)*) oraz kwasem 3-aminofenyloboronowym, której schemat przedstawiony jest na rysunku 3.

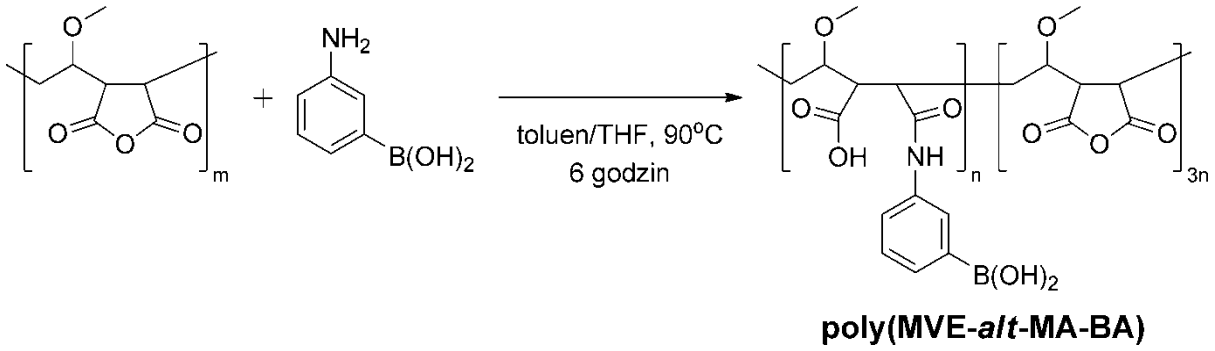

Rysunek 3. Schemat otrzymywania polimeru zawierającego receptory boronowe.

W wyniku reakcji nie uzyskuje się pełnego przereagowania wszystkich grup bezwodnikowych znajdujących się w poly(MVE-*alt*-MA), dlatego do dalszych badań niezbędne było wyznaczenie, ile receptorów boronowych znajduje się w produkcie oznaczonym jako poly(MVE-*alt*-MA-BA). Wartość tę wyznaczono techniką spektroskopii ^{1}H NMR poprzez porównanie intensywności sygnałów pochodzących od protonów aromatycznych, obecnych tylko w grupach fenyloboronowych, z intensywnością sygnałów od pozostałych protonów, których ilość nie zmieniła się w trakcie procesu funkcjonalizacji. Okazało się, że w końcowym produkcie na trzy nieprzereagowane grupy bezwodnikowe przypada jeden receptor boronowy. W kolejnym etapie badań wyznaczyłem stałe trwałości kompleksów między receptorami boronowymi, znajdującymi się w strukturze poly(MVE-*alt*-

MA-BA), oraz diolami i cukrami o różnej budowie. W tym celu zastosowałem metodę zaproponowaną przez Springsteena i Wanga [7] wykorzystującą alizarynę S (ARS, ang. *Alizarin Red S*), która tworząc kompleks z receptorem boronowym zmienia swoją barwę z czerwonej na żółtą. W momencie, gdy do tak uzyskanego układu wprowadza się diol, wypiera on alizarynę S z kompleksu, przywracając tym samym czerwoną barwę całej mieszaninie. Oznacza to, że mierząc zmiany absorbancji roztworu w trakcie miareczkowania roztworem diolu oraz znając stałą trwałości kompleksu receptor boronowy – alizaryna S (wyznaczoną za pomocą metody Benesiego–Hildebranda) byłem w stanie wyznaczyć stałe trwałości kompleksu receptor boronowy – diol. Schemat opisanego układu przedstawia rysunek 4.

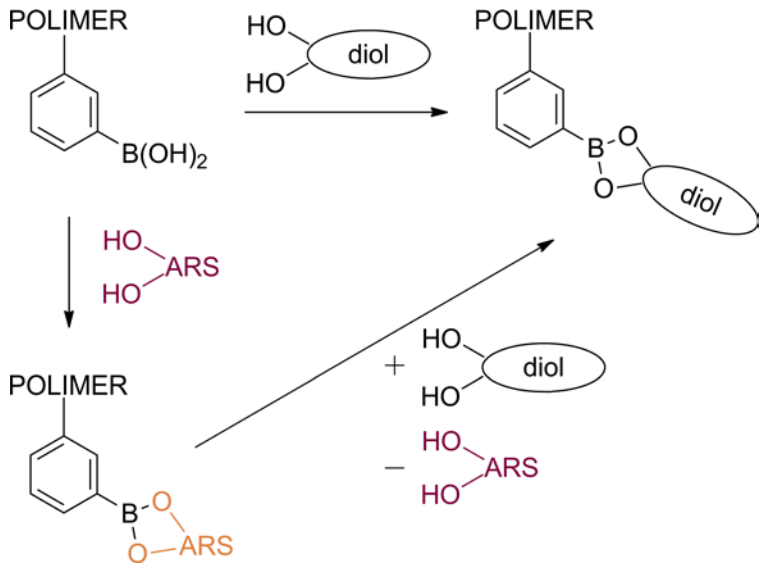

Rysunek 4. Schemat układu wykorzystywanego do wyznaczania stałych trwałości kompleksu receptor boronowy – diol.

W wyniku przeprowadzonych pomiarów wykazałem, że uzyskany polimer charakteryzował się zdecydowanie większe powinowactwo do rybonukleozydów cytydyny oraz urydyny, niż do jakiegokolwiek innego przebadanego cukru. Ponadto zaobserwowałem, iż podczas próby pomiaru stałej trwałości kompleksów z wszystkimi aldopentozami oraz niektórymi innymi związkami, uzyskana mieszanina przyjmuje kolor purpurowo-czerwony, co najprawdopodobniej wskazuje na zachodzenie procesu redoks w badanym układzie. Nie udało mi się jednakże zbadać dokładnego mechanizmu tego procesu, ani znaleźć informacji na ten temat w literaturze.

Polimery, które zdolne są do tworzenia kompleksów z kationami metali znajdują szerokie zastosowanie w oczyszczaniu wód, odzyskiwaniu cennych metali oraz w katalizie heterogenicznej. Temat ten został przeze mnie szerzej opisany w rozdziale monografii pt.

„*Functional polymers forming complexes with metal ions*”. W celu uzyskania polimeru zdolnego do adsorpcji konkretnych kationów metali, niezbędne jest zaprojektowanie lub wybranie odpowiedniego receptora.

W publikacji pt. “*Removal of heavy metal ions with the use of chelating polymers obtained by grafting pyridine–pyrazole ligands onto polymethylhydrosiloxane*” problemem badawczym jaki podjąłem była synteza receptorów pirydyno-pirazolowych, przyłączenie ich do powierzchni poli(metylowodorosiloksanu) (PMHS, ang. *polymethylhydrosiloxane*) oraz sprawdzenie zdolności sorpcyjnych tak uzyskanych materiałów w stosunku do kationów miedzi(II), kadmu(II), chromu(III), niklu(II) oraz kobaltu(II). Wybrałem receptory pirydyno-pirazolowe, gdyż pochodne pirazolu znane są ze swoich zdolności do tworzenia trwałych związków koordynacyjnych z kationami metali. W rozdziale monografii pt. „*Synthesis of pyrazole-based bidentate and tridentate supramolecular ligands*” przedstawiłem zagadnienia dotyczące syntezy oraz właściwości pochodnych pirazolu, jako ligandów supramolekularnych. Wybór PMHS na polimer macierzysty spowodował, iż musiałem zaprojektować ligandy zdolne do przyłączenia się do powierzchni polimeru w wyniku reakcji hydrosililowania. W tym celu przeprowadziłem szereg reakcji, przedstawionych na rysunku 5, prowadzących do otrzymania ligandów **3** i **6**, które różnią się długością linkera łączącego je z łańcuchem głównym polimeru. Moim celem było sprawdzenie również, czy długość linkera oraz obecność dodatkowych atomów donorowych tlenu w przypadku liganda **6** ma wpływ na zdolności sorpcyjne ostatecznego polimeru. W wyniku reakcji hydrosililowania uzyskałem dwa polimery, które oznaczyłem jako PMHS-*g*-PyPzAllyl (uzyskany z zastosowaniem liganda **3**) oraz PMHS-*g*-PyPz$(OEt)_2$Allyl (uzyskany z zastosowaniem liganda **6**). Dla kationów miedzi(II), kadmu(II), chromu(III), niklu(II) oraz kobaltu(II) wyznaczyłem izotermy adsorpcji, kinetykę adsorpcji, wpływ temperatury oraz pH na proces adsorpcji. Ponadto sprawdziłem, jak cykle adsorpcji/desorpcji wpływają na zdolności sorpcyjne polimeru oraz wykazałem, że uzyskane polimery efektywnie adsorbują kationy metali z zanieczyszczonych nimi ciekłych odpadów przemysłowych. Wartości maksymalnej adsorpcji, obliczone na podstawie izotermy Langmuira, wykazały różnice między właściwościami PMHS-*g*-PyPzAllyl oraz PMHS-*g*-PyPz$(OEt)_2$Allyl względem przebadanych kationów metali. Okazało się, że PMHS-*g*-PyPz$(OEt)_2$Allyl, dzięki obecności dłuższego linkera, jest bardziej uniwersalny w procesie adsorpcji kationów, gdyż różnice między wartościami maksymalnej adsorpcji między kationami były zdecydowanie mniejsze niż w przypadku PMHS-*g*-PyPzAllyl. Jest to najprawdopodobniej związane z większą elastycznością receptora, który jest w stanie lepiej dostosować się do rozmiarów określonych kationów metali.

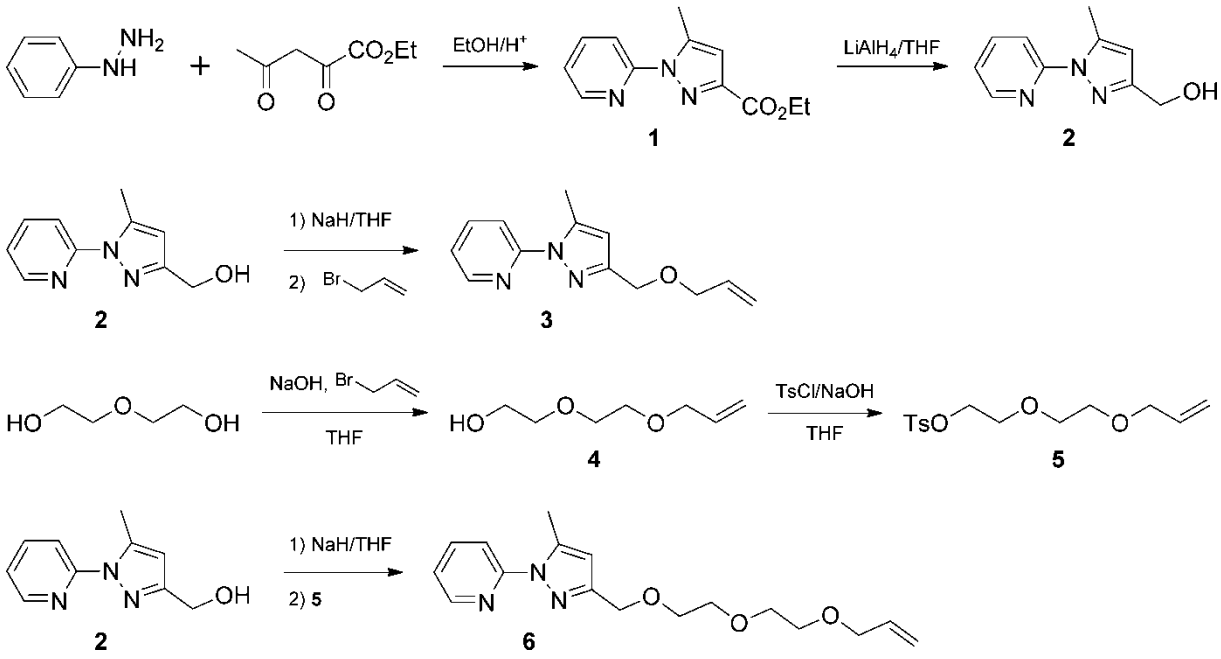

Rysunek 5. Schemat syntez prowadzących do otrzymania ligandów **3** i **6**.

Zasady Schiffa, zawierające w swojej strukturze atomy azotu i tlenu, są znane z tworzenia trwałych kompleksów z kationami metali przejściowych. Są to najczęściej związki, które można otrzymać w wyniku prostej kondensacji lub kilku kondensacji zachodzących podczas pojedynczego etapu syntezy. Poprzez przyłączenie zasad Schiffa do polimerów uzyskuje się materiały zdolne do adsorpcji kationów metali poprzez receptory o dobrze zdefiniowanej strukturze [8]. Kolejnym zagadnieniem, które realizowałem w trakcie wykonywania pracy doktorskiej dotyczyło syntezy polimerów sfunkcjonalizowanych za pomocą zasad Schiffa. Syntezę polimeru zawierającego w swojej strukturze zasady Schiffa oraz sprawdzenie właściwości sorpcyjnych tak uzyskanego materiału w stosunku do kationów miedzi(II), kadmu(II), chromu(III), niklu(II) oraz kobaltu(II) przedstawiłem w publikacji pt. "*Preparation of Porous Resin with Schiff Base Chelating Groups for Removal of Heavy Metal Ions from Aqueous Solutions*". Polimerem jaki zdecydowałem się poddać funkcjonalizacji był poly(MVE-*alt*-MA), co oznaczało, iż zastosowany receptor musiał być w stanie przyłączyć się do grup bezwodnikowych. W tym celu zdecydowałem się na otrzymanie zasady Schiffa w wyniku reakcji 2-acetylopirydyny oraz hydrazydu kwasu 4-aminobenzoesowego, która posiada grupę aminową, zdolną do reakcji z grupami bezwodnikowymi. Schemat otrzymywania ostatecznego polimeru przedstawiłem na rysunku 6.

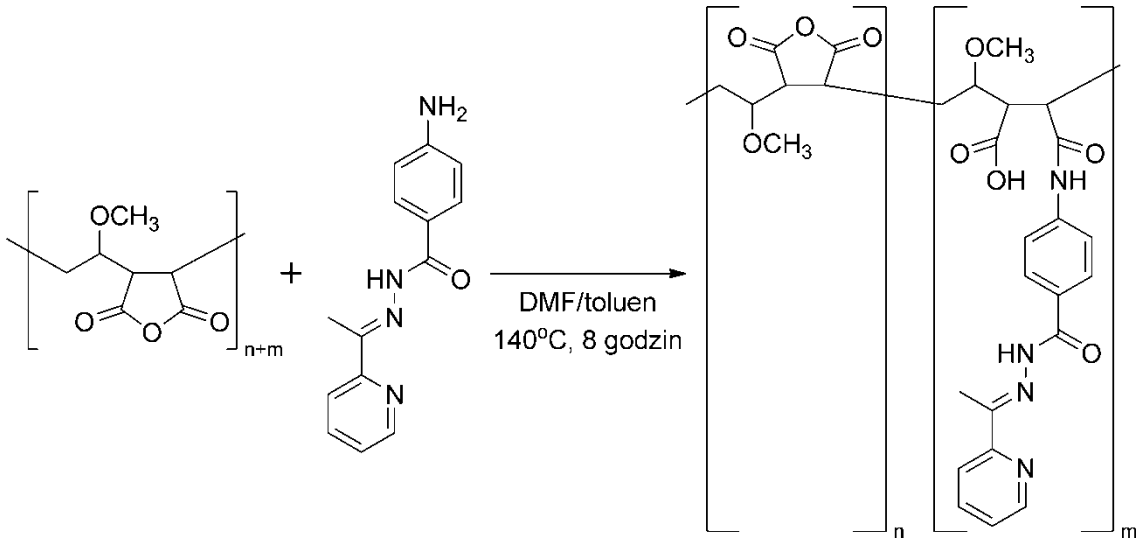

Rysunek 6. Schemat otrzymywania polimeru zawierającego w swojej strukturze zasady Schiffa.

Uzyskany materiał scharakteryzowałem za pomocą spektroskopii w podczerwieni, analizy elementarnej, termograwimetrii, skaningowej kalorymetrii różnicowej, sorptometrii azotu oraz skaningowej mikroskopii elektronowej. Okazało się, że otrzymany polimer wykazuje interesującą, porowatą strukturę, a jego powierzchnia właściwa wyznaczona z izotermy BET wynosi 2,051 m^2/g, co jest wartością zbliżoną do wartości uzyskiwanych dla innych chelatujących polimerów [9]. Dla kationów miedzi(II), kadmu(II), chromu(III), niklu(II) oraz kobaltu(II) wyznaczyłem izotermy adsorpcji, kinetykę adsorpcji, wpływ temperatury oraz pH na proces adsorpcji. Okazało się, że procesowi adsorpcji najlepiej odpowiada model Langmuira, a kinetyce model pseudo-drugiego rzędu. Sprawdziłem także przydatność polimeru po kilku cyklach adsorpcji/desorpcji, w których zastosowałem dwa odczynniki desorbujące: kwas solny oraz EDTA. Zaskakującym faktem była obserwacja, iż adsorpcja polimeru w stosunku do większości kationów zwiększa się po pierwszym etapie desorpcji z zastosowaniem kwasu solnego. Wytłumaczyłem to reakcją hydrolizy pozostałych grup bezwodnikowych, co w konsekwencji prowadzi do utworzenia się grup karboksylowych na powierzchni polimeru, które zwiększają jego zdolności sorpcyjne w stosunku do niektórych kationów metali przejściowych. Uzyskany przeze mnie polimer był w stanie zaadsorbować większe ilości kationów kadmu(II) oraz miedzi(II) niż inne sorbenty opisane w literaturze [10, 11].

Literatura

[1] S. Xu, Y. Li, H. Zou, J. Qiu, Z. Guo, B. Guo, Carbon Nanotubes as Assisted Matrix for Laser Desorption/Ionization Time-of-Flight Mass Spectrometry, Anal. Chem., 75 (2003) 6191-6195.

[2] S.-f. Ren, Y.-l. Guo, Oxidized carbon nanotubes as matrix for matrix-assisted laser desorption/ionization time-of-flight mass spectrometric analysis of biomolecules, Rapid Commun. Mass Spectrom., 19 (2005) 255-260.

[3] C. Pan, S. Xu, L. Hu, X. Su, J. Ou, H. Zou, Z. Guo, Y. Zhang, B. Guo, Using oxidized carbon nanotubes as matrix for analysis of small molecules by MALDI-TOF MS, J. Am. Soc. Mass Spectrom., 16 (2005) 883-892.

[4] D. Shiino, Y. Murata, K. Kataoka, Y. Koyama, M. Yokoyama, T. Okano, Y. Sakurai, Preparation and characterization of a glucose-responsive insulin-releasing polymer device, Biomaterials, 15 (1994) 121-128.

[5] D. Shiino, Y. Murata, A. Kubo, Y.J. Kim, K. Kataoka, Y. Koyama, A. Kikuchi, M. Yokoyama, Y. Sakurai, T. Okano, Amine containing phenylboronic acid gel for glucose-responsive insulin release under physiological pH, J. Control. Release., 37 (1995) 269-276.

[6] W. Takayoshi, M. Imajo, M. Iijima, M. Suzuki, H. Yamamoto, Y. Kanekiyo, Multicolor saccharide-sensing chips created via layer-by-layer adsorption of boronic acid-containing polymers, Sensor. Actuat. B-Chem., 192 (2014) 776-781.

[7] G. Springsteen, B. Wang, A detailed examination of boronic acid–diol complexation, Tetrahedron, 58 (2002) 5291-5300.

[8] P.A. Vigato, S. Tamburini, The challenge of cyclic and acyclic schiff bases and related derivatives, Coord. Chem. Rev., 248 (2004) 1717-2128.

[9] M. Monier, D.A. Abdel-Latif, Modification and characterization of PET fibers for fast removal of Hg(II), Cu(II) and Co(II) metal ions from aqueous solutions, J. Hazard. Mater., 250–251 (2013) 122-130.

[10] R. Hua, Z. Li, Sulfhydryl functionalized hydrogel with magnetism: Synthesis, characterization, and adsorption behavior study for heavy metal removal, Chem. Eng. J., 249 (2014) 189-200.

[11] Q. Wang, W. Gao, Y. Liu, J. Yuan, Z. Xu, Q. Zeng, Y. Li, M. Schröder, Simultaneous adsorption of Cu(II) and SO42− ions by a novel silica gel functionalized with a ditopic zwitterionic Schiff base ligand, Chem. Eng. J., 250 (2014) 55-65.

PODSUMOWANIE

Celem naukowym rozprawy doktorskiej pod tytułem „Funkcjonalizacja polimerów i nanomateriałów węglowych z zastosowaniem niskocząsteczkowych receptorów molekularnych" było opracowanie metod syntezy i otrzymanie nowych, funkcjonalnych polimerów i materiałów węglowych zawierających receptory molekularne o określonych, założonych właściwościach. Tak otrzymane, sfunkcjonalizowane nanorurki węglowe miały znaleźć zastosowanie w spektrometrii mas jako matryce w technice MALDI-MS, natomiast sfunkcjonalizowane polimery jako układy zdolne do wiązania analitów w chemii analitycznej i środowiskowej.

Uzyskane wyniki przedstawiłem w pięciu oryginalnych publikacjach naukowych. Na podstawie literatury przedstawiłem w rozdziale monografii pt. „*Synthesis of pyrazole-based bidentate and tridentate supramolecular ligands*" właściwości pochodnych pirazolu jako ligandów supramolekularnych, natomiast w rozdziale monografii pt. "*Functional polymers forming complexes with metal ions*" omówiłem zagadnienia dotyczące syntezy oraz badań funkcjonalnych polimerów.

W wyniku przeprowadzonych badań opracowałem metody syntezy i otrzymałem:

- sfunkcjonalizowane kwasem sinapowym nanorurki węglowe, które z powodzeniem zastosowałem jako nowe, efektywne matryce w analizie MALDI-MS,
- rozpuszczalny w wodzie polimer poly(MVE-alt-MA-BA), zawierający receptory boronowe; wyznaczyłem stałe trwałości kompleksów między receptorami boronowymi, znajdującymi się w strukturze polimeru i różnymi diolami,
- otrzymałem polimery krzemoorganiczne, zawierające w swojej strukturze receptory pirydyno-pirazolowe oraz zastosowałem je do adsorpcji kationów metali przejściowych,
- uzyskałem polimer będący pochodną poly(MVE-alt-MA), zwierający w swojej strukturze zasady Schiffa oraz wykorzystałem go do adsorpcji kationów metali przejściowych.

Otrzymane w wyniku syntezy sfunkcjonalizowane nanorurki węglowe oraz sfunkcjonalizowane polimery posiadały założone przed syntezą właściwości i mogą znaleźć zastosowanie w spektrometrii mas, w chemii analitycznej jako selektywne receptory oraz do oczyszczania wód z jonów metali ciężkich.

Streszczenie rozprawy doktorskiej pt.

„Funkcjonalizacja polimerów i nanomateriałów węglowych z zastosowaniem niskocząsteczkowych receptorów molekularnych”

mgr Michał Cegłowski

promotor: prof. dr hab. Grzegorz Schroeder

Kontrolowana, funkcjonalizacja chemiczna materiałów poprzez wprowadzanie do ich struktury określonych grup funkcyjnych umożliwia zmianę ich właściwości fizykochemicznych lub nadawanie im specjalnych zastosowań. Jest to jedna z podstawowych strategii syntezy stosowanych w chemii supramolekularnej, która umożliwia uzyskiwanie materiałów funkcjonalnych, posiadających w swojej strukturze receptory molekularne. Układy tego typu zachowują większość unikalnych właściwości początkowego materiału, a ponadto dzięki obecności receptorów molekularnych, zdolne są do tworzenia selektywnych oddziaływań z innymi cząsteczkami.

Nanorurki węglowe wykazują niezwykłe właściwości elektryczne oraz mechaniczne, co sprawia, że są badane jako obiecujące materiały do zastosowań w elektronice jako półprzewodniki, chemii materiałowej jako składniki wytrzymałych materiałów kompozytowych oraz chemii analitycznej do detekcji substancji przy bardzo niskich stężeniach. Większość z tych zastosowań wymaga wcześniejszej funkcjonalizacji powierzchni nanorurek węglowych.

Funkcjonalizacja polimerów umożliwia otrzymanie szerokiej grupy materiałów polimerowych o specjalistycznych zastosowaniach. Dużym zainteresowaniem badaczy cieszą się polimery zdolne do selektywnego wychwytywania, ze swojego otoczenia określonych związków chemicznych. Tego typu materiały otrzymuje się w kontrolowanej polimeryzacji funkcjonalnych monomerów lub poprzez funkcjonalizację odpowiedniego polimeru. Druga z opisanych metod jest wydajna i łatwa do przeprowadzenia, pod warunkiem, że receptor użyty do funkcjonalizacji posiada grupy funkcyjne zdolne do trwałego wiązania się z głównym łańcuchem polimeru. Oznacza to, że niezbędne w tej metodzie jest otrzymanie cząsteczki receptora z grupami funkcyjnymi reaktywnymi względem określonego polimeru. Zaletą funkcjonalnych polimerów jest najczęściej: łatwa synteza, niski koszt otrzymywania oraz zdolność do wielokrotnego zastosowania w tym samym procesie po etapie regeneracji.

Celem naukowym mojej pracy jest opracowanie metody syntezy i otrzymanie nowych, funkcjonalnych materiałów węglowych i polimerów zawierających receptory molekularne. Układy te mają wykazywać zdolność selektywnego wiązania jonów i cząsteczek oraz zdefiniowane właściwości.

W celu otrzymania nowych matryc dla techniki MALDI-MS (ang. *matrix-assisted laser desorption/ionization mass spectrometry*), które nie generowałyby sygnałów na widmie mas w rejonie niskich mas cząsteczkowych, przeprowadziłem funkcjonalizację wielościennych nanorurek węglowych poprzez przyłączenie do ich powierzchni kwasu sinapowego w sposób kowalencyjny lub poprzez utworzenie kompleksu jonowego. Uzyskane w ten sposób materiały zastosowałem jako matryce w analizie MALDI-MS surfaktantów, kwasu foliowego oraz wankomycyny. Wykazałem, że widma masowe zarejestrowane z zastosowaniem przygotowanych przeze mnie materiałów mają, dla większości zbadanych analitów, wyższą całkowitą intensywność oraz lepszy stosunek sygnału do szumu niż widma zarejestrowane z zastosowaniem niezmodyfikowanych nanorurek węglowych. Ponadto stwierdziłem, że widma uzyskane z zastosowaniem przygotowanych przeze mnie funkcjonalizowanych nanorurek węglowych posiadają mniej sygnałów pochodzących od matrycy w rejonie niskich mas cząsteczkowych, które przeszkadzają w analizie widm, niż widma uzyskane z zastosowaniem czystego kwasu sinapowego jako matrycy.

Przeprowadzenie funkcjonalizacji określonych polimerów wymagało ode mnie uzyskania receptorów, które jednocześnie będą selektywne wobec odpowiedniego analitu i reaktywne względem grup funkcyjnych obecnych w strukturze polimeru. Pierwszym celem funkcjonalizacji polimerów było uzyskanie materiałów zdolnych do selektywnego oddziaływania z cukrami i diolami. W tym celu do poli(eteru metylowo-winylowego-*alt*-bezwodnika maleinowego) (poly(MVE-*alt*-MA), ang. *poly(methyl vinyl ether-alt-maleic anhydride)*) przyłączyłem kwas 3-aminofenyloboronowy. Do roztworu tak otrzymanego polimeru dodałem następnie alizaryny S, która utworzyła z nim barwny kompleks. Śledzenie zmian absorpcji uzyskanego kompleksu podczas miareczkowania za pomocą cukrów i dioli pozwoliło mi na wyznaczenie stałych trwałości między otrzymanym, polimerem funkcjonalnym oraz badanymi diolami. Wykazałem, że spośród badanych dioli, uzyskany polimer miał największe powinowactwo do nukleozydów (cytydyny oraz urydyny).

Drugim celem funkcjonalizacji polimerów było uzyskanie materiałów zdolnych do adsorpcji kationów metali przejściowych. Otrzymałem w tym celu trzy polimery: dwie pochodne poli(metylowodorosiloksanu) (PMHS, ang. *polymethylhydrosiloxane*) sfunkcjonalizowane za pomocą różnych ligandów pirydyno-pirazolowych oraz poly(MVE-*alt*-MA) sfunkcjonalizowany za pomocą zasady Schiffa uzyskanej w wyniku reakcji 2-acetylopirydyny oraz hydrazydu kwasu 4-aminobenzoesowego. Następnie zbadałem wpływ stężenia jonów metali, czasu, temperatury oraz pH na proces adsorpcji kationów miedzi(II), kadmu(II), chromu(III), niklu(II) oraz kobaltu(II). Wykazałem, że pochodne PMHS mają

największe powinowactwo do jonów miedzi(II) oraz kadmu(II), a najmniejsze do jonów chromu(III) i kobaltu(II). Sfunkcjonalizowany poly(MVE-*alt*-MA) ma największe powinowactwo do jonów kadmu(II), a najmniejsze do jonów chromu(III). Wszystkie uzyskane polimery okazały się efektywne podczas procesu usuwania kationów metali z zanieczyszczonych nimi ciekłych odpadów przemysłowych.

Summary of doctoral dissertation on

“Functionalization of polymers and carbon nanomaterials with low molecular weight receptors”

Michał Cegłowski

PhD supervisor: Prof. Grzegorz Schroeder

Controlled chemical functionalization of materials achieved by introduction of defined functional groups to their structure, permits endowing the materials with specific target properties. It is one of the fundamentals synthetic strategies used in supramolecular chemistry, leading to functional materials comprising molecular receptors in their structure. The materials obtained preserve most of the properties of the initial material, but thanks to the presence of molecular receptors they are capable of selective interactions with other molecules.

Carbon nanotubes show unusual electric and mechanical properties and thus are promising materials to be used as semiconductors in electronics, components of highly resistant composites and as detectors of substances present at trace amounts. Most of these applications need preliminary functionalization of carbon nanotubes surfaces.

Functionalization of polymers permits getting a wide range of polymer materials showing defined properties. Recently, much interest has been paid to polymers capable of selective scavenging of certain chemical compounds or pollutants. They are obtained either as a result of controlled polymerisation of functionalised monomers or by functionalization of the polymer. The second approach is efficient and easy to perform on condition that the receptor used for the functionalization has functional groups capable of making permanent bonds with the main polymer chain. This condition implies the necessity of obtaining a molecular receptor with the functional groups reactive towards a given polymer. The benefits of functionalized polymers include easy synthesis, low cost and ability to multiple application in the same process after regeneration.

The aim of my doctoral dissertation was to design a method for the synthesis and to synthesise new functionalized carbon materials and polymers, containing molecular receptors capable of selective binding ions or molecules and showing defined properties.

One of my tasks was to obtain new matrices to be employed for matrix-assisted laser desorption/ionization mass spectrometry (MALDI-MS), which would not generate signals in the mass spectra in the region of low molecular mass. I performed multiwall carbon nanotubes functionalized on the surface with sinapic acid via covalent bonds or via formation of ionic complex. The materials obtained were applied as matrices in the MALDI-MS analyses of

surfactants, folic acid and vancomycin. I proved that the mass spectra recorded using the matrix proposed show higher total intensity and higher signal to noise ratio than the spectra recorded with unmodified carbon nanotubes. Moreover, the spectra obtained with the functionalized carbon nanotubes as a matrix showed less signals coming from the matrix in the low molecular mass range (that interfere with spectra analysis) than those recorded with pure sinapic acid as a matrix.

In order to functionalize certain polymers, it was necessary to obtain receptors that would be selective towards a given analyte and reactive towards the functional groups present in the polymer structure. The first task was to obtain materials capable of selective interactions with sugars and diols. For this purpose I proposed attachment of 3-aminephenylboronic acid to poly(methyl vinyl ether-*alt*-maleic anhydride) (poly(MVE-*alt*-MA). To a solution of thus obtained polymer, Alizarin Red S was added to make a coloured complex. Observation of changes in the absorption of the complex obtained upon titration with sugars and diols permitted a determination of the stability constants of complexes of the functionalized polymer and the diols studied. I proved that from among the diols studied the polymer showed the highest affinity to nucleosides, in particular cytidine and uridine.

The second aim of polymer functionalization was to obtain materials capable of adsorption of transition metal cations. I synthesised three polymers: two derivatives of polymethylhydrosiloxane (PMHS) functionalized with different pyridine-pyrazole ligands and poly(MVE-*alt*-MA) functionalized with a Schiff base obtained as a result of the reaction of 2-acetylpyridine and 4-aminobenzoic hydrazide. The influence of the metal ions concentration, contact time, temperature and pH on the adsorption processes of copper(II), cadmium(II), chromium(II), nickel(II) and cobalt(II) ions. The PMHS derivatives obtained were found to show the highest affinity to copper(II) and cadmium(II) ions and the lowest to chromium(III) and cobalt(II) ions. Functionalized poly(MVE-*alt*-MA) showed the highest affinity to cadmium(II) ions and the lowest to chromium(III) ions. All polymers obtained were efficient adsorbents in the process of removal of metal cations from wastewater.

Research Article

Rapid Communications in Mass Spectrometry

Received: 1 August 2012 Revised: 19 October 2012 Accepted: 21 October 2012 Published online in Wiley Online Library

Rapid Commun. Mass Spectrom. **2013**, *27*, 258–264
(wileyonlinelibrary.com) DOI: 10.1002/rcm.6448

Laser desorption/ionization mass spectrometric analysis of surfactants on functionalized carbon nanotubes

Michał Cegłowski* and Grzegorz Schroeder

Faculty of Chemistry, Adam Mickiewicz University in Poznan, Umultowska 89b, 61-614, Poznań, Poland

RATIONALE: Recently, unmodified and carboxylated carbon nanotubes have been used as assisting surfaces laser desorption/ionization (LDI) in mass spectrometry. The functionalization of carbon nanotubes with organic compounds should lead to a gamut of other promising LDI-assisting surfaces.
METHODS: Carboxylated carbon nanotubes were functionalized with sinapinic acid either covalently or by creating an ionic macro-complex. Polyether-based surfactants were used as analytes to examine the properties of these new matrices. Mass spectrometric analysis was conducted on a LDI-quadrupole time-of-flight (QTOF) mass spectrometer. Carbon nanotube surfaces were deposited from suspension using the dried-droplet method.
RESULTS: The functionalization of the carbon nanotubes was confirmed with Fourier transform infrared (FTIR) spectroscopy. The usefulness of each material was examined with two poly(ethylene glycol) hexadecyl ether amphiphiles (Brij® 52 and Brij® 56) and a poly(ethylene glycol) monomethyl ether as analytes. Generally, the mass spectra obtained with carbon nanotubes covalently functionalized with sinapinic acid as a matrix had peaks with higher intensities than those obtained with carbon nanotubes functionalized by ionic macro-complex formation.
CONCLUSIONS: The presented new materials based on functionalized carbon nanotubes are effective in the LDI mass analysis of polyether amphiphiles and poly(ethylene glycol) monomethyl ether. This type of assisting surfaces can be highly modified by appropriate functionalization procedures. Copyright © 2012 John Wiley & Sons, Ltd.

Matrix-assisted laser desorption/ionization (MALDI)[1,2] mass spectra are normally obtained with the use of a mixture of the analyte and an appropriate matrix such as sinapinic acid or 2,5-dihydroxybenzoic acid (DHB). This requirement is the main drawback of this method – the inability to obtain well-defined spectra of small analyte molecules, because their signals interfere with a variety of signals generated from the ions produced by the matrix. In the original work by Tanaka *et al.*, inorganic compounds such as fine cobalt powder mixed with glycerol[2] were proposed as matrices. Since then many other inorganic substances such as graphite,[3–5] diamond nanowires,[6] activated carbon,[7] carbon powder,[8] porous silicon,[9–11] silicon thin film,[12] single-crystal silicon surface,[13] silicon nanowires,[14,15] nanostructured silicon plates,[16] and frozen solutions of solid organic compounds[17] have been used as assisting surfaces for obtaining LDI mass spectra.

Since the report by Iijima in 1991,[18] carbon nanotubes (CNTs) have attracted the attention of many scientists from different fields. Their unique physical properties and a possibility to covalently or noncovalently modify their surface make them a promising material in a variety of applications.[19] Xu *et al.* have used CNTs as an efficient assisting surface for LDI analysis of biomolecules such as small peptides.[20] In order to provide an additional proton source, eliminate the carbon impurities that produce additional signals in mass spectra and increase the solubility of the CNTs, Ren and Guo[21] used oxidized CNTs containing carboxylic groups on their surface, as assisting surface for obtaining LDI mass spectra of oligosaccharides, peptides and insulin. Oxidized CNTs have also successfully been used for the qualitative and quantitative determination of small molecules by Pan *et al.*[22] Ren and Guo[23] introduced the use of CNTs functionalized with 2,5-dihydroxybenzoyl hydrazine for obtaining LDI mass spectra of trace peptides. Derivatization with this compound introduced phenyl and phenolic hydroxyl groups onto the surface of CNTs. Groups of this type can improve the effectiveness of CNTs as a proton source, with the carbon nanotube surface being responsible for the absorption of the pulse laser energy.

Polyether-based amphiphiles have been widely applied in biomedical and pharmaceutical areas, mostly as nanocarriers of hydrophobic drugs. They exhibit good chemical stability, high water solubility, low toxicity, weak interaction with blood components, and are highly biocompatible.[24] Nevertheless, they have some drawbacks such as possible degradation under stress, accumulation in the body above certain levels, or interaction with the immune system that can generate unwanted immune responses.[24] Thus, a rapid and sensitive method is required in order to estimate the presence of these compounds in biological samples.

In this paper we present a convenient method for functionalizing CNTs in order to obtain functional-assisting surfaces for obtaining LDI mass spectra. The new materials were designed

* *Correspondence to:* M. Cegłowski, Faculty of Chemistry, Adam Mickiewicz University in Poznan, Umultowska 89b, 61-614 Poznań, Poland.
E-mail: ceglowski.m@gmail.com

as derivatives of CNTs to which sinapinic acid, a conventional MALDI matrix, has been attached in two different ways. One of the matrices was designed as an ionic macro-complex between sinapinic acid and modified CNTs, while the other is a product of covalent functionalization of carboxylated CNTs with sinapinic acid. These routes of functionalization allow a combination of the high absorption of laser energy by CNTs with the effectiveness of sinapinic acid as a proton source. The usefulness of these assisting surfaces was examined with polyether amphiphiles [poly(ethylene glycol) hexadecyl ethers] and poly(ethylene glycol) monomethyl ether.

EXPERIMENTAL

Chemicals and materials

Polyether amphiphiles (poly(ethylene glycol) hexadecyl ethers: Brij® 52 and Brij® 56), poly(ethylene glycol) monomethyl ether of average $M_n = 750$, sinapinic acid (≥99.0%, matrix substance for MALDI-MS), sodium perchlorate monohydrate and potassium perchlorate were obtained from Sigma-Aldrich (St. Louis, MO, USA). Carboxylated CNTs (multi-walled nanotubes, -COOH functionalized, >95% purity) with average diameter of 10–20 nm and average length 10–30 μm were obtained from Nanostructured & Amorphous Materials, Inc. (Houston, TX, USA). The methanol used in our experiments was HPLC grade (Sigma-Aldrich). The other chemical reagents were of analytical grade and were used without further purification.

Synthesis of CNTs with sinapinic acid attached covalently (Fig. 1)

A sample of carboxylated CNTs (100 mg) was refluxed with 20 mL of thionyl chloride for 20 h. The excess thionyl chloride was then removed under reduced pressure and the resulting powder was dried in vacuum at 80 °C.

The obtained material was suspended in 20 mL of anhydrous tetrahydrofuran (THF) and 100 mg of sinapinic acid and 300 μL of triethylamine were added. The resulting mixture was stirred for 24 h. The final product (CNT-SA) was isolated by centrifugation, washed thoroughly with THF, then with methanol and dried at 80 °C.

Synthesis of CNTs with sinapinic acid attached as ionic macro-complex (Fig. 2)

A sample of carboxylated CNTs (150 mg) was refluxed with 25 mL of thionyl chloride for 20 h. The excess thionyl chloride was then removed under reduced pressure and the resulting powder was dried in vacuum at 80 °C.

The obtained material was suspended in 20 mL of anhydrous THF and 1 mL (large excess) of ethylenediamine was added. The mixture thus obtained was refluxed for 5 h. The resulting black powder was isolated by centrifugation, washed thoroughly with water, then with methanol and dried at 80 °C.

Of the obtained material 50 mg were sonicated in 30 mL of a sinapinic acid/methanol solution (2 mg mL^{-1}) for 30 min and the mixture was then stirred overnight. The resulting product ([CNT-NH_3^+][SA^-]) was isolated by centrifugation, washed three times with methanol and dried at 80 °C.

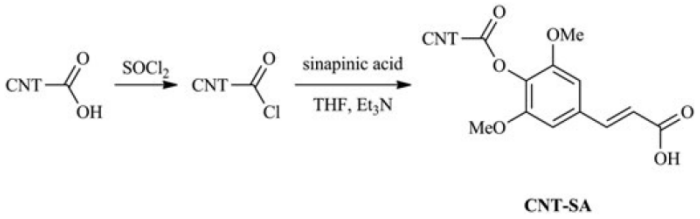

Figure 1. Synthetic route to CNT-SA material.

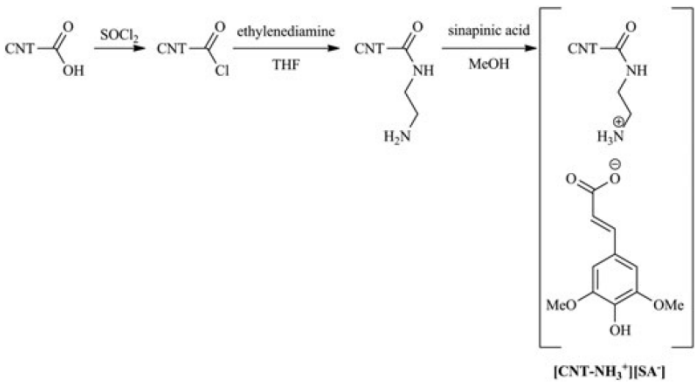

Figure 2. Synthetic route to [CNT-NH_3^+][SA^-] material.

LDIMS analysis

Each matrix obtained (2 mg) (CNT-SA and [CNT-NH_3^+][SA^-]) was suspended in 1 mL MeOH/H_2O (50:50 v/v) using ultrasonic dispersion for 10 min. About 0.7 μL of the obtained suspension was applied to a stainless steel target probe and 0.7 μL of the analyte solution (Brij® 52, Brij® 56 or poly(ethylene glycol) monomethyl ether methanolic solutions (10^{-3} M)) was pipetted on top of the CNT layer. If $KClO_4$ or $NaClO_4$ solutions were used, 0.7 μL of a 0.2 M water solution of the appropriate salt was applied on top of the CNT layer. Every drop applied to a target probe was allowed to dry at room temperature.

Instrumental conditions

The LDIQTOF mass spectra were obtained on a Q-TOF Premier mass spectrometer (software MassLynx version 4.1, Waters/Micromass Manchester, UK) with a 200 Hz repetition rate Nd/YAG laser (λ = 355 nm, power density 10^7 W/cm^2).

Infrared spectra were recorded on a IFS 66 s spectrometer (Bruker Polska Sp. z.o.o., Poznan, Poland), using KBr pellets (about 0.15 mg of sample in 200 mg of KBr).

RESULTS AND DISCUSSION

Synthesis of CNT-SA and [CNT-NH_3^+][SA^-] materials

Functionalization of CNTs with sinapinic acid was achieved in two different ways. One procedure involved the reaction of carboxylated CNTs with thionyl chloride, which produced CNTs containing acyl chloride functional groups. These reactive groups were subsequently reacted with sinapinic acid in order to produce ester bonds that covalently attached sinapinic acid to the CNT surface, yielding CNT-SA. Formation of the product was confirmed by FTIR analysis (Fig. 3). The band at 1730 cm^{-1} of the carboxylated CNTs is assigned to C=O stretching vibrations[25] and that at 1630 cm^{-1} to -COONa groups formed when the CNTs are rinsed with deionized water.[26] The CNT-SA FTIR spectra show the band at 1717 cm^{-1} which can be assigned to C=O stretching vibrations of the ester groups formed. Moreover, the lack of a strong band at 1630 cm^{-1} indicates that all the -COONa groups have undergone the reaction. Thus, the FTIR analysis indicates that the functionalization was successful.

The second procedure of functionalization involved the production of CNTs containing acyl chloride functional groups with the use of the same procedure. These groups were subsequently reacted with ethylenediamine in order to produce free amine groups attached to the surface of CNTs via amide bonding. After the reaction with sinapinic acid, the amine groups formed the sinapinic acid salt of the amine, a new ionic macro-complex [CNT-NH_3^+][SA^-]. Formation of the product was confirmed by FTIR analysis (Fig. 4). The band at 1654 cm^{-1} can be assigned to the C=O stretching vibrations of the amide groups formed. The almost complete disappearance of the band at 1730 cm^{-1}, that is present in the FTIR spectrum of carboxylated CNTs, indicates that most of the carboxylic groups reacted with ethylenediamine. Moreover, the appearance of weak bands at 1464 cm^{-1} and 1436 cm^{-1}, which are strong bands in the spectrum of pure sinapinic acid, indicates that sinapinic acid formed the expected ionic macro-complex.

LDIQTOF MS analysis of Brij® 52, Brij® 56 and poly(ethylene glycol) monomethyl ether using new assisting surfaces

A series of LDIQTOF mass spectra was obtained using Brij® 52, Brij® 56 and poly(ethylene glycol) monomethyl ether with the new assisting surfaces CNT-SA and [CNT-NH_3^+][SA^-]. Generally Na^+ and K^+ cations are present in the solvent used for the sample preparation for the LDI experiments. Consequently the LDITOF mass spectra show multiple adducts if no salt is added.[27] To avoid this problem and reduce complexity of the spectra, Na^+ or K^+ cations were applied in excess on the CNTs surface. With the concentration of salt being about 200 times higher than the concentration of the sample in solution before deposition, the oligomers were almost completely cationized by the appropriate cation. The mass of the ion formed from an oligomer can be described as the sum of the mass of the chain end plus the sum of *n* times the mass of ethoxy repeat unit plus the mass of the cation. The aim of the study was to determine the usefulness of each assisting surface with respect to enhancement of the intensity of the analyte signals and to reduce the chemical noise caused by CNTs impurities.

Figure 5 shows the mass spectra obtained using Brij® 52 in the LDI experiments with the two new assisting surfaces. Molecular masses can be calculated from the end group, cetyl

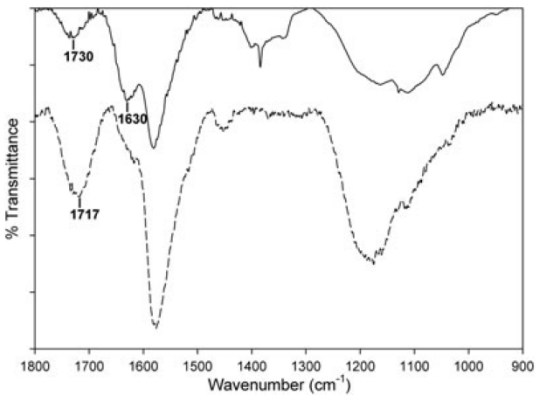

Figure 3. FTIR spectra of carboxylated CNTs (top) and CNT-SA (bottom).

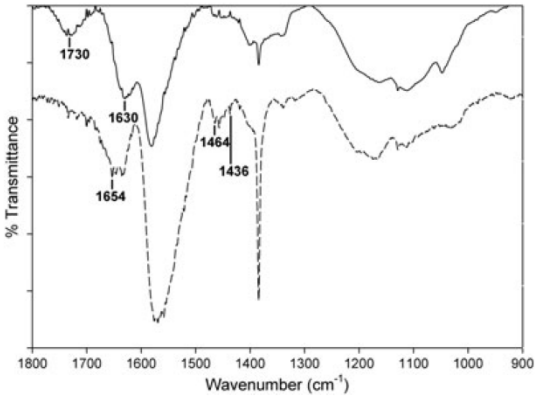

Figure 4. FTIR spectra of carboxylated CNTs (top) and [CNT-NH_3^+][SA^-] (bottom).

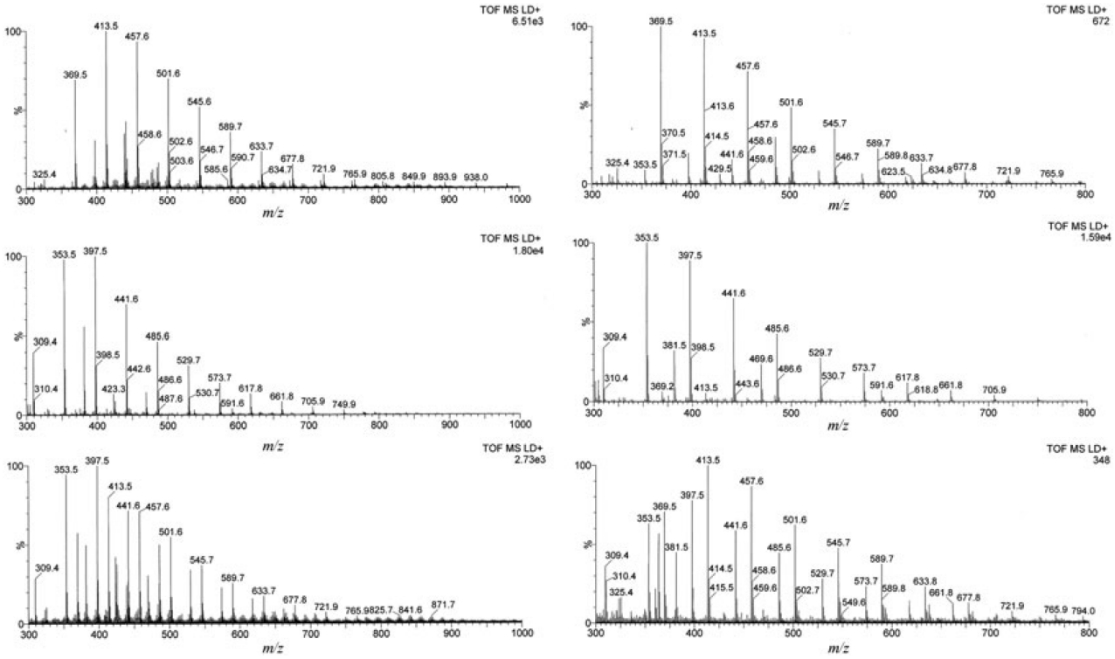

Figure 5. LDIQTOF mass spectra of 1 nmol/spot Brij® 52 recorded with CNT-SA- (left column) or [CNT-NH_3^+][SA^-]-assisting surface (right column) with excess of potassium (upper row) or sodium cation (middle row) or without addition of cations (bottom row).

alcohol ($m = 242$ u), plus $n \times 44$ u for the polyoxyethylene unit and mass of metal ion (23 u for sodium or 39 u for potassium). The spectrum of Brij® 52 when cationized with an excess of sodium cations had its most intense peak at m/z 397.5 ($n = 3$) and a distribution representing $n = 1$–11 for spectra obtained on both types of CNTs. When cationized with an excess of potassium cations the spectrum of Brij® 52 had its most intense peak at m/z 413.5 ($n = 3$) and a distribution representing $n = 2$–12 for spectra obtained on both types of CNTs. For spectra obtained without an excess of any cations the intensities of the corresponding sodiated or potassiated peaks were similar for both assisting surfaces. The main difference between our results and those obtained with previously published data available for the MALDI-TOF MS analysis of Brij® 52 is the narrower distribution of oligomers ($n = 2$–12 compared with $n = 3$–19 presented by Raith *et al.*[28]). The mass spectrum of Brij® 52 on the CNT-SA-assisting surface showed peaks of intensities higher than those in the spectrum recorded on the [CNT-NH_3^+][SA^-] surface regardless of the presence of an excess of sodium or potassium cations. However, the spectrum of Brij® 52 observed on the [CNT-NH_3^+][SA^-]-assisting surface had lower background matrix peaks and therefore a better signal-to-noise ratio.

Figure 6 shows the mass spectra obtained using Brij® 56 with the two new assisting surfaces. The masses of the ions obtained can be calculated in the same way as for Brij® 52 (cetyl alcohol, plus $n \times 44$ u for the polyoxyethylene unit and the mass of the appropriate metal ion). The spectrum of Brij® 56 when cationized with an excess of sodium cations on both types of CNTs had its most intense peak at m/z 617.7 ($n = 8$) and showed peaks representing $n = 3$–21. The spectrum of Brij® 56 cationized with an excess of potassium cations on both types of CNTs had its most intense peak at m/z 633.7 ($n = 8$) and showed peaks corresponding to $n = 3$–20. For spectra obtained without excess of any cations the intensities of the sodiated peaks were much greater than those of the potassiated ones for both assisting surfaces. Similarly to the spectra recorded for Brij® 52, the peaks in the mass spectra taken on the CNT-SA-assisting surface for Brij® 56 had higher intensities than those in the spectra obtained on [CNT-NH_3^+][SA^-]-assisting surface regardless of the presence of excess of sodium or potassium cations. The spectra obtained on the [CNT-NH_3^+][SA^-]-assisting surface had lower background matrix peaks.

Figure 7 shows the mass spectra obtained using poly(ethylene glycol) monomethyl ether with the two new assisting surfaces. The masses of the ions obtained can be calculated from the end group, the methyl alcohol ($m = 32$ u), plus $n \times 44$ u for the polyoxyethylene unit and the mass of the metal ion (23 u for sodium or 39 u for potassium). The spectrum of poly(ethylene glycol) monomethyl ether when cationized with an excess of sodium cations had its most intense peak at m/z 715.7 ($n = 15$) and showed peaks corresponding to $n = 10$–24 for spectra obtained on both types of CNTs. When cationized with an excess of potassium cations the spectrum of Brij® 52 had its most intense peak at m/z 731.6 ($n = 15$) and showed peaks corresponding to $n = 9$–24 for spectra obtained on both types of CNTs. For spectra obtained without an excess of any cations the intensities of sodiated peaks were greater than those of the potassiated ones for both assisting surfaces. Similarly to the spectra recorded for the other two analytes, the peaks in the mass spectra taken on the CNT-SA-assisting surface for poly (ethylene glycol) monomethyl ether had higher intensities than

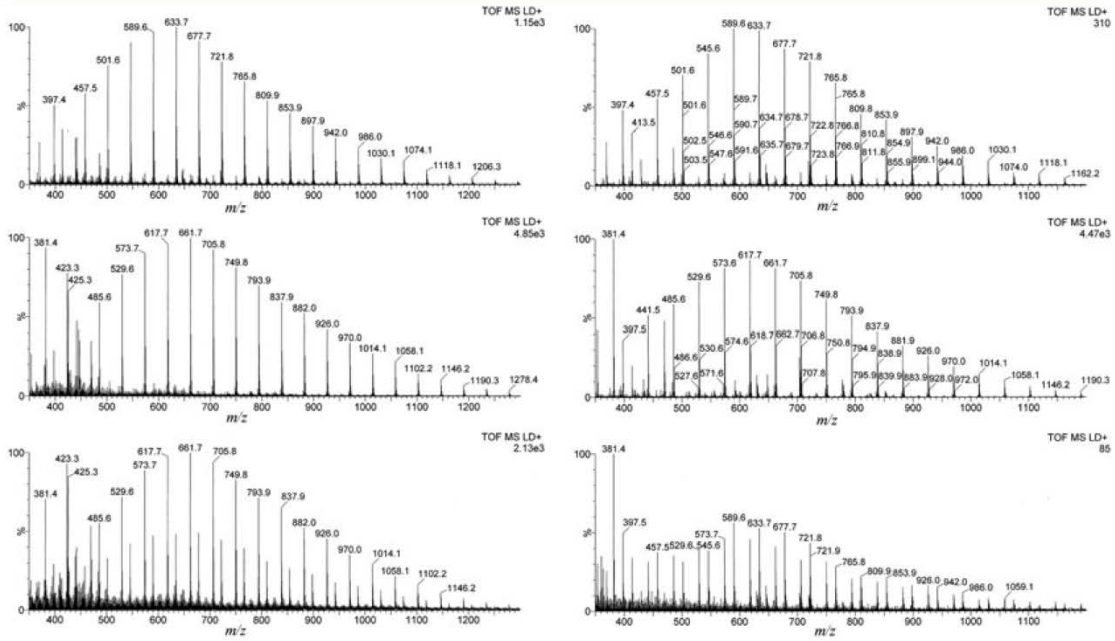

Figure 6. LDIQTOF mass spectra of 1 nmol/spot Brij® 56 recorded with CNT-SA- (left column) or [CNT-NH_3^+][SA^-]-assisting surface (right column) with excess of potassium (upper row) or sodium cation (middle row) or without addition of cations (bottom row).

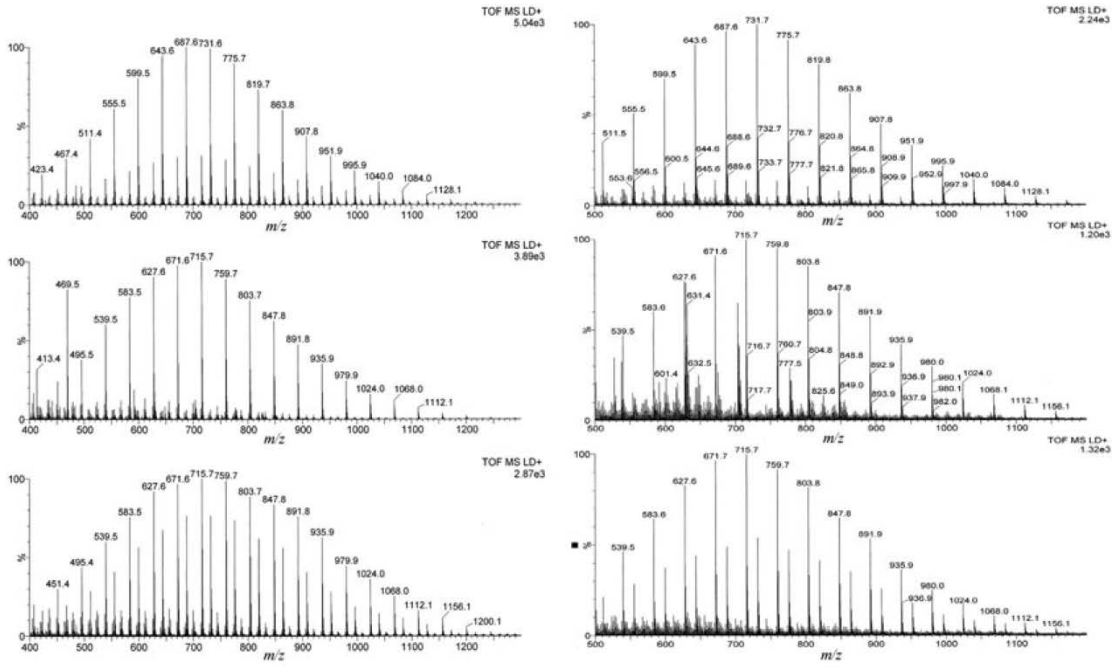

Figure 7. LDIQTOF mass spectra of 1 nmol/spot poly(ethylene glycol) monomethyl ether recorded with CNT-SA- (left column) or [CNT-NH_3^+][SA^-]-assisting surface (right column) with excess of potassium (upper row) or sodium cation (middle row) or without addition of cations (bottom row).

Table 1. Average molecular weights in number $(\bar{M}_n(g/mol))$ and in weight $(\bar{M}_w(g/mol))$, average degrees of polymerization $(\bar{DP}_n)$ and polydispersity indices (Ip) of the analytes studied determined by LDIQTOF with different assisting surfaces and excess of sodium cation. The intensity of peaks was assumed to be proportional to the concentration of the oligomers

Analyte	Assisting surface	$\bar{M}_n(g/mol)$	$\bar{M}_w(g/mol)$	$\bar{DP}_n$	Ip
Brij® 52	CNT-SA	436	451	9,9	1,03
Brij® 52	[CNT-NH_3^+][SA^-]	439	455	10,0	1,03
Brij® 56	CNT-SA	671	714	15,3	1,06
Brij® 56	[CNT-NH_3^+][SA^-]	698	741	15,9	1,06
poly(ethylene glycol) monomethyl ether	CNT-SA	723	753	16,4	1,04
poly(ethylene glycol) monomethyl ether	[CNT-NH_3^+][SA^-]	739	767	16,8	1,04

those observed in the spectra obtained on the [CNT-NH_3^+][SA^-]-assisting surface regardless of the presence of an excess of sodium or potassium cations. The spectra obtained on the [CNT-NH_3^+][SA^-]-assisting surface had lower background matrix peaks.

All the analytes formed sodiated and potassiated molecules so the presence of sodium and potassium cations in the LDI sample spot was required to obtain mass spectra of these compounds. The CNT-SA material has free carboxylic groups on its surface that can be donors of sodium and potassium cations, whereas the [CNT-NH_3^+][SA^-] material does not have groups of this kind. The fact that the spectra obtained on the CNT-SA-assisting surface had peaks of higher intensity can be attributed to the amount of sodium and potassium ions that are present at the surface of the material and the ability of the material to transfer these ions to the analyte. The observation that the spectra obtained on the [CNT-NH_3^+][SA^-] material had lower background matrix peaks can be attributed to the transfer of excess laser energy to the sinapinic acid that is bonded noncovalently. This process may cause breaking of the ionic bond and desorption of sinapinic acid but it also preserves the structure of the CNTs whose fragments are the main source of the unwanted background matrix peaks. Table 1 shows all the results of calculations obtained from the LDIQTOF mass spectra of the analytes when cationized with an excess of sodium cations on both types of assisting CNTs surfaces.

CONCLUSIONS

The LDIQTOF MS detection of polyether amphiphiles and poly(ethylene glycol) monomethyl ether is shown to be effective on two new assisting surfaces that are based on carbon nanotube derivatives. These materials were designed to have two different types of functionalization of CNTs with sinapinic acid: in the covalent and ionic macro-complex forms. These new assisting surfaces can be used for LDI analysis without any special preparation of the LDI target plate. Such assisting surfaces can be useful for the LDI-MS detection of other polyether amphiphiles that are used as nanocarriers of hydrophobic drugs.

Acknowledgements

Supported by the Polish Ministry of Science and Higher Education (Grant No. N 204 028636) in the years 2009–2012.

REFERENCES

[1] M. Karas, D. Bachmann, F. Hillenkamp. Influence of the wavelength in high-irradiance ultraviolet laser desorption mass spectrometry of organic molecules. *Anal. Chem.* **1985**, *57*, 2935.
[2] K. Tanaka, H. Waki, Y. Ido, S. Akita, Y. Yoshida, T. Yoshida, T. Matsuo. Protein and polymer analyses up to m/z 100 000 by laser ionization time-of-flight mass spectrometry. *Rapid Commun. Mass Spectrom.* **1988**, *2*, 151.
[3] J. Sunner, E. Dratz, Y.-C. Chen. Graphite surface-assisted laser desorption/ionization time-of-flight mass spectrometry of peptides and proteins from liquid solutions. *Anal. Chem.* **1995**, *67*, 4335.
[4] M. J. Dale, R. Knochenmuss, R. Zenobi. Graphite/liquid mixed matrices for laser desorption/ionization mass spectrometry. *Anal. Chem.* **1996**, *68*, 3321.
[5] K.-H. Park, H.-J. Kim. Analysis of fatty acids by graphite plate laser desorption/ionization time-of-flight mass spectrometry. *Rapid Commun. Mass Spectrom.* **2001**, *15*, 1494.
[6] Y. Coffinier, S. Szunerits, H. Drobecq, O. Melnyk, R. Boukherroub. Diamond nanowires for highly sensitive matrix-free mass spectrometry analysis of small molecules. *Nanoscale* **2012**, *4*, 231.
[7] Y.-C. Chen, M.-F. Tsai. Using surfactants to enhance the analyte signals in activated carbon, surface-assisted laser desorption/ionization (SALDI) mass spectrometry. *J. Mass Spectrom.* **2000**, *35*, 1278.
[8] J.-Y. Wu, Y.-C. Chen. A novel approach of combining thin-layer chromatography with surface-assisted laser desorption/ionization (SALDI) time-of-flight mass spectrometry. *J. Mass Spectrom.* **2002**, *37*, 85.
[9] J. Wei, J. M. Buriak, G. Siuzdak. Desorption-ionization mass spectrometry on porous silicon. *Nature* **1999**, *399*, 243.
[10] R. A. Kruse, X. Li, P. W. Bohn, J. V. Sweedler. Experimental factors controlling analyte ion generation in laser desorption/ionization mass spectrometry on porous silicon. *Anal. Chem.* **2001**, *73*, 3639.
[11] Z. Shen, J. J. Thomas, C. Averbuj, K. M. Broo, M. Engelhard, J. E. Crowell, M. G. Finn, G. Siuzdak. Porous silicon as a versatile platform for laser desorption/ionization mass spectrometry. *Anal. Chem.* **2000**, *73*, 612.
[12] J. D. Cuiffi, D. J. Hayes, S. J. Fonash, K. N. Brown, A. D. Jones. Desorption−ionization mass spectrometry using deposited nanostructured silicon films. *Anal. Chem.* **2001**, *73*, 1292.
[13] S. H. Bhattacharya, T. J. Raiford, K. K. Murray. Infrared Laser Desorption/Ionization on Silicon. *Anal. Chem.* **2002**, *74*, 2228.
[14] G. l. Piret, H. Drobecq, Y. Coffinier, O. Melnyk, R. Boukherroub. Matrix-free laser desorption/ionization mass spectrometry on silicon nanowire arrays prepared by chemical etching of crystalline silicon. *Langmuir* **2009**, *26*, 1354.

[15] G. l. Piret, R. m. Desmet, E. Diesis, H. Drobecq, J. r. Segers, C. Rouanet, A.-S. Debrie, R. Boukherroub, C. Locht, O. Melnyk. Chips from chips: Application to the study of antibody responses to methylated proteins. *J. Proteome Res.* **2010**, *9*, 6467.
[16] M. Dupré, Y. Coffinier, R. Boukherroub, S. Cantel, J. Martinez, C. Enjalbal. Laser desorption ionization mass spectrometry of protein tryptic digests on nanostructured silicon plates. *J. Proteomics* **2012**, *75*, 1973.
[17] P. Kraft, S. Alimpiev, E. Dratz, J. Sunner. Infrared, surface-assisted laser desorption ionization mass spectrometry on frozen aqueous solutions of proteins and peptides using suspensions of organic solids. *J. Am. Soc. Mass Spectrom.* **1998**, *9*, 912.
[18] S. Iijima. Helical microtubules of graphitic carbon. *Nature* **1991**, *354*, 56.
[19] P. M. Ajayan. Nanotubes from carbon. *Chem. Rev.* **1999**, *99*, 1787.
[20] S. Xu, Y. Li, H. Zou, J. Qiu, Z. Guo, B. Guo. Carbon nanotubes as assisted matrix for laser desorption/ionization time-of-flight mass spectrometry. *Anal. Chem.* **2003**, *75*, 6191.
[21] S.-f. Ren, Y.-l. Guo. Oxidized carbon nanotubes as matrix for matrix-assisted laser desorption/ionization time-of-flight mass spectrometric analysis of biomolecules. *Rapid Commun. Mass Spectrom.* **2005**, *19*, 255.
[22] C. Pan, S. Xu, L. Hu, X. Su, J. Ou, H. Zou, Z. Guo, Y. Zhang, B. Guo. Using oxidized carbon nanotubes as matrix for analysis of small molecules by MALDI-TOF MS. *J. Am. Soc. Mass Spectrom.* **2005**, *16*, 883.
[23] S.-f. Ren, Y.-l. Guo. Carbon nanotubes (2,5-dihydroxybenzoyl hydrazine) derivative as pH adjustable enriching reagent and matrix for MALDI analysis of trace peptides. *J. Am. Soc. Mass Spectrom.* **2006**, *17*, 1023.
[24] S. Gupta, R. Tyagi, V. S. Parmar, S. K. Sharma, R. Haag. Polyether based amphiphiles for delivery of active components. *Polymer* **2012**, *53*, 3053.
[25] A. Kuznetsova, D. B. Mawhinney, V. Naumenko, J. T. Yates, J. Liu, R. E. Smalley. Enhancement of adsorption inside of single-walled nanotubes: opening the entry ports. *Chem. Phys. Lett.* **2000**, *321*, 292.
[26] Q. Zhao, J. Qian, M. Zhu, Q. An. Facile fabrication of polyelectrolyte complex/carbon nanotube nanocomposites with improved mechanical properties and ultra-high separation performance. *J. Mater. Chem.* **2009**, *19*, 8732.
[27] G. Cheguillaume, W. Buchmann, B. Desmazières, J. Tortajada. Liquid chromatography-mass spectrometry hyphenation for exhaustive and unambiguous characterization of polyoxyethylene surfactants. *Chromatographia* **2004**, *60*, 561.
[28] K. Raith, C. E. H. Schmelzer, R. H. H. Neubert. Towards a molecular characterization of pharmaceutical excipients: Mass spectrometric studies of ethoxylated surfactants. *Int. J. Pharmaceut.* **2006**, *319*, 1.

Research Article

Rapid Communications in Mass Spectrometry

Received: 8 April 2013 Revised: 29 August 2013 Accepted: 2 September 2013 Published online in Wiley Online Library

Rapid Commun. Mass Spectrom. **2013**, *27*, 2631–2638
(wileyonlinelibrary.com) DOI: 10.1002/rcm.6728

Laser desorption/ionization mass spectrometric analysis of folic acid, vancomycin and Triton® X-100 on variously functionalized carbon nanotubes

Michał Cegłowski*, Szymon Jasiecki and Grzegorz Schroeder

Faculty of Chemistry, Adam Mickiewicz University in Poznan, Umultowska 89b, 61-614 Poznan, Poland

RATIONALE: Carbon nanotubes (CNTs) have been ascertained to constitute versatile assisting matrices for laser desorption/ionization mass spectrometric analysis of different molecules. The functionalization thereof can lead to obtaining laser desorption/ionization assisting surfaces that would allow the detection of molecules at lower concentration and produce spectra with a better signal-to-noise ratio.
METHODS: Pristine, -OH and -COOH functionalized multi-walled CNTs were obtained from commercial suppliers. Gallic or sinapinic acid was attached covalently to the CNT surfaces by forming an ester bond. Folic acid, vancomycin and Triton® X-100 were used as analytes to examine properties of these new assisting surfaces. Mass spectrometry analysis was conducted on a matrix-assisted laser desorption/ionization quadrupole time-of-flight (MALDIQTOF) mass spectrometer.
RESULTS: The functionalization of CNTs was confirmed with Fourier transform infrared (FTIR) spectroscopy. The obtained mass spectra revealed that all the assisting surfaces are capable of transferring energy to the analytes; moreover, the presence of carboxyl groups in the structures of CNTs highly enhances their ionization properties. Nevertheless, the presence of sinapinic acid on CNT surfaces does not increase their properties to absorb pulse laser energy.
CONCLUSIONS: The presented assisting surfaces are effective in LDI mass analysis of folic acid, vancomycin and Triton® X-100. The appropriate functionalization of CNTs can lead to the production of assisting surfaces that can become highly effective in the ionization of particular types of analytes. Copyright © 2013 John Wiley & Sons, Ltd.

The main drawback of the matrix-assisted laser desorption/ionization mass spectrometry (MALDI-MS)[1,2] technique constitutes the requirement of using an appropriate matrix such as sinapinic acid, 2,5-dihydroxybenzoic acid or α-cyano-4-hydroxycinnamic acid, since there is no universal matrix.[3] The matrix produces a gamut of its own signals that may interfere with the signals derived from the analyte molecules. Moreover, the matrix signals are principally present in the low-mass region of the spectra. Therefore, obtaining good spectra of small molecules by the MALDI technique poses a substantial challenge. In order to circumvent this problem different inorganic or organic materials such as graphite,[4] carbon powder,[5] activated carbon,[6] graphene,[7,8] porous silicon,[9,10] platinum,[11] TiO_2 nanoparticles,[12] nanostructured silicon plates,[13] biomineralized cell walls of microalgae,[14] 9-aminoacridine,[15–17] 1,5-naphthalene derivatives,[18] 1,8-bis (dimethylamino)naphthalene,[19] conductive polymers,[20] ionic liquids,[21,22] or *meso*-tetrakis(pentafluorophenyl)porphyrin[23–25] have been used as assisting surfaces or matrices for LDI mass analysis of different molecules.

Carbon nanotubes (CNTs)[26] have unique physical properties that have attracted scientists representing numerous fields of science. The possibility of modifying their structures prevailingly by oxidizing their sidewalls and then carrying out reactions on the resulting carboxylic groups makes them a material that has found a multitude of potential applications.[27] Xu *et al*. have used CNTs, prepared from coal by an arc discharge method, as assisted matrix for laser desorption/ionization time-of-flight (LDITOF) mass spectrometric analysis of peptides and β-cyclodextrin.[28] Chen *et al*. have used CNTs as an assisting matrix for MALDI analysis of peptides and small proteins. Moreover, citric acid treated CNTs were employed as affinity probes to selectively concentrate traces of analytes from aqueous solutions.[29] Ren and Guo have used CNTs oxidized by nitric acid as a matrix for MALDI analysis of oligosaccharides, peptides and insulin. The incorporation of carboxylic groups onto the surface of CNTs has provided a proton source and allowed a better dispersion of polar analytes, that led to a better shot-to-shot reproducibility.[30] Zhang, Wang and Guo have demonstrated that 20 common amino acids can be analyzed by MALDI-MS with CNTs as a matrix. The most intense peaks corresponded to sodium ion adducts and under optimal conditions only a few or no background peaks appeared in the low-mass region.[31] Ren *et al*. have used a type of polyurethane adhesive to immobilize CNTs on the target, to avoid their dissipating. A material prepared in this way was used as a matrix for MALDI-MS analysis of small carbohydrates.[32] Pan *et al*. have used oxidized CNTs for qualitative determination of small molecules and quantitative determination of jatrorrhizine and palmatine.[33] Quantitative analysis with the use of oxidized CNTs as a matrix for MALDI-MS has been applied to monitor enzyme activity and screen enzyme inhibitors by Hu *et al*.[34]

* *Correspondence to:* M. Cegłowski, Faculty of Chemistry, Adam Mickiewicz University in Poznan, Umultowska 89b, 61-614 Poznan, Poland.
E-mail: ceglowski.m@gmail.com

Ren and Guo have used CNTs functionalized with 2,5-dihydroxybenzoyl hydrazine as a pH-adjustable enriching agent and a matrix used in the MALDI-MS analysis of trace peptides.[35] Oxidized CNTs have been used as preconcentrating probes and assisting surfaces for the quantitative determination of cationic surfactants in water samples using atmospheric pressure MALDIMS by Shrivas and Wu.[36] Li *et al.* have demonstrated a successful use of magnetite/silica/oxidized CNTs composite as a magnetic solid-phase extraction sorbent and a matrix for the MALDIMS detection of benzo[*α*]pyrene. This composite material can be used to detect benzo[*α*]pyrene from organic solvents or aqueous solution.[37] Carroccio *et al.* have used MALDI-MS to discriminate between grafted or adsorbed functionalized molecules onto the surface of CNTs.[38] Our group have recently introduced CNTs functionalized with sinapinic acid, which is a conventional MALDI-MS matrix. The functionalization was achieved in two different ways: by producing a covalent bond or by forming an ionic macro-complex between the surface of the CNTs and sinapinic acid. The resulting materials proved successful as assisting surfaces for the LDI-MS detection of polyether amphiphiles.[39]

In this paper we analyze the influence of functionalization of CNTs on their usefulness as assisting surfaces for LDI mass analysis and compare it with sinapinic acid, a commonly used MALDI matrix. The absorption of laser energy by unmodified CNTs is excellent, but their ability to transfer it to the analyte is not that effective. Moreover, CNTs do not possess any groups that can be a source of protons; therefore, ionization of the analyte is also challenging. In order to examine the influence of functionalization of CNTs as assisting surfaces in LDI, mass analysis was studied for different groups introduced onto their surface, namely the CNTs unmodified, hydroxylated, carboxylated, with gallic or sinapinic acid attached covalently were examined. Hydroxylated CNTs have been chosen because there is no literature data as to whether the presence of hydroxyl groups exerts any impact on the properties of CNTs as LDI-assisting surfaces. From our previous study[39] we acknowledged that functionalization of CNTs with sinapinic acid grandly improves their usefulness in LDI experiments. However, it was not clear whether sinapinic acid is only a proton source or whether it helps to absorb pulse laser energy and subsequently transfers it to the analyte. In order to answer this question functionalization of CNTs with gallic acid, a compound that is not used as a MALDI matrix but has a similar acid dissociation constant to sinapinic acid, was carried out. The usefulness of every assisting surface was investigated with three chemically different substances that can be found in biological samples: folic acid, which has many functions in living organisms, for example it is needed to synthesize and repair DNA; vancomycin, an antibiotic which is used in treatment of infections caused by Gram-positive bacteria; Triton® X-100, which apart from being used as a surfactant in cleaning agents is also an ingredient of different types of vaccines.[40]

EXPERIMENTAL

Chemicals and materials

Folic acid, vancomycin hydrochloride, Triton® X-100, gallic acid and sinapinic acid were obtained from Sigma-Aldrich (St. Louis, MO, USA). CNTs (multi-walled nanotubes) with average diameter of 10–20 nm and average length 10–30 μm, denoted as CNT, hydroxylated CNTs (multi-walled nanotubes, -OH functionalized, >95% purity) with average diameter of 10–20 nm and average length 10–30 μm, denoted as CNT-OH, carboxylated CNTs (multi-walled nanotubes, -COOH functionalized, >95% purity) with average diameter of 10–20 nm and average length 10–30 μm, denoted as CNT-COOH, were obtained from Nanostructured & Amorphous Materials, Inc. (Houston, TX, USA). Methanol used in our experiments was HPLC grade (Sigma-Aldrich). The other chemical reagents were of analytical grade and were used without further purification.

Synthesis of CNTs with gallic acid attached covalently

A sample of CNT-COOH (100 mg) was refluxed with 20 mL of thionyl chloride for 20 h. Subsequently, thionyl chloride was removed under reduced pressure and the resulting powder was dried in vacuum at 80 °C.

The obtained material was suspended in 20 mL of anhydrous tetrahydrofuran (THF) and 100 mg of gallic acid and 300 μL of triethylamine were added; the resulting mixture was then stirred for 24 h. The final product (CNT-GA) was isolated by centrifugation, washed thoroughly with THF, then with methanol and dried at 80 °C. The synthetic scheme is presented in Fig. 1.

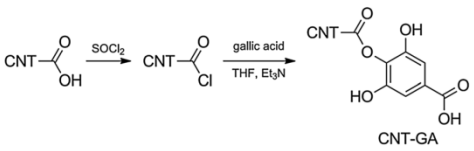

Figure 1. Synthetic route to CNT-GA material.

Synthesis of CNTs with sinapinic acid attached covalently

A sample of CNT-COOH (100 mg) was refluxed with 20 mL of thionyl chloride for 20 h. Thereupon, thionyl chloride was removed under reduced pressure and the resulting powder was dried in vacuum at 80 °C.

The obtained material was suspended in 20 mL of anhydrous THF and 100 mg of sinapinic acid and 300 μL of triethylamine were added; the resulting mixture was then stirred for 24 h. The final product (CNT-SA) was isolated by centrifugation, washed thoroughly with THF, then with methanol and dried at 80 °C. The synthetic scheme is presented in Fig. 2.

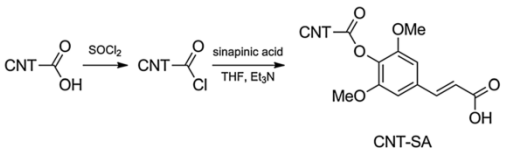

Figure 2. Synthetic route to CNT-SA material.

LDI-MS analysis

A sample of 2 mg of each material obtained (CNT, CNT-OH, CNT-COOH, CNT-GA and CNT-SA) was suspended in 1 mL MeOH/H_2O (50:50, v/v) using ultrasonic dispersion for 10 min. About 0.7 µL of the so-obtained suspension was applied to a stainless steel target probe, then 0.7 µL of the analyte solution (folic acid alkaline water solution (10^{-3} M), vancomycin hydrochloride water solution (10^{-3} M) and Triton® X-100 methanolic solution (10^{-3} M)) was pipetted on top of the layer of CNTs (crystals of analytes were not visible on the layers). Similarly, 0.7 µL of a saturated solution of sinapinic acid (water/acetonitrile/trifluoroacetic acid 70:30:0.3) was applied to a stainless steel target probe and then 0.7 µL of the appropriate analyte solution was pipetted on top of the matrix. Every drop applied to a target probe was allowed to dry at room temperature.

Instrumental conditions

The LDIQTOF mass spectra were obtained on a Waters/Micromass (Manchester, UK) Q-TOF Premier mass spectrometer in positive ion mode. Desorption/ionization was obtained by using a 355 Nd/YAG laser (200 Hz repetition rate, power density 10^7 W/cm^2) with a 4 ns pulse width. Available acceleration potential was in the range of ±20 kV. The spectra shown represent the sum of 100 laser shots and are the average of 10 spectra recorded (all spectra were almost identical). Because CNTs form a inhomogeneous layer on a stainless steel target probe, 'sweet spots' were used to generate mass spectra. Examination and processing of mass spectra data were performed using MassLynx 4.1 software (Waters/Micromass).

Infrared spectra were recorded on an IFS 66 s spectrometer (Bruker, Karlsruhe, Germany), using KBr pellets (about 0.15 mg of sample in 200 mg of KBr).

Transmission electron microscope (TEM) images were recorded using a FEI Tecnai G^2 20 X-TWIN (Hillsboro, OR, USA) electron microscope with a point resolution of 0.25 nm operating at 200 kV.

RESULTS AND DISCUSSION

Synthesis of CNT-GA and CNT-SA materials

The functionalization of CNT-COOH with gallic and sinapinic acid was achieved in a similar way. CNT-COOH were reacted with thionyl chloride to produce CNTs containing acyl chloride functional groups. These groups were subsequently reacted with gallic or sinapinic acid in order to produce ester bonds that covalently attached gallic or sinapinic acid to the surface of the CNTs, yielding CNT-GA or CNT-SA, respectively. The isolated products were analyzed by FTIR analysis (Figs. 3 and 4). The band at 1733 cm^{-1} is assigned to C=O stretching vibrations of CNT-COOH,[41] whereas the band at 1630 cm^{-1} is appropriated to –COONa groups that are formed while CNTs are rinsed with water that contains still small amounts of sodium ions.[42] The band at 1384 cm^{-1} is assigned to the carboxylic –O-H bending vibrations.[43] FTIR spectra of CNT-GA show the band at 1731 cm^{-1} which can be assigned to the C=O stretching vibrations of ester groups formed, whereas the spectra of CNT-SA show this band at 1717 cm^{-1}. Moreover, lack of strong

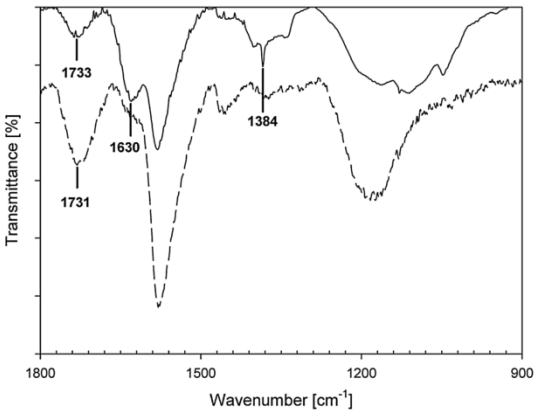

Figure 3. FTIR spectra of CNT-COOH (top) and CNT-GA (bottom).

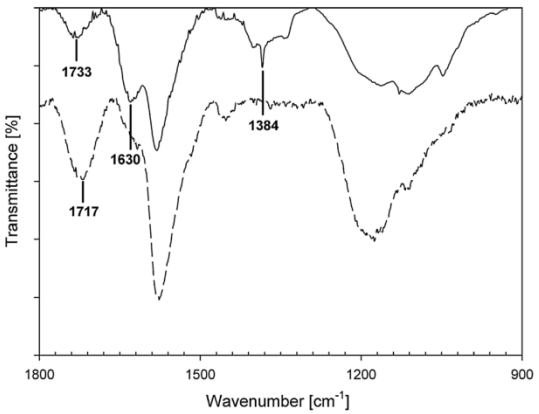

Figure 4. FTIR spectra of CNT-COOH (top) and CNT-SA (bottom).

bands at 1630 cm^{-1} and 1384 cm^{-1} indicated that almost all the carboxylic groups from the CNT-COOH surface had undergone the desired reaction.

TEM images of functionalized CNTs are mostly identical for all materials obtained. The functionalization with gallic and sinapinic acid is based on the reaction with sidewall defects introduced by the oxidation process. Nevertheless, the functionalization with these compounds does not introduce any defects beyond those already present in the structure of the CNTs. The sample TEM images of CNT-SA material are presented in Fig. 5. All examined CNTs were multi-walled carbon nanotubes of high purity with a hollow internal channel. The length and diameter of these materials were not influenced by the functionalization process.

LDIQTOF MS analysis of folic acid, vancomycin and Triton® X-100 using CNTs and CNT derivatives as assisting surfaces

LDIQTOF mass spectra of vancomycin, folic acid and Triton® X-100 were obtained on CNT, CNT-OH, CNT-COOH, CNT-GA and CNT-SA as assisting surfaces. The presented LDIQTOF

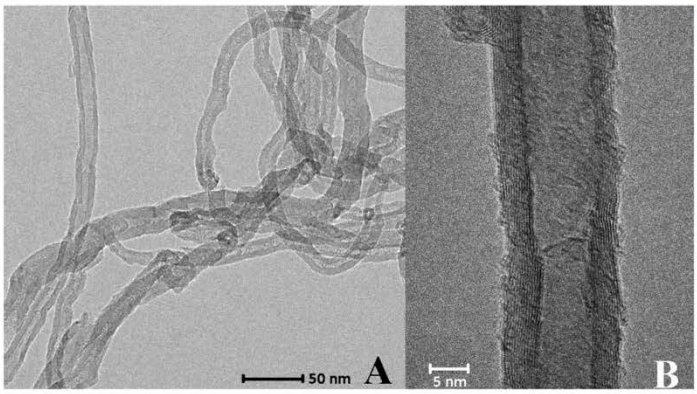

Figure 5. TEM images of CNT-SA material: (A) a bundle of CNT-SA and (B) high-resolution image of CNT-SA.

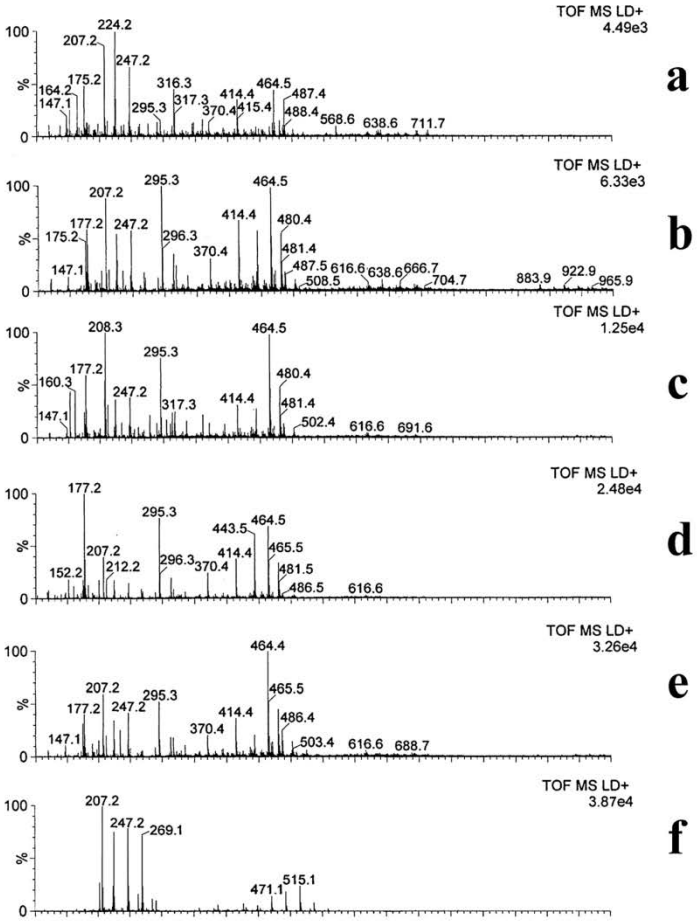

Figure 6. LDIQTOF mass spectra of 0.7 nmol/spot folic acid recorded with CNT (a), CNT-OH (b), CNT-COOH (c), CNT-GA (d), CNT-SA (e), and sinapinic acid (f).

mass spectra obtained usually show signals originating from sodiated or potassiated analyte molecules because of the presence of Na^+ and K^+ cations in solvents used for the sample preparation. The aim of the study was to identify the differences between assisting surfaces produced and to evaluate the usefulness of each assisting surface for enhancement of an intensity of the analyte signals.

Figure 6 shows the mass spectra of folic acid recorded with the use of CNTs and CNT derivatives as assisting surfaces. All spectra, apart from other signals, present a peak observed at *m/z* 464.5, which corresponds to $[M+Na]^+$. This result is in accordance with literature data presented by Cha and Kim, who have obtained a MALDI mass spectrum of folic acid with *α*-cyano-4-hydroxycinnamic acid as matrix.[44] All LDIQTOF spectra obtained have high absolute intensities, but the spectra obtained on CNT and CNT-OH have about one order of magnitude worse analyte intensities than those obtained on CNT-COOH, CNT-GA and CNT-SA as assisting surfaces. Furthermore, the spectrum recorded on CNT-SA as an assisting surface represents the best signal-to-noise (S/N) ratio from among the other spectra obtained. In contrast, the spectra of folic acid recorded with sinapinic acid as a matrix do not show any signal that can be assigned to folic acid (Fig. 6). All major peaks can be attributed to sinapinic acid (SA): $[SA–H_2O+H]^+$ *m/z* 207.2, $[SA+Na]^+$ *m/z* 247.2, $[SA–H+2Na]^+$ *m/z* 269.1, $[2SA+Na]^+$ *m/z* 471.1, $[2SA–H+2Na]^+$ *m/z* 493.1, $[2SA–2H+3Na]^+$ *m/z* 515.1. This clearly indicates that assisting surfaces based on functionalized CNTs are more useful in LDI analysis of low molecular compounds such as folic acid.

Figure 7 shows the mass spectra of vancomycin in the LDI experiments on CNTs and CNT derivatives as assisting surfaces. All the spectra show peaks at *m/z* 1473.4 corresponding to $[M+Na]^+$, *m/z* 1306.2 corresponding to the loss of an aminocarbohydrate group $[M–C_7H_{15}NO_2+H]^+$ and *m/z* 1166.1 corresponding to the loss of two carbohydrate

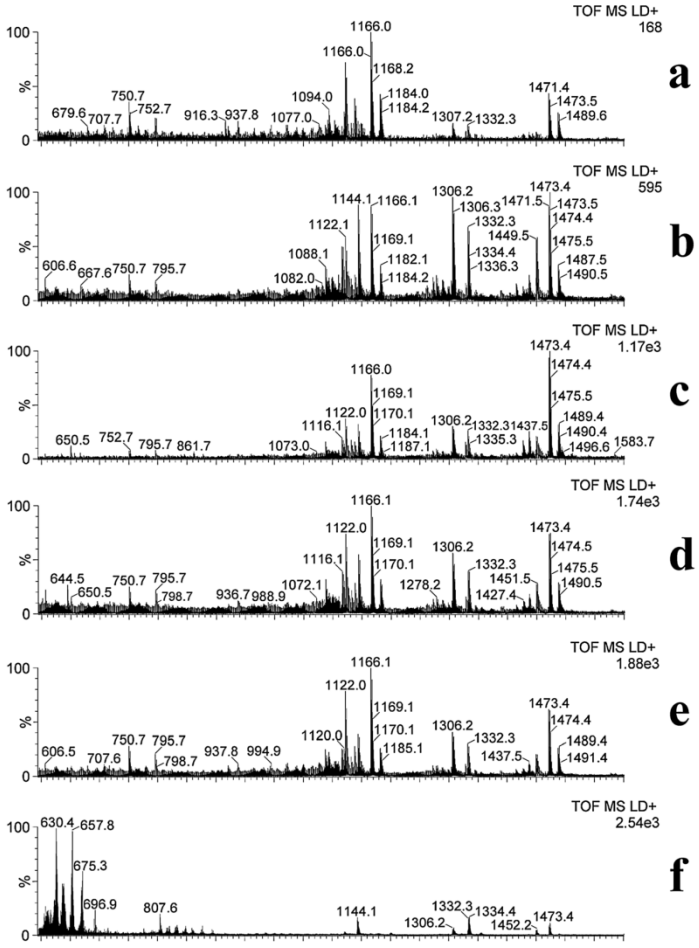

Figure 7. LDIQTOF mass spectra of 0.7 nmol/spot vancomycin recorded with CNT (a), CNT-OH (b), CNT-COOH (c), CNT-GA (d), CNT-SA (e), and sinapinic acid (f)

units $[M–C_{13}H_{25}NO_7 + Na]^+$. The LDIQTOF spectra obtained on CNT and CNT-OH again have about one order of magnitude worse analyte intensities than those obtained on CNT-COOH, CNT-GA and CNT-SA as assisting surfaces. From all vancomycin spectra, the spectrum obtained on CNT-COOH has the best S/N ratio and additionally it has the highest relative intensity of $[M + Na]^+$ signal. The spectrum recorded with sinapinic acid as a matrix shows peaks at *m/z* 1473.4 and 1306.2 (Fig. 7). In the presented mass range the intensities of those signals are fairly low, but the overall spectra intensity is greater than that of the spectra obtained with CNTs as assisting surfaces. This indicates that the effectiveness of functionalized CNTs in LDI analysis of vancomycin is similar to that of the commonly used MALDI matrices.

Figure 8 shows the mass spectra of Triton® X-100 recorded with CNTs and CNT derivatives as assisting surfaces. Molecular masses can be calculated from the end group 4-*tert*-octylphenol (m = 206 u), plus $n \times 44$ u for the polyoxyethylene unit and the mass of metal ion (23 u for sodium or 39 u for potassium). All Triton® X-100 spectra present sodiated and potassiated peaks, yet the signals originating from sodiated molecules have higher intensities. The peaks form into a bell-shaped curve, which is common typical for polymeric substances and is related to a wide distribution of molecular weights. The results are in accordance with the data presented by Raith, Schmelzer and Neubert, who obtained the MALDI mass spectrum of Triton® X-100 with *α*-cyano-4-hydroxycinnamic acid as a matrix.[45] Similarly to other analytes, the spectra obtained on CNT and CNT-OH have notably worse analyte intensities than those recorded with the use of other assisting surfaces. The spectrum obtained on CNT-GA as an assisting surface has the best S/N ratio. In contrast, the spectra of Triton® X-100 recorded with sinapinic acid as a matrix show only a few signals that can be assigned to the analyte. No

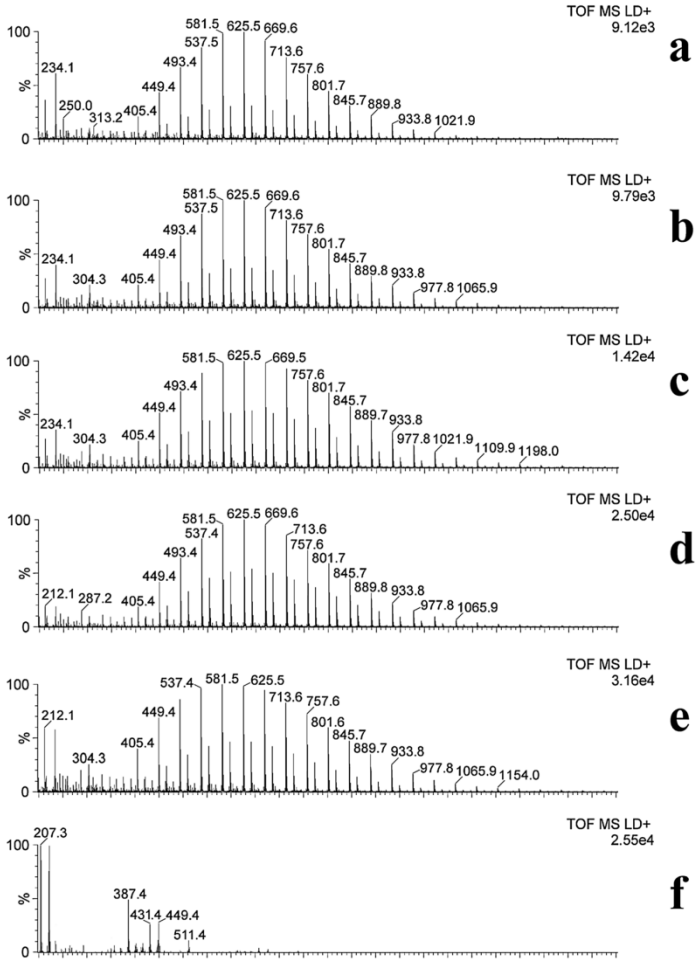

Figure 8. LDIQTOF mass spectra of 0.7 nmol/spot Triton® X-100 recorded with CNT (a), CNT-OH (b), CNT-COOH (c), CNT-GA (d), CNT-SA (e), and sinapinic acid (f).

characteristic bell-shaped distribution of molecular weights related to the polymeric structure of Triton® X-100 can be observed. This observation indicates that functionalized CNTs are more effective in LDI analysis of Triton® X-100 and similar compounds than the commonly used MALDI matrices.

All presented assisting surfaces were able to efficiently absorb and transfer pulse laser energy to the analyte and therefore to obtain the LDI mass spectra, which is related to their similar, overall structure. Nevertheless, the spectra of all analytes obtained on CNT and CNT-OH have worse intensities than the spectra recorded on the other CNT derivatives as assisting surfaces. Except the groups that appear in the defect sites, CNT does not have any functional groups that can be a proton or alkali ion source. CNT-OH has hydroxyl groups, but their efficiency in being a proton source is not very high. Moreover, hydroxyl groups are not very effective in binding sodium or potassium ions from a solution; therefore, their ability to generate sodiated or potassiated analyte molecules also proves not efficient enough. In contrast to these two materials, CNT-COOH, CNT-GA and CNT-SA possess carboxylic groups on their surfaces. These groups are very efficient in being a proton source and can bind sodium and potassium ions from solution, and subsequently transfer them to the analytes during LDI experiments. Therefore, CNT-COOH, CNT-GA and CNT-SA assisting surfaces produce spectra with higher intensities of analyte peaks than CNT and CNT-OH materials. The similar intensities of spectra produced with CNT-GA and CNT-SA indicate that binding sinapinic acid to the surface of CNTs does not affect the properties of CNTs to absorb pulse laser energy, but only introduces carboxylic groups onto their surface. The S/N ratio of CNT-COOH, CNT-GA and CNT-SA varies depending on the analyte used and is probably related to both the structure of the analyte and an assisting surface. In order to obtain the best result, it is necessary to choose the most suitable assisting surface to a specific analyte.

To be able to compare the effectiveness of functionalized CTNs and sinapinic acid as matrices, the concentration of deposited analyte solution must remain constant. The lack of signals coming from folic acid and low number of signals coming from Triton® X-100 can be attributed to the high ratio of sinapinic acid to the analyte. The signals of sinapinic acid dominate in the low-mass region so the analyte signals are buried among them. In contrast, functionalized CNTs produce only a few signals in the low-mass region; therefore, the amount of the analyte that has to be applied on them in LDI experiments is much lower than on sinapinic acid. Moreover, higher signals of Triton® X-100 in LDI experiments with functionalized CNTs as assisting surfaces can be attributed to well-known interactions between CNTs and surfactants.[46,47] Triton® X-100 molecules wrap around CNTs,[48,49] which allows effective transfer of the energy from CNTs to the analyte in the laser desorption process.

CONCLUSIONS

Carbon nanotubes and functionalized carbon nanotubes have been proven to be effective assisting surfaces in LDIQTOF mass analysis of vancomycin, folic acid and Triton® X-100. Due to the presence of carboxylic groups, CNT-COOH, CNT-GA and CNT-SA materials appeared to be more efficient in ionization of analyte molecules. The choice of an appropriate assisting surface to a designated analyte allows an increase in the signal-to-noise ratio. These assisting surfaces have proven to be more effective in LDIQTOF mass analysis of folic acid and Triton® X-100 than sinapinic acid, a commonly used MALDI matrix. The materials obtained can be used for LDI analysis without any special preparation of LDI plates and can be useful in the detection of other bioactive molecules.

Acknowledgement

Supported by the Ministry of Science and Higher Education (Grant No. 2011/03/B/ST5/01573) in the years 2012–2015.

REFERENCES

[1] M. Karas, D. Bachmann, F. Hillenkamp. *Anal. Chem.* **1985**, *57*, 2935.
[2] K. Tanaka, H. Waki, Y. Ido, S. Akita, Y. Yoshida, T. Yoshida, T. Matsuo. *Rapid Commun. Mass Spectrom.* **1988**, *2*, 151.
[3] S. M. A. B. Batoy, E. Akhmetova, S. Miladinovic, J. Smeal, C. L. Wilkins. *Appl. Spectrosc. Rev.* **2008**, *43*, 485.
[4] K.-H. Park, H.-J. Kim. *Rapid Commun. Mass Spectrom.* **2001**, *15*, 1494.
[5] J.-Y. Wu, Y.-C. Chen. *J. Mass Spectrom.* **2002**, *37*, 85.
[6] Y.-C. Chen, M.-F. Tsai. *J. Mass Spectrom.* **2000**, *35*, 1278.
[7] X. Dong, J. Cheng, J. Li, Y. Wang. *Anal. Chem.* **2010**, *82*, 6208.
[8] Y. Liu, J. Liu, C. Deng, X. Zhang. *Rapid Commun. Mass Spectrom.* **2011**, *25*, 3223.
[9] J. Wei, J. M. Buriak, G. Siuzdak. *Nature* **1999**, *399*, 243.
[10] S. Okuno, M. Nakano, G.-e. Matsubayashi, R. Arakawa, Y. Wada. *Rapid Commun. Mass Spectrom.* **2004**, *18*, 2811.
[11] H. Kawasaki, T. Ozawa, H. Hisatomi, R. Arakawa. *Rapid Commun. Mass Spectrom.* **2012**, *26*, 1849.
[12] M. Radisavljević, T. Kamčeva, I. Vukićević, M. Radoičić, Z. Šaponjić, M. Petković. *Rapid Commun. Mass Spectrom.* **2012**, *26*, 2041.
[13] M. Dupré, Y. Coffinier, R. Boukherroub, S. Cantel, J. Martinez, C. Enjalbal. *J. Proteomics* **2012**, *75*, 1973.
[14] T. Jaschinski, A. Svatoš, G. Pohnert. *Rapid Commun. Mass Spectrom.* **2013**, *27*, 109.
[15] R. Shroff, A. Muck, A. Svatoš. *Rapid Commun. Mass Spectrom.* **2007**, *21*, 3295.
[16] S. Vaidyanathan, R. Goodacre. *Rapid Commun. Mass Spectrom.* **2007**, *21*, 2072.
[17] M. Eibisch, J. Schiller. *Rapid Commun. Mass Spectrom.* **2011**, *25*, 1100.
[18] I. Osaka, M. Sakai, M. Takayama. *Rapid Commun. Mass Spectrom.* **2013**, *27*, 103.
[19] C. D. Calvano, C. G. Zambonin, F. Palmisano. *Rapid Commun. Mass Spectrom.* **2011**, *25*, 1757.
[20] L. J. Soltzberg, P. Patel. *Rapid Commun. Mass Spectrom.* **2004**, *18*, 1455.
[21] M. Zabet-Moghaddam, E. Heinzle, A. Tholey. *Rapid Commun. Mass Spectrom.* **2004**, *18*, 141.
[22] C. A. Serrano, Y. Zhang, J. Yang, K. A. Schug. *Rapid Commun. Mass Spectrom.* **2011**, *25*, 1152.
[23] F. O. Ayorinde, P. Hambright, T. N. Porter, Q. L. Keith. *Rapid Commun. Mass Spectrom.* **1999**, *13*, 2474.
[24] F. O. Ayorinde, K. Garvin, K. Saeed. *Rapid Commun. Mass Spectrom.* **2000**, *14*, 608.
[25] F. O. Ayorinde, D. Z. Bezabeh, I. G. Delves. *Rapid Commun. Mass Spectrom.* **2003**, *17*, 1735.
[26] S. Iijima. *Nature* **1991**, *354*, 56.
[27] P. M. Ajayan. *Chem. Rev. (Washington, DC, U. S.)* **1999**, *99*, 1787.

[28] S. Xu, Y. Li, H. Zou, J. Qiu, Z. Guo, B. Guo. *Anal. Chem.* **2003**, *75*, 6191.
[29] W.-Y. Chen, L.-S. Wang, H.-T. Chiu, Y.-C. Chen, C.-Y. Lee. *J. Am. Soc. Mass Spectrom.* **2004**, *15*, 1629.
[30] S.-f. Ren, Y.-l. Guo. *Rapid Commun. Mass Spectrom.* **2005**, *19*, 255.
[31] Z. Jing, W. Hao-Yang, G. Yin-Long. *Chin. J. Chem.* **2005**, *23*, 185.
[32] S.-f. Ren, L. Zhang, Z.-h. Cheng, Y.-l. Guo. *J. Am. Soc. Mass Spectrom.* **2005**, *16*, 333.
[33] C. Pan, S. Xu, L. Hu, X. Su, J. Ou, H. Zou, Z. Guo, Y. Zhang, B. Guo. *J. Am. Soc. Mass Spectrom.* **2005**, *16*, 883.
[34] L. Hu, G. Jiang, S. Xu, C. Pan, H. Zou. *J. Am. Soc. Mass Spectrom.* **2006**, *17*, 1616.
[35] S.-f. Ren, Y.-l. Guo. *J. Am. Soc. Mass Spectrom.* **2006**, *17*, 1023.
[36] K. Shrivas, H.-F. Wu. *Anal. Chim. Acta* **2008**, *628*, 198.
[37] X.-S. Li, J.-H. Wu, L.-D. Xu, Q. Zhao, Y.-B. Luo, B.-F. Yuan, Y.-Q. Feng. *Chem. Commun. (Cambridge, U. K.)* **2011**, *47*, 9816.
[38] S. C. Carroccio, G. Curcuruto, N. Tz. Dintcheva, C. Gambarotti, S. Coiai, G. Filippone. *Rapid Commun. Mass Spectrom.* **2013**, *27*, 1359.
[39] M. Cegłowski, G. Schroeder. *Rapid Commun. Mass Spectrom.* **2013**, *27*, 258.
[40] R. C. Seid Jr, J. L. Look, C. Ruiz, V. Frolov, D. Flyer, J. Schafer, L. Ellingsworth. *Vaccine* **2012**, *30*, 4349.
[41] A. Kuznetsova, D. B. Mawhinney, V. Naumenko, J. T. Yates, J. Liu, R. E. Smalley. *Chem. Phys. Lett.* **2000**, *321*, 292.
[42] Q. Zhao, J. Qian, M. Zhu, Q. An. *J. Mater. Chem.* **2009**, *19*, 8732.
[43] S. B. Dibyendu, *et al.*, *Smart Materials and Structures* **2004**, *13*, 1263.
[44] S. Cha, H.-J. Kim. *Bull. Korean Chem. Soc.* **2003**, *24*, 1308.
[45] K. Raith, C. E. H. Schmelzer, R. H. H. Neubert. *Int. J. Pharm.* **2006**, *319*, 1.
[46] V. A. Gigiberiya, I. A. Ar'ev, N. I. Lebovka. *Colloid J.* **2012**, *74*, 663.
[47] Y. Dong, R. Wang, S. Li, H. Yang, M. Du, Y. Fu. *J. Colloid Interface Sci.* **2013**, *391*, 8.
[48] M. Calvaresi, M. Dallavalle, F. Zerbetto. *Small* **2009**, *5*, 2191.
[49] N. R. Tummala, A. Striolo. *ACS Nano* **2009**, *3*, 595.

Journal of Applied Polymer Science

Poly(methyl vinyl ether-*alt*-maleic anhydride) Functionalized with 3-Aminophenylboronic Acid: A New Boronic Acid Polymer for Sensing Diols in Neutral Water

Michał Cegłowski, Błażej Gierczyk, Grzegorz Schroeder
Department of Supramolecular Chemistry, Faculty of Chemistry, Adam Mickiewicz University in Poznan, Umultowska 89b, 61-614, Poznań, Poland
Correspondence to: M. Cegłowski (E-mail: ceglowski.m@gmail.com)

ABSTRACT: Amidation of poly(methyl vinyl ether-*alt*-maleic anhydride) with 3-aminophenylboronic acid was used to prepare a new boronic acid polymer. The binding of catechol dye, Alizarin Red S to the polymer obtained resulted in getting a stable, colored sensor which was used to establish association constants with different diols in competitive assay. The binding of different diols was readily detected by color change and absorbance values measured at 450 nm were used to calculate the association constants. The polymer obtained formed high-affinity complexes with ribonucleosides, particularly cytidine and uridine. © 2014 Wiley Periodicals, Inc. J. Appl. Polym. Sci. **2014**, *131*, 40778.

KEYWORDS: functionalization of polymers; molecular recognition; sensors and actuators

Received 31 October 2013; accepted 27 March 2014
DOI: 10.1002/app.40778

INTRODUCTION

Boronic acids are well known to form complexes with diol-containing compounds through reversible ester formation. The high-affinity interaction between these molecules has been extensively investigated by many researches[1–6] and resulted in application of boronic acids as sensors for saccharides,[7,8] carbohydrate transporters,[9,10] and for separation of carbohydrates and glycoproteins.[11,12] Nevertheless, to understand the properties and stability of boronate ester formed, a method is needed for measurements of association constants of complexes between diols and boronic acid. The easiest and most versatile method is to measure changes in fluorescence or absorption spectra during titration experiments. This method is however limited only to boronic acids that are fluorescent or possess a chromophoric group which is sensitive to binding process. Springsteen and Wang[1,13] have developed a method which allows determination of binding constants even if the boronic acid is not fluorescent or does not contain an appropriate chromophoric group. They have proposed a system consisting of a three-component competitive assay, containing boronic acid, diol compound and Alizarin Red S (ARS) which is anthraquinone dye changing color in response to formation of high-affinity complexes with boronic acids.

Boronic acid polymers have found many applications in medicine, particularly in drug delivery[14–19] and sensing of biologically relevant compounds.[20,21] The main benefits of boronic acid polymers are connected with their increased activity caused by multivalency and the possibility to control drug release by using targeted biodistribution.[22] Moreover, polymers due to their macromolecular structure have increased circulation time in body because their large size slows down the glomerular filtration.[23] In comparison to small molecules they are not as readily detected by mononuclear phagocyte system, which also increases their circulation time.[24] Boronic acid polymers have found application in detection of biologically relevant compounds such as dopamine,[25] glucose,[26–28] diols,[29] ATP,[30] or nucleotides.[31] They also appeared useful in carbohydrate and glycoconjugate purification and identification,[32] preparation of materials of high mechanical[33] and thermal[34–36] stability, synthesis of polyurethane foams[37] and field-flow fractionation/adhesion chromatography.[38]

Saccharide sensing using boronic acid polymers is based on changes in optical or conductivity properties taking place upon binding with a carbohydrate molecule. Optical changes resulting in color shift are especially relevant, because they offer immediate response without need to use any additional apparatus. These polymers are of much interest and numerous examples have been reported in recent studies. Films composed of copolymers of aniline and 3-aminophenylboronic acid have been reported to undergo hypsochromic shift of absorption maximum on addition of saccharides.[39] Translucent boronic acid-carrying nanolatexes with bonded ARS[40] and copolymers with boronic acid residues[41] have been used for selective visual detection of fructose. ARS have been coupled with thermoresponsive

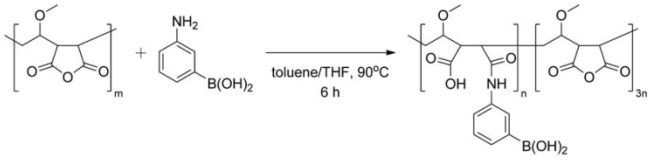

Figure 1. Synthesis of poly(MVE-*alt*-MA-BA).

copolymer[29] or boronic acid terminated polylactide[42] to obtains sensor for the recognition of hydroxyl-containing molecules. Boronic acid-appended azobenzene dye attached to poly(ethyleneimine) showed a significant change in the UV-Vis absorption spectra upon addition of glucose.[43] A porous hydrogel film incorporated with ARS have been used to monitor concentration of glucose in the range from 0.1 to 1 m*M*.[26]

In this article we report the synthesis of new boronic acid polymer and its application in sensing diols in water solutions. The polymer was synthesized by grafting 3-aminophenylboronic acid onto poly(methyl vinyl ether-*alt*-maleic anhydride) by partial amidolysis. The binding of ARS to the boronic acid groups in this polymer gave an optical sensor for diols. It was used to establish the association constants in a competitive assay between diols and the polymer obtained. The binding of diols was readily observed by a color change of the sensor.

EXPERIMENTAL

Materials

All reagents used are commercial products. Poly(methyl vinyl ether-*alt*-maleic anhydride) (poly(MVE-*alt*-MA); average $M_w = 216{,}000$, average $M_n = 80{,}000$), 3-aminophenylboronic acid monohydrate, all carbohydrates, nucleosides, and other diols were purchased from Sigma-Aldrich (St. Louis, MO). All the chemicals were of the analytical grade and used without further purification. Toluene, tetrahydrofuran (THF), diethyl ether and all other solvents were of purity grade p.a., were obtained from POCH (Gliwice, Poland) and were used without further purification.

Synthesis

To a stirred solution of poly(MVE-*alt*-MA) (0.5 g) in toluene (20 mL), 3-aminophenylboronic acid monohydrate (0.44 g, 3.21 mmol) in THF (10 mL) was slowly added. The mixture was refluxed at 90°C for 6 h. After cooling to room temperature, the final product was isolated by filtration, washed thoroughly with toluene, THF, diethyl ether, and dried in vacuo yielding poly(MVE-*alt*-MA-BA) as a white solid (0.59 g). The synthetic scheme is presented in Figure 1.

Apparatus

The FTIR spectra of polymers were recorded on a Bruker IFS 66s spectrometer (Billerica, MA) using KBr pellets (about 1.5 mg of sample in 200 mg of KBr). NMR spectra were recorded on an Agilent 800 MHz NMR spectrometer (Santa Clara, CA) in D_2O at 298 K using residual HDO signal as a reference. Elemental analyses were carried out by a Vario EL III Element Analyzer (Hanau, Germany). Thermal data were obtained by using a Setaram Setsys 1200 (Caluire, France). The thermal stability of polymers was investigated by thermogravimetric analysis and derivative scanning calorimetry in an air stream at a heating rate of 10°C min^{-1}. The pH measurements were performed using Elmetron CP-505 apparatus (Zabrze, Poland) equipped with a combined pH electrode. UV–Vis measurements were made on an Agilent 8453 (Santa Clara, CA) spectrophotometer using 1 cm plastic cuvettes. UV–Vis absorbance spectra were measured at room temperature within 190–1100 nm.

Determination of the Association Constant of ARS with Poly(MVE-*alt*-MA-BA)

A 0.15 m*M* solution of ARS was prepared in 150 m*M* phosphate buffer of pH 6.9 (Solution A). The poly(MVE-*alt*-MA-BA) solution with a concentration of 5.43 mg mL^{-1} (Solution B) was prepared using Solution A as a solvent to avoid dilution of ARS during titration. Because of a long solubility time of poly(MVE-*alt*-MA-BA), determined by partial hydrolysis of anhydride groups, all poly(MVE-*alt*-MA-BA) solutions were prepared 24 h before measurements, in order to obtain clear solutions. 1 mL of ARS solution (Solution A) was placed in a cuvette and treated stepwise with 0–16.29 mg of poly(MVE-*alt*-MA-BA) (0–3.0 mL of solution B). After every addition of the latter solution, the mixture was equilibrated for 3 min and then the spectrum was measured. The UV-Vis curves from the titration of ARS with poly(MVE-*alt*-MA-BA) solution are presented in Figure 2. The association constant was determined using the Benesi-Hildebrand method. For all calculations the absorbance at 450 nm was used, because the changes in absorbance at this wavelength were the highest.

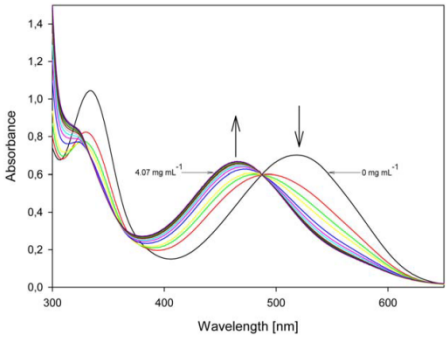

Figure 2. Absorption spectra changes of ARS (0.15 m*M*) with increasing concentration of poly(MVE-*alt*-MA-BA) in phosphate buffer (150 m*M*, pH = 6.9). Concentration of poly(MVE-*alt*-MA-BA) from 0 to 4.07 mg mL^{-1} (indicated in the figure). [Color figure can be viewed in the online issue, which is available at wileyonlinelibrary.com.]

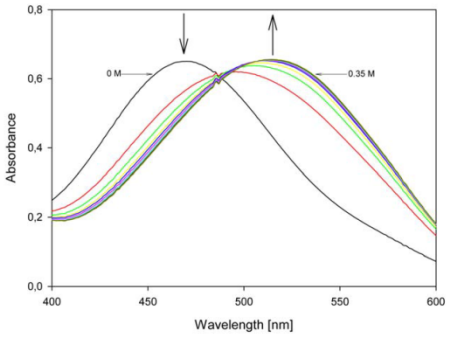

Figure 3. Absorption spectra changes of ARS (0.15 m*M*) and poly(MVE-*alt*-MA-BA) mixture (1.17 mg mL^{-1}) with increasing concentration of fructose in phosphate buffer (150 m*M*, pH = 6.9). Concentration of fructose from 0 to 0.35*M* (indicated in the figure). [Color figure can be viewed in the online issue, which is available at wileyonlinelibrary.com.]

Determination of the Association Constants of Diols with Poly(MVE-*alt*-MA-BA)

In the ARS solution (0.15 m*M* in 150 m*M* phosphate buffer of pH 6.9 – Solution A), poly(MVE-*alt*-MA-BA) was dissolved, to the concentration of 1.17 mg mL^{-1} (Solution C). To acquire clear solution, this mixture was prepared 24 h before any measurements. The solutions of diols were prepared using Solution C to avoid dilution during titration. A portion of 1 mL of Solution C was placed in a cuvette and treated stepwise with the diol solution. Arabinose, dopamine hydrochloride, fructose, galactose, glucose, lactose, maltose, mannitol, mannose, ribose, sorbitol, sorbose, sucrose, tagatose, and xylose were used in concentrations from the 0 to 0.35 *M* range. Because of their low solubilities, the concentration ranges of the following compounds are specified after their names: adenosine 0–0.019, catechol 0–0.037, cytidine 0–0.125, galactitol 0–0.121, guanosine 0–0.002, *myo*-inositol 0–0.038, lyxose 0–0.214, and uridine 0–0.131 *M*. After each addition, the mixture was equilibrated for 3 min before the spectrum was measured. For all calculations the absorbance at 450 nm was used. Figure 3 shows an exemplary result of competitive titration of a mixture of poly(MVE-*alt*-MA-BA) and ARS with fructose.

RESULTS AND DISCUSSION

Synthesis and Characterization of Poly(MVE-*alt*-MA-BA)

The new boronic acid polymer was synthesized by partial amidolysis of maleic anhydride groups of poly(methyl vinyl ether-*alt*-maleic anhydride) in the reaction with 3-aminophenylboronic acid. Poly(MVE-*alt*-MA) is known to react with amines or alcohols to produce polymers with functional side chains. Nevertheless, not all anhydride groups undergo amidation or alcoholysis and even under excess of amine or alcohol some of them remain unreacted.[44,45] To assess how many functional groups were introduced into polymer structure it is necessary to use additional experimental techniques.

The ^{1}H-NMR poly(MVE-*alt*-MA-BA) spectrum (Figure 4), the polymer was allowed dissolve in D_2O for 24 h and the water signals were suppressed with selective presaturation. The signals at 1.1–1.3 ppm come from residual -C**H**$_3$ and -C**H**$_2$- protons, those at 1.4–2.3 ppm come from the main chain -C**H**$_2$- protons, those at 2.3–3.8 ppm come from -O-C**H**, -C**H**(COOH)- and -C**H**(CONHR)- protons. In the aromatic part of the spectra, the signals at 6.9–7.8 ppm can be attributed to Ph-**H** protons of phenylboronic acid moiety. The ratio of intensities of the NMR signals assigned to aromatic protons (introduced into polymer in the reaction with 3-aminophenylboronic acid) to those assigned to alkyl protons, whose amount has not changed during functionalization process, is 11 : 88. This clearly indicates

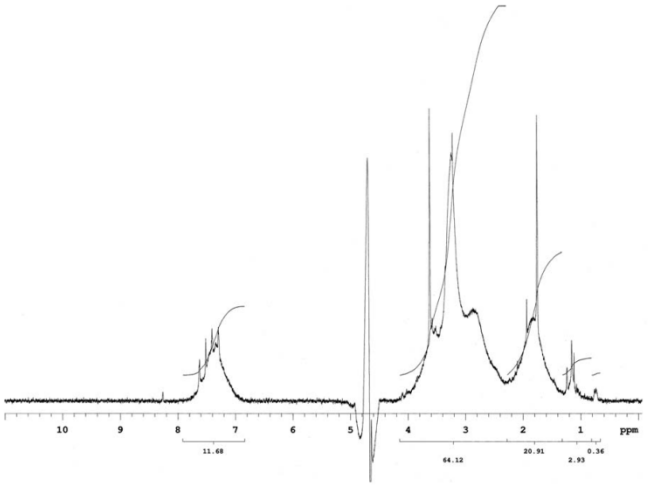

Figure 4. ^{1}H-NMR spectrum of poly(MVE-*alt*-MA-BA).

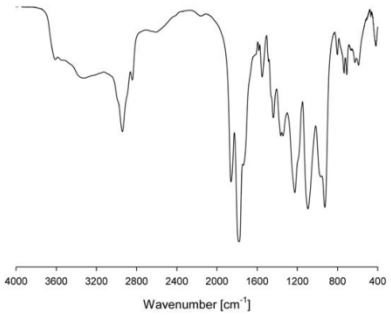

Figure 5. FTIR spectrum of poly(MVE-*alt*-MA-BA).

that statistically there is one anhydride group that has undergone amidation reaction per three unreacted anhydride groups. This information allowed the calculation of molar concentration of boronic acid moieties ([P] parameter) in poly(MVE-*alt*-MA-BA) solution, that were further used to calculate K_{ars} and K_a values. For 5.43 mg mL^{-1} solution of poly(MVE-*alt*-MA-BA), the concentration of boronic acid moieties was 7.13 m*M*, whereas for 1.17 mg mL^{-1} solution of poly(MVE-*alt*-MA-BA) it was 1.54 m*M*.

Elemental analysis of poly(MVE-*alt*-MA-BA) gave the following results (%): C, 53.48; H, 5.21; N, 1.67. To calculate theoretical amounts of each element, the model structure proposed by ^{1}H-NMR spectroscopy was used. Calculated elemental analysis gave the result (%): C, 53.63; H, 5.30; N, 1.84 which was in good agreement with experimental result. This confirms that during functionalization with 3-aminophenylboronic acid, one per four anhydride groups has undergone amidation reaction.

The FTIR spectrum of poly(MVE-*alt*-MA-BA) is presented in Figure 5. The structure of poly(MVE-*alt*-MA-BA) is confirmed by the appearance of the following characteristic absorption bands (cm^{-1}): at 3340 (medium broad peak for ν BO—H overlapped with carboxylic ν O—H and amide ν N—H), 2945 (ν C—H in CH_2 and CH_3), 2842 (ν C—H in CH_2 chain backbone of MVE unit), 1863 (ν C=O in anhydride groups), 1781 (ν C=O in anhydride groups), 1738 (ν C=O in carboxyl groups), 1630 (ν NH—C=O partially overlapped with ν C=O), 1550 (ν C=C), 1440 (δ CH_3, CH_2), 1366 and 1343 (δ CH_3 in CH_3—O), 1226 (ν C—O), 1095 (ν C—B overlapped with ν C—O—C), 923 (γ C—O), 735 and 710 (γ CH_2).[46]

The thermogravimetric analysis (TGA) and differential scanning calorimetry (DSC) results for poly(MVE-*alt*-MA-BA) are presented in Figure 6. In the temperature range 40–245°C, only a small loss of mass is observed. It can be attributed to the physisorbed residual water or solvent molecules as well as evaporation of volatile organic components. The polymer undergoes a three step decomposition process. The first step starts at 245°C and ends at 280°C and is probably related to decomposition and oxidation of the most reactive part of the polymer. The total mass loss at this step is 24.5%. The second step starts at 280°C and ends at 500°C. In this relatively long step, the polymer is slowly decomposed and oxidized with the total mass loss of 29.7%. The last step start at 500°C, ends at 620°C and is related to complete oxidation of all organic material. The residual mass is ~1.4%. The DSC curve presents two exothermic effects, both corresponding to the first and third decomposition steps. The second decomposition step is very slow therefore it is not represented by any peaks in the DSC curve.

Binding of ARS to Poly(MVE-*alt*-MA-BA)

Alizarin Red S displays a significant change in color in response to complex formation with boronic acid. This property was used for determination of association constants in competitive assays, between boronic acids and other diol-containing compounds.[1] The ARS binding to poly(MVE-*alt*-MA-BA) permitted a construction of an optical sensor of diols employing the reversible boronate ester formation.

The equilibrium in the solution of boronic acid polymer (P) and ARS dye (A) can be described as:

$$P + A \overset{K_{ars}}{\longleftrightarrow} PA$$

where K_{ars} $[M^{-1}]$ is the association constant of PA complex formation and P symbolizes one boronic acid residue of the polymer chain. The Benesi-Hildebrand[47] analysis of K_{ars} involves the measurements of absorbance as a function of $[P]$ when $[P]>>[A]$. Using the Benesi-Hildebrand equation:

$$\frac{[A]_0}{Abs} = \left(\frac{1}{[P]}\right)\left(\frac{1}{\varepsilon K_{ars}}\right) + \frac{1}{\varepsilon} \quad (1)$$

one can plot $x = 1/[P]$ vs. $y = [A]_0/Abs$ to receive the y-intercept $= 1/\varepsilon$ and slope $= (1/K_{ars}\varepsilon)$. The parameters of the equations are the following: $[A]_0$ (mol L^{-1}) is the total concentration of ARS dye, [P] (mol L^{-1}) is the total concentration of boronic groups from poly(MVE-*alt*-MA-BA) (varied), *Abs* is the absorbance measured at 450 nm, and ε is the molar absorptivity.

After addition of poly(MVE-*alt*-MA-BA) the color of a buffered solution of ARS changed from burgundy to orange indicating formation of boronate ester. The maximum amount of ARS that poly(MVE-*alt*-MA-BA) is capable to bond was established to be 1.31 m*M* per gram of polymer. By using titration monitored by UV-Vis spectroscopy at 450 nm it was possible to

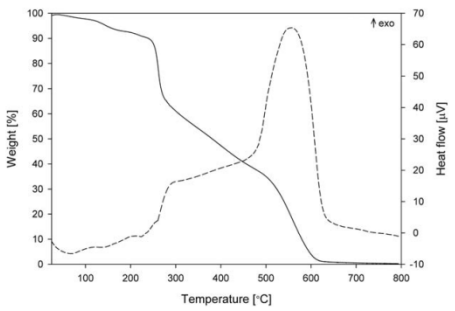

Figure 6. TGA (solid line) and DSC (dashed line) results for poly(MVE-*alt*-MA-BA).

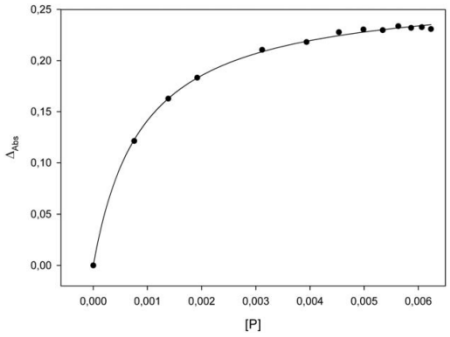

Figure 7. Plot of Δ_{Abs} (at 450 nm) versus [*P*] for ARS (0.15 m*M*) upon titration with poly(MVE-*alt*-MA-BA) (concentrations from 0 to 4.07 mg mL^{-1}) in phosphate buffer (150 m*M*, pH = 6.9) where [*P*] is the total concentration of boronic groups from poly(MVE-*alt*-MA-BA).

establish K_{ars} value of 1080 M^{-1}. The titration curve obtained by plotting Δ_{Abs} vs. [*P*] is presented in Figure 7. Although the color change was almost immediate, after every titration step the mixture was stirred for 3 min to equilibrate all boronic acid moieties that were built-in into the polymer structure. The measured K_{ars} value was smaller than for phenylboronic acid itself (1500 M^{-1} at pH 7.0)[1] which can be attributed to substitution of phenylboronic ring by amide group and to additional steric effects that have occurred in the polymer structure.

Binding of Diols to Poly(MVE-*alt*-MA-BA)

The solution of poly(MVE-*alt*-MA-BA) was used to bind and measure association constants with various diols in competitive assays. In competitive assay the reporter (ARS) and the receptor (boronic acid polymer) associate under the measurement conditions. The complex of the receptor and the reporter dissociates in the presence of a guest (diol).

The two equilibriums in the complex solution during titration of boronic acid polymer (*P*) and ARS dye (*A*) with a diol substrate (*D*) are:

$$P + A \overset{K_{ars}}{\longleftrightarrow} PA$$

$$P + D \overset{K_a}{\longleftrightarrow} PD$$

where K_a $[M^{-1}]$ is the association constant for PD complex formation. The association constant K_a can be calculated from the following eqs. (2–4):

$$Q = \frac{[A]}{[PA]} = \frac{Abs_{PA} - Abs}{Abs - Abs_A} \quad (2)$$

where *Abs* is absorbance measured, Abs_{PA} is the initial absorbance of ARS – poly(MVE-*alt*-MA-BA) solution and Abs_A is the absorbance of ARS;

$$L = [p]_0 - \frac{1}{QK_{Ars}} - \frac{[A]_0}{Q+1} \quad (3)$$

where $[A]_0$ (mol L^{-1}) is the total concentration of ARS and $[P]_0$ (mol L^{-1}) is the total concentration of boronic groups from poly(MVE-alt-MA-BA);

$$\frac{[D]}{L} = \frac{K_{ars}}{K_a} Q + 1 \quad (4)$$

where [*D*] (mol/L) is the diol concentration (varied). To obtain K_a value one must plot $x = Q$ vs. $y = [D]/[L]$ to receive a slope = K_{ars}/K_a. The *y*-intercept should be 1, but we obtained its different values. This is however in accordance with the results of other groups also reporting to have obtained different values of the *y*-intercept.[1,2] The values of the association constants measured are presented in Table I.

The binding of diols to poly(MVE-*alt*-MA-BA) results in release of free ARS which is connected with color change of the solution from orange to burgundy. Titration with increasing concentration of appropriate diol allows measurements of the association constants by monitoring the decrease in absorption at 450 nm by UV-Vis spectroscopy. The measured association constants are generally in good agreement with the values reported by Springsteen and Wang.[1] For all compounds they are lower than those measured for phenylboronic acid, which can be explained by the same factors that are responsible for the low binding constant with ARS: additional substitution of phenylboronic ring and steric effects that are present in polymer structure. Springsteen and Wang have shown that the values of association constants continue to decrease in the following order: ARS > sorbitol > fructose > tagatose > mannitol = sorbose. In our studies this order of decrease in K_a values is similar: ARS > sorbitol > fructose > mannitol > tagatose > sorbose. The difference in K_a value between mannitol and tagatose is very small (9 in our studies, 10 reported by Springsteen, and Wang) therefore, the change in the above presented order is acceptable and is probably related to small changes in binding properties of boronic residues in polymer structure. More surprising is the relatively big difference in K_a values between tagatose and sorbose (according to Springsteen and Wang the K_a value for these

Table I. Association Constants (K_a) with Poly(MVE-*alt*-MA-BA) at pH 6.9, 150 m*M* Phosphate Buffer

Diol	K_a $[M^{-1}]$	Diol	K_a $[M^{-1}]$
ARS	1080	maltose	0[a]
cytidine	130	mannose	0[a]
uridine	81	sucrose	0[a]
sorbitol	46	adenosine	–[b]
fructose	40	guanosine	–[b]
mannitol	34	arabinose	–[c]
tagatose	25	catechol	–[c]
sorbose	9	dopamine	–[c]
galactitol	0[a]	galactose	–[c]
glucose	0[a]	lyxose	–[c]
myo-inositol	0[a]	ribose	–[c]
lactose	0[a]	xylose	–[c]

[a] The values were too low to be accurately measured with this method.
[b] The solubility of those compounds was too low to allow measurement of association constant.
[c] The compounds reacted with ARS which was indicated by a change in solution color to reddish brown.

compounds was identical) but the reason for this effect has not been established yet. Unfortunately, we were unable to measure accurately K_a values for glucose, lactose, maltose, mannose, and sucrose because there were no significant differences in their absorption spectra during titration, therefore the K_a value was established as 0 for these compounds. According to Springsteen and Wang, the K_a values for these carbohydrates are in the range 13–0.67. We observed K_a values generally lower than those measured by Springsteen and Wang, therefore K_a value of 0 is consistent with our expectations.

Measurements of K_a for all aldopentoses (arabinose, lyxose, ribose, and xylose), galactose, catechol, and dopamine (which is a catecholamine) has not given any satisfactory results. The color of solution instead of changing into burgundy (the color of free ARS) changed into reddish brown. The assumption that this change in color is connected with reaction of ARS with examined diol molecules was confirmed by mixing buffered ARS solution (without poly(MVE-*alt*-MA-BA)) with these diols. The new absorption band that is produced interferes with the band at 450 nm which is used to calculate K_a values, so it was impossible to obtain accurate K_a values. The fact that aldopentoses as well as catechol and its derivative react with ARS is not surprising. All these compounds possess reactive groups that can undergo reduction–oxidation reactions leading to products with different absorption properties. Unfortunately, we were unable to explain why from among all aldohexoses studied only galactose underwent a reaction that led to unusual change in color. It is worth noting that this reaction is not instant at low concentrations, used in fluorescence measurements, it can take more time than needed to accomplish titration procedure. This is probably the reason why Springsteen and Wang and other researchers that used ARS method to establish association constants have not reported this unusual change in color.

Measurements of K_a for ribonucleosides (adenosine, cytidine, guanosine, uridine) indicated that cytidine and uridine produce high-affinity complexes with boronic acid moieties. The measured K_a values were 130 and 81 M^{-1} respectively, so much higher than for any other carbohydrates. Unfortunately we were unable to measure K_a values for adenosine and guanosine, because of their too low solubility that made them inapplicable for this method. Investigation of boron with nucleosides and nucleic acid has recently been a subject of profound interest because of a wide range of their potential medicinal, biotechnological or analytical applications.[48] In view of the above, the synthesis of boronic acid polymer that can form high-affinity complexes with nucleosides is a substantial achievement.

CONCLUSIONS

A new boronic acid polymer was prepared by amidation of anhydride groups of poly(MVE-*alt*-MA) with 3-aminophenylboronic acid. The resulting polymer was characterized by chemical and spectroscopic methods. It was established that 25% of anhydride groups underwent amidation reaction. After solubilization in phosphate buffered solution this polymer was associated with ARS to produce colored optical sensor that was further used to measure the association constants with different diols in competitive assays. Generally, all K_a values were lower than those measured for phenylboronic acid. The poly(MVE-*alt*-MA) polymer showed higher affinity to ribonucleosides, particularly cytidine and uridine, than to any carbohydrate examined.

With different amines or alcohols the presented procedure can be used to prepare a variety of boron-containing diol-responsive polymers. The ARS method allows easy measurements of association constant between boronic acid residue of the polymer chain and a particular diol. Owing to the reversible binding properties and high water solubility, boronic acid polymers of this type can find applications in biology or medicine for example for carbohydrate detection, drug delivery or isolation of nucleosides.

ACKNOWLEDGMENTS

This work was supported by the Polish National Science Center (NCN; decision no. DEC-2012/05/N/ST5/01274).

REFERENCES

1. Springsteen, G.; Wang, B. *Tetrahedron* **2002**, *58*, 5291.
2. Dowlut, M.; Hall, D. G. *J. Am. Chem. Soc.* **2006**, *128*, 4226.
3. Gierczyk, B.; Kazmierczak, M.; Schroeder, G.; Sporzynski, A. *New J. Chem.* **2013**, *37*, 1056.
4. Adamczyk-Woźniak, A.; Brzózka, Z.; Cyrański, M. K.; Filipowicz-Szymańska, A.; Klimentowska, P.; Żubrowska, A.; Żukowski, K.; Sporzyński, A. *Appl. Organomet. Chem.* **2008**, *22*, 427.
5. Adamczyk-Woźniak, A.; Jakubczyk, M.; Jankowski, P.; Sporzyński, A.; Urbański, P. M. *J. Phys. Org. Chem.* **2013**, *26*, 415.
6. Rogowska, P.; Cyrański, M. K.; Sporzyński, A.; Ciesielski, A. *Tetrahedron Lett.* **2006**, *47*, 1389.
7. James, T. D.; Sandanayake, K. R. A. S.; Shinkai, S. *Angew. Chem., Int. Ed. Engl.* **1996**, *35*, 1910.
8. Edwards, N. Y.; Sager, T. W.; McDevitt, J. T.; Anslyn, E. V. *J. Am. Chem. Soc.* **2007**, *129*, 13575.
9. Duggan, P. J.; Houston, T. A.; Kiefel, M. J.; Levonis, S. M.; Smith, B. D.; Szydzik, M. L. *Tetrahedron* **2008**, *64*, 7122.
10. Altamore, T. M.; Barrett, E. S.; Duggan, P. J.; Sherburn, M. S.; Szydzik, M. L. *Org. Lett.* **2002**, *4*, 3489.
11. Ren, L.; Liu, Z.; Dong, M.; Ye, M.; Zou, H. *J. Chromatogr., A* **2009**, *1216*, 4768.
12. Zhou, W.; Yao, N.; Yao, G.; Deng, C.; Zhang, X.; Yang, P. *Chem. Commun. (Cambridge, U. K.)* **2008**, *0*, 5577.
13. Springsteen, G.; Wang, B. *Chem. Commun. (Cambridge, U. K.)* **2001**, *0*, 1608.
14. Huang, Y.; Liu, M.; Wang, L.; Gao, C.; Xi, S. *React. Funct. Polym.* **2011**, *71*, 666.
15. Ahsan Uddin, K. M.; Ye, L. *J. Appl. Polym. Sci.* **2013**, *128*, 1527.
16. Çimen, E. K.; Rzaev, Z. M. O.; Pişkin, E. *J. Appl. Polym. Sci.* **2005**, *95*, 573.
17. Sershen, S.; West, J. *Adv. Drug Delivery Rev.* **2002**, *54*, 1225.

18. Shiino, D.; Murata, Y.; Kubo, A.; Kim, Y. J.; Kataoka, K.; Koyama, Y.; Kikuchi, A.; Yokoyama, M.; Sakurai, Y.; Okano, T. *J. Control. Release.* **1995**, *37*, 269.
19. Shiino, D.; Murata, Y.; Kataoka, K.; Koyama, Y.; Yokoyama, M.; Okano, T.; Sakurai, Y. *Biomaterials* **1994**, *15*, 121.
20. Takayoshi, W.; Imajo, M.; Iijima, M.; Suzuki, M.; Yamamoto, H.; Kanekiyo, Y. *Sensor. Actuat. B-Chem.* **2014**, *192*, 776.
21. Xu, Z.; Uddin, K. M. A.; Ye, L. *Macromolecules* **2012**, *45*, 6464.
22. Cambre, J. N.; Sumerlin, B. S. *Polymer* **2011**, *52*, 4631.
23. Seymour, L. W.; Duncan, R.; Strohalm, J.; Kopeček, J. *J. Biomed. Mater. Res.* **1987**, *21*, 1341.
24. Stenzel, M. H. *Chem. Commun. (Cambridge, U. K.)* **2008**, *0*, 3486.
25. Plesu, N.; Kellenberger, A.; Taranu, I.; Taranu, B. O.; Popa, I. *React. Funct. Polym.* **2013**, *73*, 772.
26. Hajizadeh, S.; Ivanov, A. E.; Jahanshahi, M.; Sanati, M. H.; Zhuravleva, N. V.; Mikhalovska, L. I.; Galaev, I. Y. *React. Funct. Polym.* **2008**, *68*, 1625.
27. Matsumoto, A.; Yoshida, R.; Kataoka, K. *Biomacromolecules* **2004**, *5*, 1038.
28. Matsumoto, A.; Ikeda, S.; Harada, A.; Kataoka, K. *Biomacromolecules* **2003**, *4*, 1410.
29. Elmas, B.; Senel, S.; Tuncel, A. *React. Funct. Polym.* **2007**, *67*, 87.
30. Sreenivasan, K. *J. Appl. Polym. Sci.* **2004**, *94*, 2088.
31. Özdemir, A.; Tuncel, A. *J. Appl. Polym. Sci.* **2000**, *78*, 268.
32. Chalagalla, S.; Sun, X.-L. *React. Funct. Polym.* **2010**, *70*, 471.
33. Zhou, C.; Wang, B.; Zhang, F.; Xu, K.; Han, C.; Hu, H.; Liu, Y.; Wang, P.; Xin, J. H. *J. Appl. Polym. Sci.* **2013**, *130*, 2345.
34. Kızılcan, N.; Dinçer, P. *J. Appl. Polym. Sci.* **2013**, *129*, 2813.
35. Guo, Z.; Li, H.; Han, W.; Zhao, T. *J. Appl. Polym. Sci.* **2013**, *128*, 3356.
36. Ullah, S.; Ahmad, F.; Yusoff, P. S. M. M. *J. Appl. Polym. Sci.* **2013**, *128*, 2983.
37. Lubczak, J.; Łukasiewicz, B.; Myśliwiec, B. *J. Appl. Polym. Sci.* **2013**, *127*, 2057.
38. Ikeya, T.; Kataoka, K.; Okano, T.; Sakurai, Y. *React. Funct. Polym.* **1998**, *37*, 251.
39. Pringsheim, E.; Terpetschnig, E.; Piletsky, S. A.; Wolfbeis, O. S. *Adv. Mater. (Weinheim, Ger.)* **1999**, *11*, 865.
40. Cannizzo, C.; Amigoni-Gerbier, S.; Larpent, C. *Polymer* **2005**, *46*, 1269.
41. Okasaka, Y.; Kitano, H. *Colloids Surf., B* **2010**, *79*, 434.
42. Cross, A. J.; Davidson, M. G.; Garcia-Vivo, D.; James, T. D. *RSC Adv.* **2012**, *2*, 5954.
43. Egawa, Y.; Gotoh, R.; Seki, T.; Anzai, J.-I. *Mater. Sci. Eng., C* **2009**, *29*, 115.
44. Cao, Y.-C.; Wang, X.; Scott, K. *J. Power Sources* **2012**, *201*, 226.
45. Weber, J.; Boyko, V.; Arndt, K.-F. *Macromol. Chem. Phys.* **2007**, *208*, 643.
46. Türk, M.; Rzayev, Z.; Kurucu, G. *Health* **2010**, *2*, 51.
47. Benesi, H. A.; Hildebrand, J. H. *J. Am. Chem. Soc.* **1949**, *71*, 2703.
48. Martin, A. R.; Vasseur, J. J.; Smietana, M. *Chem. Soc. Rev.* **2013**, *42*, 5684.

Chemical Engineering Journal 259 (2015) 885–893

Contents lists available at ScienceDirect

Chemical Engineering Journal

journal homepage: www.elsevier.com/locate/cej

Removal of heavy metal ions with the use of chelating polymers obtained by grafting pyridine–pyrazole ligands onto polymethylhydrosiloxane

Michał Cegłowski *, Grzegorz Schroeder

Faculty of Chemistry, Adam Mickiewicz University in Poznan, Umultowska 89b, 61-614 Poznań, Poland

HIGHLIGHTS

- Pyridine–pyrazole ligands were grafted onto polymethylhydrosiloxane.
- Two different linkers were used for grafting reaction.
- Extraction of Cu^{2+}, Cd^{2+}, Cr^{3+}, Ni^{2+} and Co^{2+} from aqueous solution was achieved.
- The length of linker influences the amount of ions extracted.
- The polymer with the shorter linker is more selective towards Cu^{2+} ion.

GRAPHICAL ABSTRACT

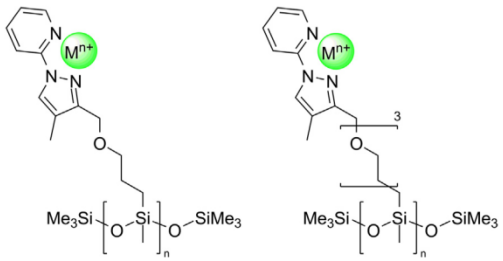

ARTICLE INFO

Article history:
Received 1 July 2014
Received in revised form 13 August 2014
Accepted 14 August 2014
Available online 27 August 2014

Keywords:
Chelating polymer
Hydrosilylation
Liquid–liquid extraction
Heavy metal ion
Adsorption

ABSTRACT

New chelating polymers soluble in organic non-polar solvents were synthesized by hydrosilylation reaction of polymethylhydrosiloxane with pyridine–pyrazole ligands. Two types of linkers were used to graft pyridine–pyrazole ligands onto polymethylhydrosiloxane. The composition and properties of the polymers obtained were studied by NMR spectroscopy, Fourier transform infrared spectroscopy, elemental analysis, thermogravimetric analysis and derivative scanning calorimetry. The effects of various parameters such as initial metal ion concentration, contact time, temperature and pH were examined in the processes of extraction of Cu^{2+}, Cd^{2+}, Cr^{3+}, Ni^{2+} and Co^{2+}. The equilibrium data were best represented by Langmuir isotherm and the uptake capacities of polymers obtained varied between 0.24 mmol (for Co^{2+}) and 1.48 mmol (for Cu^{2+}) per 1 g of polymer. The adsorption kinetics was found to follow the pseudo-second-order kinetic model. The polymers adsorption capacity was more than 90% level after five cycles of adsorption–desorption. Treatment of real wastewater samples showed good ability of the polymers to absorb metal ions.

1. Introduction

Heavy metal ions from industrial wastes pose threat to the environment and human health, therefore their quantitative removal and a constant monitoring of their concentration are important issues. Although some of them are fundamental for human metabolism and are well known as dietary minerals, all of them are potentially toxic at higher concentrations. Copper in human organism is carried by ceruloplasmin, an enzyme that facilitates iron uptake. Cadmium is a nonessential metal for human organism and is toxic even at low concentrations [1]. It can damage liver, kidneys and inhaled with dust can cause problems with respiratory tract. Chromium is an essential nutrient, which is required for appropriate sugar and fat metabolism [2]. At high concentrations chromium(III) can lead to DNA damage [3], whereas

* Corresponding author. Tel.: +48 618291565.
E-mail address: ceglowski.m@gmail.com (M. Cegłowski).

http://dx.doi.org/10.1016/j.cej.2014.08.058
1385-8947/

chromium(VI) damages kidneys, the liver and blood cells. Nickel deficiency in human organism causes lowering of specific activities of many enzymes involved in carbohydrate and amino acid metabolism, nevertheless no enzymes or cofactors that include nickel are known in higher organisms [4]. Cobalt is an important cofactor in Vitamin B_{12}, which is responsible for proper functioning of the brain and nervous system and for formation of blood [5]. Excessive amounts of cobalt may produce goiter and reduce thyroid activity [6].

One of the most popular techniques used to remove a wide variety of substances is adsorption. This technique allows the use of environmentally friendly materials whose cost of production is usually very low [7]. Adsorption is widely used in preconcentration procedures, which are mandatory for many analytical techniques [8–20]. Polymers and chelating resins are among the most popular absorbents used for removal of metal ions from aqueous solutions. These materials have been widely used because they are reusable, easy to handle and characterized by high adsorption rate and high adsorption efficiencies as well as high selectivity to some metal ions [21–26].

Liquid–liquid extraction, also known as solvent extraction (SX), allows separation of a particular compound or many compounds from one liquid and its transfer into another immiscible liquid. This process usually involves vigorous stirring of both liquids in order to allow mass transfer of the solute from one phase to another. After a specific time the stirring is stopped and both liquid phases are allowed to coalescence. By choosing an appropriate solvent, it is possible to selectively recover high amounts of the solute. Metal extraction from aqueous phase requires the use of an organic solution of a special extractant that will allow solubilization of the metal salts in the organic phase. This method has been proven to be effective in removal of cadmium(II) [27], copper(II) [28], chromium(III) [29], chromium(VI) [30], palladium(II) [31], nickel(II) [32,33], and alkali metal ions [34]. Extractants can be used as pure compounds or they can be immobilized on a resin or polymer surface [35,36].

Polysiloxane-based polymers are used in a wide range of applications because of their good thermal and oxidative stability, high functionality, low toxicity combined with physiological inertness and relatively low cost of synthesis [37]. Chelating groups can be incorporated into polysiloxane network to produce new materials that find applications in areas such as extraction and recovery of metal ions from aqueous solutions [38]. The introduction of chelating groups into polysiloxane network can be achieved by two strategies. The first one involves hydrolysis and polycondensation reaction of tetraethoxysilane with functional tri- or di-alkoxysilane that already contains a chelating group. The second strategy is a modification of the post-polysiloxane that contains a reactive group (e.g. R—Cl or R—NH_2) with a complexing unit [39]. With the use of these methods a wide range of immobilized-polysiloxane ligand systems have been obtained [40–43].

In this study, two polymers prepared by grafting pyridine–pyrazole ligands onto polymethylhydrosiloxane (PMHS) were synthesized and used for extraction of trace metal ions from water. A new strategy, based on the hydrosilylation reaction for grafting ligands on polysiloxane precursor was proposed. The influence of factors affecting the extraction of Cu^{2+}, Cd^{2+}, Cr^{3+}, Ni^{2+} and Co^{2+} such as concentration, contact time, temperature and pH was examined.

2. Experimental

2.1. Materials and chemicals

All reagents used are commercial products. Poly(methylhydrosiloxane) (PMHS; average M_n = 1700–3200), ethyl 2, 4-dioxovalerate, 2-hydrazinopyridine, diethylene glycol, allyl bromide, *p*-toluenesulfonyl chloride, lithium aluminum hydride, anhydrous tetrahydrofuran (THF) and Karstedt's catalyst (Platinum(0)-1,3-divinyl-1,1,3,3-tetramethyldisiloxane complex solution in xylene) were obtained from Sigma–Aldrich (St. Louis, MO, USA). Metal perchlorates: $Cu(ClO_4)_2 * 6H_2O$, $Cd(ClO_4)_2 * 6H_2O$, $Cr(ClO_4)_3 * 6H_2O$, $Ni(ClO_4)_2 * 6H_2O$ and $Co(ClO_4)_2 * 6H_2O$ used for extraction experiments were also obtained from Sigma–Aldrich. Anhydrous ethyl alcohol and all other solvents of the purity grade p.a., were obtained from POCH (Gliwice, Poland) and were used without further purification. Anhydrous toluene used for hydrosilylation reaction was dried by distillation from sodium hydride. Wastewater samples were obtained from PRESSEKO (Bolechowo near/Poznan, Poland) company.

2.2. Instrument

Shimadzu AA-7000 atomic absorption spectrophotometer (Shimadzu, Japan) was used for determination of Cu^{2+}, Cd^{2+}, Cr^{3+}, Ni^{2+} and Co^{2+} concentrations. The determination of metals was performed in 3 replications, and the % RSD did not exceed 5%. The FTIR spectra of polymers were recorded on a Bruker IFS 66s spectrometer (Billerica, MA, USA) using a thin film. NMR spectra were recorded on Varian VNMR-S 400 MHz (Palo Alto, CA, USA). Elemental analyses were carried out by a Vario EL III Element Analyzer (Hanau, Germany). Thermal data were obtained by using a Netzsch STA 409 CD (Kraków, Poland). The thermal stability of polymers was investigated by thermogravimetric analysis and derivative scanning calorimetry in an argon stream at a heating rate of 8 °C min^{-1}. The pH measurements were performed using Elmetron CP-505 apparatus (Zabrze, Poland) equipped with a combined pH electrode.

2.3. Synthesis of chelating polymers

Synthesis of polymers PMHS-*g*-PyPzAllyl and PMHS-*g*-PyPz$(OEt)_2$Allyl, presented in Fig. 1, is described in detail in Supporting Information.

2.4. Adsorption experiments

Adsorption studies were performed for $Cu(ClO_4)_2$, $Cd(ClO_4)_2$, $Cr(ClO_4)_3$, $Ni(ClO_4)_2$ and $Co(ClO_4)_2$. To prepare each isotherm, a series of samples containing 10 mg of the polymer dissolved in 5 mL of dichloromethane and 5 mL of metal perchlorate solution were used. The adsorptions capacities were measured for seven different concentrations (0.1, 0.5, 1, 2.5, 5, 10 and 20 mM). The water solutions of metal ions were buffered to pH 5 (acetic acid/sodium acetate buffer). The solutions were stirred for 24 h at

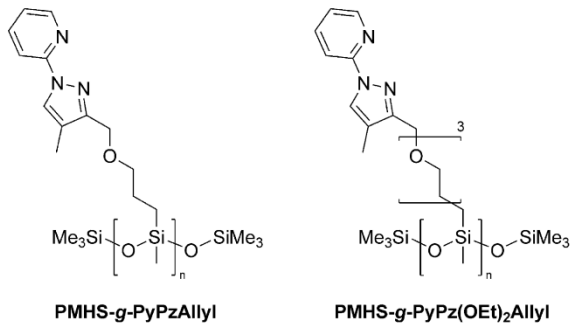

Fig. 1. Structures of the polymers obtained.

298 ± 1 K. The starting (C_0; mmol L^{-1}) and post-equilibration (C_{eq}; mmol L^{-1}) concentrations of metal ions were measured by atomic absorption spectrophotometry. The amount of metal adsorbed (q_{eq}; mmol g^{-1}) after equilibration was calculated from the difference between C_0 and C_{eq}:

$$q_{eq} = \frac{(C_0 - C_{eq})V}{m} \quad (1)$$

where m is the mass of polymer (0.01 g) and V is the volume of aqueous solution (L).

For the adsorption kinetic studies, 10 mg of the polymer was dissolved in 10 mL of dichloromethane and 10 mL of buffered (pH 5) metal perchlorate solution with the initial concentration of 2.5 mM were stirred at 298 ± 1 K. The aqueous samples were taken at preset time intervals and the concentrations of metal ions were measured by atomic absorption spectrophotometry. The amount of adsorption at time t, q_t (mmol g^{-1}), was calculated from:

$$q_t = \frac{(C_0 - C_t)V}{m} \quad (2)$$

where m is the mass of polymer (0.01 g), C_0 (mmol L^{-1}) is the initial metal ion concentration, C_t (mmol L^{-1}) is the metal ion concentration at time t, V is the volume of aqueous solution (L).

Thermodynamic studies were performed for other sets of samples containing 10 mg of polymer dissolved in 5 mL of dichloromethane and 5 mL of buffered (pH 5) metal perchlorate solution with the initial concentration of 2.5 mM; they were stirred under 298 ± 1 K, 303 ± 1 K and 308 ± 1 K for 24 h. Other experimental details were as for isotherms determination.

The relations between the sorption properties of the polymers and the pH of the solution were studied in the pH range from 2 to 7. The pH of the solutions was adjusted with the buffers containing KCl/HCl (pH 2), acetic acid/sodium acetate (pH 3–6) and HEPES (4-(2-hydroxyethyl)-1-piperazineethanesulfonic acid) buffer (pH 7). The measurements were made for 20 mM metal concentration, which guaranteed large excess of ions over ligand groups. Other experimental details were as for isotherms determination.

Sorption/desorption experiments were performed as for thermodynamic studies (5 mM metal ion concentration), however samples were stirred for 12 h. Afterwards, the water phase was collected and the organic phase was stirred with 5 mL of 0.1 M HCl for 12 h. The starting and final concentrations of metal ions in aqueous phases were measured by atomic absorption spectrophotometry. To test the reusability of the polymers, this adsorption–desorption cycle was repeated five times by using the same adsorbent.

Experiments with real wastewater samples were performed by adding 2 mL of wastewater sample to a solution of polymer (20 mg) in dichloromethane (5 mL). The solutions were stirred for 24 h. The starting and final concentrations of metal ions in aqueous phases were measured by atomic absorption spectrophotometry.

3. Results and discussion

3.1. Synthesis of polymers and their characterization

The new chelating polymers with pyridine–pyrazole ligands were synthesized according to the synthetic route presented in Fig. S-1 in Supporting Information. The first step of synthesis was the condensation reaction between ethyl 2,4-dioxovalerate and 2-hydrazinopyridine that produces compound **1**. Secondly, ester group of compound **1** was reduced with lithium aluminum hydride to produce hydroxyl group, which allows further functionalization. In order to carry out hydrosilylation reaction, an allylic group must have been introduced into a pyridine–pyrazole ligand. This was achieved in two ways, by reaction of **2** under strong basic conditions with allyl bromide or linker **5**. The last step, which was the hydrosilylation reaction of **3** or **6** (the ^{1}H NMR spectra presented in Figs. S-2 and S-3, respectively in Supporting Information) with PMHS, was catalyzed by Karstedt's catalyst and was carried out until all of the allyl groups had reacted. The aim of using two types of linkers was to examine if the length of the chain and increased number of oxygen atoms affects polymer effectiveness in binding metal ions. The oxygen atoms can act as a donor atoms, therefore the use of this type of linker may increase polymer sorption properties. Moreover, increased flexibility of the chain should also affect sorption properties.

3.1.1. ^{1}H NMR spectra

The ^{1}H NMR spectra of the polymers obtained confirm the proposed structures. The ^{1}H NMR spectra of both polymers show characteristic signals at around 0.0 ppm (Si—C**H**$_3$) and 0.5 ppm (Si—C**H**$_2$) coming from siloxane chain. The lack of signals coming from allylic protons and residual signals coming from Si—H protons indicates that all substrates have undergone hydrosilylation reaction. Broadening of all ligand signals is natural of ^{1}H NMR spectra of polymers and indicates that their structure was preserved upon hydrosilylation. The ^{1}H NMR spectra of the polymers obtained are presented in Fig. S-4 in Supporting Information.

PMHS-*g*-PyPzAllyl ^{1}H NMR ($CDCl_3$) δ: −0.02 −0.24 (b, Si—C**H**$_3$); 0.55 (b, Si—C**H**$_2$—); 1.65 (b, Si—CH$_2$—C**H**$_2$—); 2.61 (b, Pz—C**H**$_3$) 3.45 (b, —O—C**H**$_2$—); 4.69 (b, Pz—C**H**$_2$—O—); 4.70 (b, Si—**H**); 6.19 (b, Pz—**H**); 7.11 (b, Py—**H**β); 7.63–7.87 (b, Py—**H**γ, δ); 8.38 (b, Py—**H**α).

PMHS-*g*-PyPz(OEt)$_2$Allyl ^{1}H NMR ($CDCl_3$) δ: −0.07 −0.22 (b, Si—C**H**$_3$); 0.49 (b, Si—C**H**$_2$—); 1.64 (b, Si—CH$_2$—C**H**$_2$—); 2.63 (b, Pz—C**H**$_3$); 3.33–3.71 (b, —O—C**H**$_2$—); 4.58 (b, Pz—C**H**$_2$—O); 4.70 (b, Si—**H**); 6.23 (b, Pz—**H**); 7.16 (b, Py—**H**β); 7.80 (b, Py-—**H**γ, δ); 8.41 (b, Py—**H**α).

3.1.2. IR spectra

The FT-IR absorbance spectra of the polymers obtained are presented in Fig. 2. The absorption bands assigned to the PDMS matrix appear at 2930 cm^{-1} (ν C—H), 2169 cm^{-1} (ν Si—H), 1260 cm^{-1} (δ Si—CH_3), 1100–1000 cm^{-1} (ν Si—O—Si) and 790 cm^{-1} (γ Si—CH_3). Ligands give the absorptions bands at 3060 cm^{-1} (ν aromatic C—H), 2930 cm^{-1} (ν C—H), 1600–1360 cm^{-1} (skeletal vibrations) and 780 cm^{-1} (δ C—H).

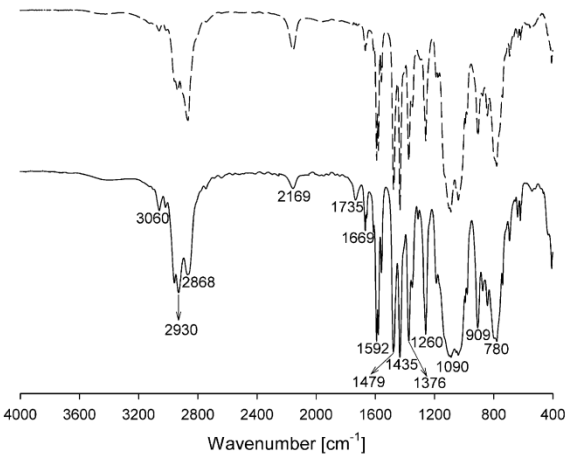

Fig. 2. FT-IR spectra of polymers obtained: PMHS-*g*-PyPzAllyl (solid line) and PMHS-*g*-PyPz(OEt)$_2$Allyl (dashed line).

The absorption bands observed are in accordance with the proposed polymer structures. Similarly to ^{1}H NMR spectra, residual Si—H bands were also observed in IR spectra. As the difference between PMHS-*g*-PyPzAllyl and PMHS-*g*-PyPz(OEt)$_2$Allyl is only in the linker chain length, their IR spectra are very similar.

3.1.3. Elemental analysis

Elemental analysis of PMHS-*g*-PyPzAllyl gave the following results (%): C, 53.15; H, 7.21; N, 11.50. In order to calculate theoretical amounts of each element, the residual Si—H groups as well as the groups formed by cross-linking of final polymer must be included. The presence of the former ones was observed in ^{1}H NMR and IR spectra. Cross-linking is a side reaction catalyzed by platinum and it results in formation of a gel-like material. A model was proposed with 15 cross-linked groups and 15 unreacted Si—H groups per 100 grafted ligand groups. Calculated elemental analysis gave the results (%): C, 53.05; H, 6.88; N, 11.81 which are in good agreement with experimental data.

Elemental analysis of PMHS-*g*-PyPz(OEt)$_2$Allyl gave the following results (%): C, 53.49; H, 7.16; N, 9.45. A similar model was proposed with 10 cross-linked groups and 5 unreacted Si—H groups per 100 grafted ligand groups. The lower amount of cross-linked groups was indicated by the fact that the polymer formed a very viscous liquid. Calculated elemental analysis gave the results (%): C, 53.56; H, 6.85; N, 9.65 which are in very good agreement with experimental data.

3.1.4. Thermal analysis

The results of thermogravimetric analysis of PMHS-*g*-PyPzAllyl and PMHS-*g*-PyPz(OEt)$_2$Allyl are presented in Fig. 3. The polymers undergo a two-step decomposition process. The first step starts at around 150 °C and ends at 260 °C for PMHS-*g*-PyPzAllyl, whereas for PMHS-*g*-PyPz(OEt)$_2$Allyl it starts at around 200 °C and ends at 300 °C. This process is probably connected with partial decomposition of the pyridine–pyrazole ligands, because it is different in the polymers studied. The second step of decomposition process is similar for both polymers, it starts at around 310 °C and ends at 590 °C.

The differential scanning calorimetry (DSC) results are presented in Fig. 4. The DSC curve of PMHS-*g*-PyPzAllyl shows an exothermic effect with a maximum at around 575 °C which is probably related to the last step of decomposition of the polymer. The DSC curve of PMHS-*g*-PyPz(OEt)$_2$Allyl shows an increased exothermic effect starting at 435 °C which is also related to the decomposition of the polymer.

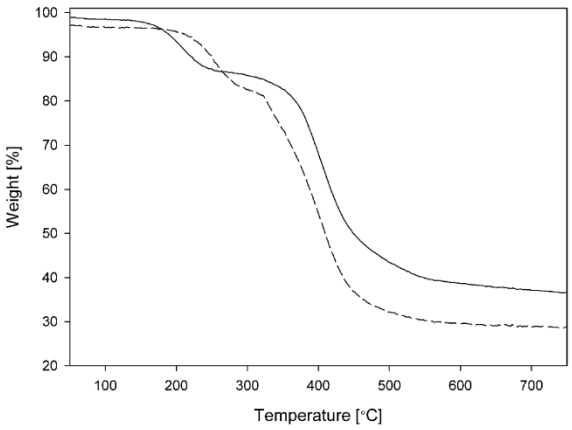

Fig. 3. Thermograms of PMHS-*g*-PyPzAllyl (solid line) and PMHS-*g*-PyPz(OEt)$_2$Allyl (dashed line).

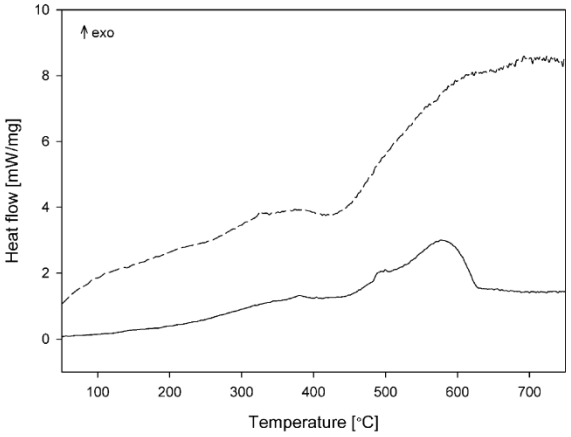

Fig. 4. DSC results of PMHS-*g*-PyPzAllyl (solid line) and PMHS-*g*-PyPz(OEt)$_2$Allyl (dashed line).

3.2. Metal ion adsorption

The ability to bind transition metal ions from water solutions was examined for both polymers obtained. Perchlorate salts were used because perchlorates are widely known to be very poor complexing agents which makes them useful as counter ions in the studies of metal cation chemistry. Moreover, perchlorates show also low reactivity as oxidants. The polymers obtained were in the form of a dense liquid or a gel-like material. Both of them had low contact surface with metal ion solutions. Moreover, these polymers were hydrophobic which made them hard to penetrate by transition metal ions. To overcome these problems the polymers obtained were dissolved in CH_2Cl_2 and used in liquid–liquid extraction experiments.

3.2.1. Adsorption isotherms

The relationships between the equilibrium concentration of metal ions and the amount of metal adsorbed on PMHS-*g*-PyPzAllyl and PMHS-*g*-PyPz(OEt)$_2$Allyl are shown in Figs. 5 and 6, respectively. For both polymers the adsorbed amount of metal ions increases with their initial concentration increasing up to a plateau value. The Langmuir, Freundlich and Temkin isotherm models were used to interpret and evaluate the adsorption data from the experiments performed at pH of 5.

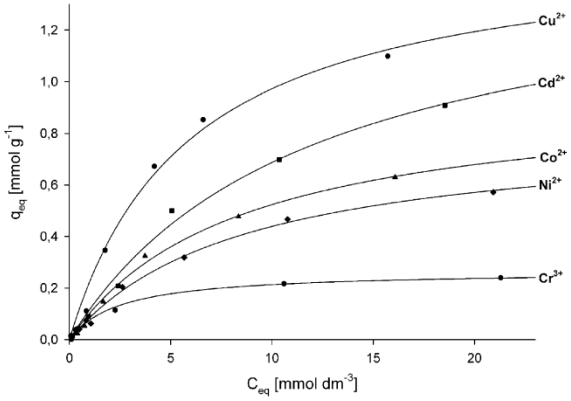

Fig. 5. Adsorption isotherms of metal ions by PMHS-*g*-PyPzAllyl.

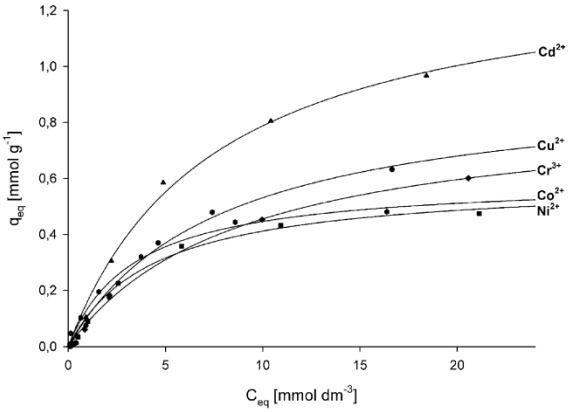

Fig. 6. Adsorption isotherms of metal ions by PMHS-*g*-PyPz(OEt)$_2$Allyl.

The Langmuir adsorption isotherm is mathematically expressed as:

$$\frac{C_{eq}}{q_{eq}} = \frac{C_{eq}}{q_m} + \frac{1}{Kq_m} \quad (3)$$

where the parameters of the equations are the following: K (dm^3 mol^{-1}) is the binding equilibrium constant, q_m (mmol g^{-1}) is the maximum amount of ions bonded, C_{eq} (mmol L^{-1}) is the equilibrium concentration of ions, and q_{eq} (mmol g^{-1}) is the amount of ions bonded at the concentration C_{eq} [44]. The Langmuir adsorption model assumes that the adsorbate forms a monolayer on a completely homogenous surface of the adsorbent. In addition, all other interactions between the adsorbed molecules are neglected. This empirical model assumes that the adsorbate forms a monolayer of one molecule thickness and the adsorption is possible only on a precise number of identical and equivalent adsorption sites. Because all sites have identical affinity to the adsorbate, this model is described as a homogenous adsorption with uniform energies [45]. The calculated K, q_m and correlation coefficient (R^2) values are given in Table 1. As follows from these data, PMHS-*g*-PyPzAllyl shows different binding capacities towards different metal ions. Very good complexation properties towards Cu^{2+} are a result of strong interactions between pyridine–pyrazole ligand and copper ion, which is in accordance with literature data [46]. Low complexation properties towards cadmium and nickel ions are a result of weak interactions in ligand–metal system but the origin of this effect has not been established yet. In PMHS-*g*-PyPzAllyl the ligand is connected to the polymer network by a relatively short linker, therefore the flexibility of the ligand groups is limited. Differences in the complexation properties can be explained by the differences in the coordination sphere geometry for the ions studied, which implies that in ligand system not all coordination centers are accessible. The PMHS-*g*-PyPz(OEt)$_2$Allyl polymer had better complexation properties towards cadmium, chromium and cobalt ion, but worse towards copper and nickel ion than PMHS-*g*-PyPzAllyl. The former polymer appeared more versatile in removal of metal ions than the latter, because the overall differences in the amounts of all metal ions adsorbed were lower. This observation can be explained by increasing flexibility of ligand groups, which can now adapt to coordination sphere geometries of different ions. Moreover, the oxygen atoms incorporated into the polymer system can form new coordination centers, which increases sorption capacity of the polymer obtained. The maximum amount of the ions bonded (q_m parameter) to both polymers obtained is similar to the values calculated in our previous work, in which we examined sorption properties of polysiloxane polymer containing polyamine groups [42]. Nevertheless, the binding equilibrium constant values (K parameter) are about an order of magnitude lower indicating that PMHS-*g*-PyPzAllyl and PMHS-*g*-PyPz(OEt)$_2$Allyl polymers form less stable complexes than the polymers previously obtained by our group.

The Freundlich adsorption isotherm is mathematically expressed as:

$$q_{eq} = K_f C_{eq}^{1/n} \quad (4)$$

$$\log\ q_{eq} = \log\ K_f + \frac{1}{n}\ \log\ C_{eq} \quad (5)$$

where K_f and n represent the Freundlich constants, C_{eq} (mmol L^{-1}) is the equilibrium concentration of the ions, and q_{eq} (mmol g^{-1}) is the amount of ions bonded at the concentration C_{eq}. The Freundlich adsorption model assumes non-ideal adsorption by formation of a multilayer of the adsorbate on a heterogeneous surface characterized by uniform energy. The $1/n$ value below one indicates a normal Langmuir isotherm, whereas $1/n$ above one indicates cooperative adsorption [47]. The K_f constant, which is related to the adsorption capacity, indicates that PMHS-*g*-PyPzAllyl polymer has high affinity to copper ion, whereas PMHS-*g*-PyPz(OEt)$_2$Allyl polymer has high affinity to cadmium and chromium ions [45]. All values calculated from Freundlich isotherm are given in Table 1.

The Temkin adsorption isotherm is mathematically expressed as:

$$q_{eq} = \frac{RT}{b}\ \ln\ (K_t C_{eq}) \quad (6)$$

$$q_{eq} = B\ \ln\ K_t + B\ \ln\ C_{eq} \quad (7)$$

where R is a gas constant, T is temperature, K_t is the equilibrium constant (L g^{-1}) related to the maximum binding energy and B is

Table 1
Parameters of metal ions adsorption by PMHS-*g*-PyPzAllyl and PMHS-*g*-PyPz(OEt)$_2$Allyl.

Polymer	Metal ion	Langmuir			Freundlich			Temkin		
		q_m (mmol g^{-1})	K (dm^3 mol^{-1})	R^2	K_f (mmol g^{-1} (L mmol^{-1})$^{1/n}$)	$1/n$	R^2	K_t (L g^{-1})	B (J mol^{-1})	R^2
PMHS-*g*-PyPzAllyl	Cu^{2+}	1.48	190	0.995	0.082	1.59	0.934	1.93	0.32	0.990
	Cd^{2+}	0.95	110	0.993	0.075	0.96	0.974	1.18	0.28	0.971
	Cr^{3+}	0.27	420	0.997	0.074	0.43	0.978	7.20	0.05	0.985
	Ni^{2+}	0.79	130	0.995	0.061	0.86	0.970	1.85	0.15	0.966
	Co^{2+}	0.24	410	0.964	0.070	0.90	0.980	2.07	0.17	0.967
PMHS-*g*-PyPz(OEt)$_2$Allyl	Cu^{2+}	1.06	100	0.966	0.079	0.86	0.982	1.93	0.17	0.963
	Cd^{2+}	1.24	190	0.998	0.087	1.48	0.968	1.94	0.26	0.980
	Cr^{3+}	0.90	100	0.977	0.064	1.59	0.990	3.20	0.13	0.941
	Ni^{2+}	0.58	230	0.991	0.075	0.99	0.989	2.40	0.13	0.987
	Co^{2+}	0.57	350	0.999	0.140	0.57	0.984	3.05	0.13	0.991

related to the heat of adsorption. The Temkin adsorption model assumes that the heat of adsorption of adsorbate molecules in a layer decreases linearly with increasing coverage which is caused by adsorbent–adsorbate interactions. Moreover, the bonding energies are distributed consistently up to some maximum binding energy. For all polymers and metal ions examined the values of K_t constants are of the same order of magnitude and are in the range 1.18–7.20 L g^{-1}. B values are also of the same order of magnitude and are in the range 0.13–0.32 J mol^{-1} indicating that the heat of adsorption is similar for all metal ions and polymers examined, except for adsorption of Cr^{3+} by PMHS-*g*-PyPzAllyl. In this case a lower value of 0.05 J mol^{-1} was obtained, however the origin of this effect is unclear. All values calculated from Temkin isotherm are given in Table 1.

3.2.2. Adsorption kinetics

Two kinetic models were considered to examine the mechanism of adsorption process. The first model applied was the pseudo-first-order model given by Langergren and Svenska [48] which can be expressed as:

$$\log\ (q_e - q_t) = \log\ q_e - \frac{k_1}{2.303} t \tag{8}$$

where q_e and q_t are the amounts of metal ions adsorbed (mmol g^{-1}) at equilibrium and at time t (h), respectively, and k_1 (h^{-1}) is the rate constant adsorption. Values of k_1 were calculated from the plots of log(q_e–q_t) versus t (Figs. S-5 and S-6 in Supporting Information). The R^2 values were relatively small proving that this model is inapplicable to describe the adsorption process of metal ions onto the polymers studied. The k_1 and R^2 values are given in Table 2.

The second model applied was the pseudo-second-order equation based on the equilibrium adsorption [49] which can be expressed as:

$$\frac{t}{q_t} = \frac{1}{k_2 q_e^2} + \frac{1}{q_e} t \tag{9}$$

where k_2 (g mmol^{-1} h^{-1}) is the rate constant of second-order adsorption. The linear plot of t/q_t versus t is shown in Figs. 7 and 8. The R^2 values are higher than 0.999 for all polymers and metal ions examined. This fact clearly indicates that this model is applicable to describe the adsorption process of metal ions onto the polymers obtained. The k_2 and R^2 values are given in Table 2.

The k_2 values characterizing adsorption of various metal ions on a particular polymer are similar in value. Moreover, the differences in k_2 values between the two polymers obtained are relatively small. This result means that the kinetic of sorption process is similar for all metal ions examined. The main reason for this phenomenon is probably related to the fact that sorption occurs in a two-phase system and the rate limiting step is the diffusion of ions from water solution into the organic phase. The formation of complex between polymer donor sites and metal ions is therefore a fast process because it occurs in a liquid phase.

Table 2
Pseudo-first-order and pseudo-second-order kinetic model parameters.

Polymer	Metal ion	Pseudo-first-order kinetic model		Pseudo-second-order kinetic model	
		k_1 (h^{-1})	R^2	k_2 (g mmol^{-1} h^{-1})	R^2
PMHS-*g*-PyPzAllyl	Cu^{2+}	2.50	0.958	60.28	0.999
	Cd^{2+}	3.20	0.957	43.99	0.999
	Cr^{3+}	0.68	0.689	43.29	0.999
	Ni^{2+}	0.97	0.921	33.38	0.999
	Co^{2+}	0.54	0.776	36.91	0.999
PMHS-*g*-PyPz(OEt)$_2$Allyl	Cu^{2+}	0.79	0.925	41.86	0.999
	Cd^{2+}	1.67	0.953	24.12	0.999
	Cr^{3+}	0.35	0.622	42.50	0.999
	Ni^{2+}	0.64	0.415	54.08	0.999
	Co^{2+}	0.54	0.678	39.21	0.999

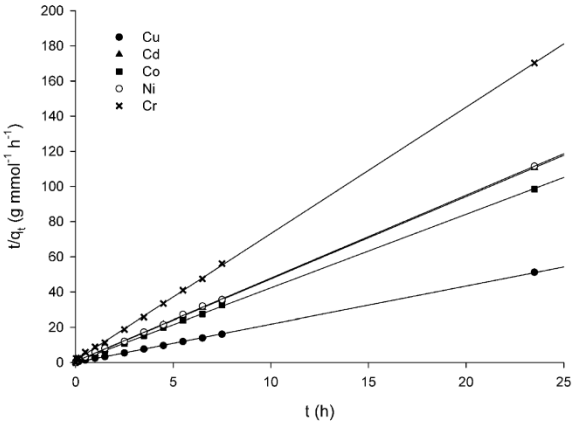

Fig. 7. Pseudo-second-order kinetics for adsorption of metal ions on PMHS-*g*-PyPzAllyl.

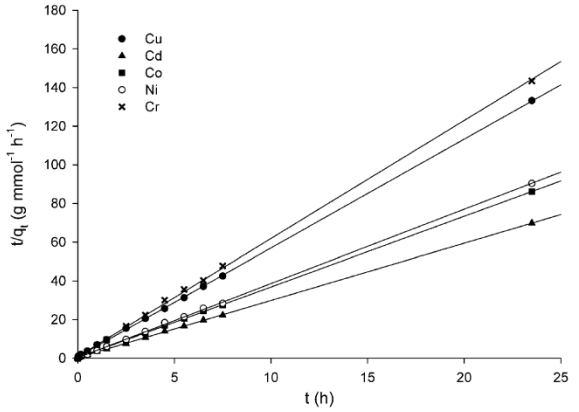

Fig. 8. Pseudo-second-order kinetics for adsorption of metal ions on PMHS-*g*-PyPz(OEt)$_2$Allyl.

3.2.3. Adsorption thermodynamics

In order to estimate the influence of temperature on the adsorption process, the thermodynamic parameters that must be considered are the changes in standard enthalpy ($\Delta H°$), standard entropy ($\Delta S°$) and Gibbs free energy ($\Delta G°$). The values of $\Delta H°$ and $\Delta S°$ were computed using the Eq. (10):

$$\ln\ K_d = \frac{\Delta S°}{R} - \frac{\Delta H°}{RT} \tag{10}$$

where R (8.314 J mol^{-1} K^{-1}) is the universal gas constant, T (K) is the solution temperature and K_d is the distribution coefficient which can be defined as:

$$K_d = \frac{C_{Ae}}{C_e} \tag{11}$$

where C_{Ae} is the amount adsorbed on solid (mmol g^{-1}) and C_e is the equilibrium concentration (mmol mL^{-1}). The values of $\Delta H°$ and $\Delta S°$

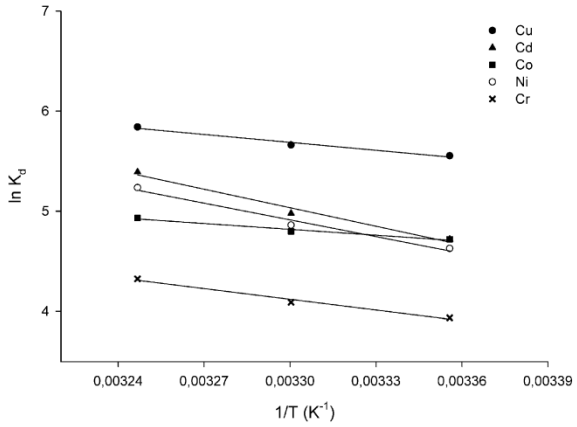

Fig. 9. Plot of $\ln K_d$ versus $1/T$ for adsorption of metal ions on PMHS-*g*-PyPzAllyl.

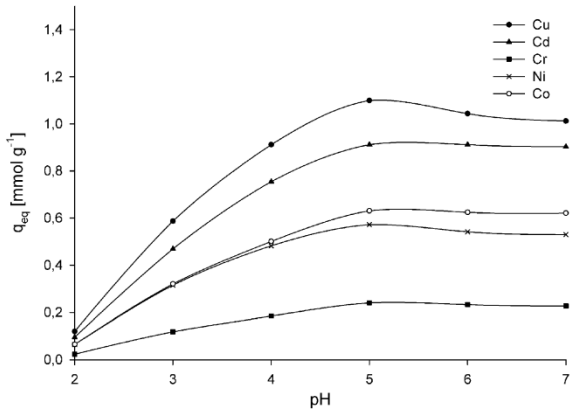

Fig. 11. The pH influence on the sorption ability of PMHS-*g*-PyPzAllyl.

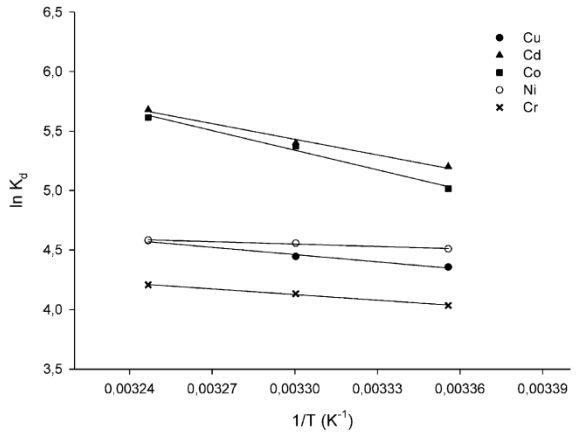

Fig. 10. Plot of $\ln K_d$ versus $1/T$ for adsorption of metal ions on PMHS-*g*-PyPz(OEt)$_2$Allyl.

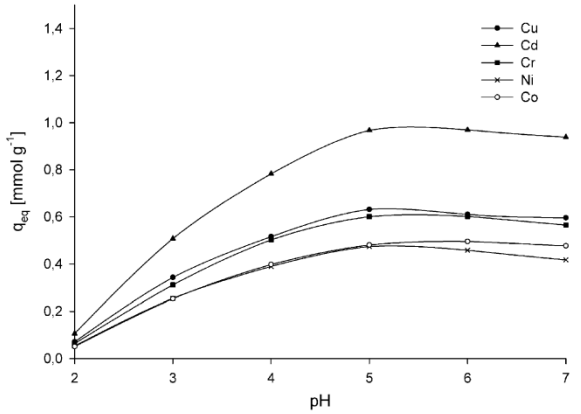

Fig. 12. The pH influence on the sorption ability of PMHS-*g*-PyPz(OEt)$_2$Allyl.

were calculated from the slope and intercept of the plot of $\ln K_d$ versus $1/T$ presented in Figs. 9 and 10. The value of ΔG° was calculated from Eq. (12):

$$\Delta G^\circ = -RT \ln K_d \quad (12)$$

The calculated values of ΔH°, ΔS° and ΔG° are listed in Table 3. It is worth noting that ΔH° values are positive, which means that the adsorption is an endothermic process. In addition, the ΔS° values are positive, suggesting that the adsorption is driven by entropy. These observations are in accordance with literature data [50]. The increase in randomness during the adsorption process is probably a result of the release of water molecules from the hydration shell [45]. Negative values of ΔG° indicate that the adsorption is a spontaneous process and the degree of spontaneity increases with temperature.

3.2.4. Influence of pH on adsorption

The influence of pH on q_{eq} of the polymers studied is illustrated in Figs. 11 and 12. At different pH values the protonation and

Table 3
Thermodynamic parameters for metal ion adsorption.

Polymer	Metal ion	ΔH° (kJ mol^{-1})	ΔS° (J mol^{-1} K^{-1})	ΔG° (kJ mol^{-1})		
				298 K	303 K	308 K
PMHS-*g*-PyPzAllyl	Cu^{2+}	21.85	119.38	−13.76	−14.26	−14.96
	Cd^{2+}	51.28	211.09	−11.69	−12.54	−13.81
	Cr^{3+}	29.62	131.99	−9.75	−10.30	−11.07
	Ni^{2+}	46.28	193.58	−11.47	−12.25	−13.41
	Co^{2+}	16.16	93.40	−11.69	−12.09	−12.63
PMHS-*g*-PyPz(OEt)$_2$Allyl	Cu^{2+}	16.92	92.92	−10.79	−11.20	−11.72
	Cd^{2+}	36.46	165.46	−12.89	−13.60	−14.54
	Cr^{3+}	13.15	77.69	−10.00	−10.41	−10.78
	Ni^{2+}	5.59	56.26	−11.17	−11.48	−11.73
	Co^{2+}	45.71	195.23	−12.43	−13.54	−14.37

Table 4
Values of q_{eq} for five cycles of sorption–desorption process.

Polymer	Cycle	q_{eq} (mmol g^{-1})				
		Cu^{2+}	Cd^{2+}	Cr^{3+}	Ni^{2+}	Co^{2+}
PMHS-*g*-PyPzAllyl	1	0.668	0.502	0.118	0.314	0.317
	2	0.662	0.498	0.117	0.307	0.313
	3	0.660	0.463	0.109	0.294	0.294
	4	0.657	0.463	0.109	0.286	0.292
	5	0.649	0.458	0.107	0.284	0.286
PMHS-*g*-PyPz(OEt)$_2$Allyl	1	0.379	0.603	0.180	0.351	0.328
	2	0.371	0.580	0.177	0.346	0.314
	3	0.369	0.562	0.174	0.342	0.310
	4	0.366	0.560	0.173	0.342	0.304
	5	0.360	0.558	0.173	0.340	0.301

Table 5
Comparison of metal ion concentration in wastewater sample before and after adding the polymer.

Metal ion	Wastewater sample (mmol L^{-1})	PMHS-*g*-PyPzAllyl (after treatment) (mmol L^{-1})	PMHS-*g*-PyPz(OEt)$_2$Allyl (after treatment) (mmol L^{-1})
Cu^{2+}	0.670	0.476	0.469
Cr^{3+}	0.787	0.522	0.493
Ni^{2+}	1.456	0.980	1.019

deprotonation of ligand groups would interfere with their structure. There are no significant differences in sorption properties of both polymers in the pH range 5–7. The protonation of ligand groups below pH 5 disturbs the interactions between metal ions and donor atoms. All ions are poorly adsorbed at pH lower than 3, which is probably caused by protonation of pyridine ring.

3.2.5. Adsorption–desorption

The results of adsorption capacity for five cycles are summarized in Table 4. The adsorption capacity does not change much for all adsorption/desorption cycles. After five cycles, both polymers obtained still retain above 90% of their initial adsorption capacity. The experimental results show that 0.1 M HCl can effectively desorb all cations examined from PMHS-*g*-PyPzAllyl as well as PMHS-*g*-PyPz(OEt)$_2$Allyl.

3.2.6. Treatment of real wastewater samples

Wastewater samples were obtained from PRESSEKO company, working on neutralization of hazardous wastes. The samples have high content of heavy metal ions because they are mixtures of wastes coming mainly from electrochemical processes. The wastewater of this type poses a serious threat to the environment and it is essential to design techniques that allow removal of heavy metal ions from it. Table 5 shows the concentration of heavy metal ions in the wastewater samples before and after the sorption process using PMHS-*g*-PyPzAllyl and PMHS-*g*-PyPz(OEt)$_2$Allyl. The results indicate, that the polymers obtained can effectively absorb heavy metal ions from wastewaters.

4. Conclusions

Two extractants were prepared by hydrosilylation reaction of polymethylhydrosiloxane with appropriate pyridine–pyrazole ligands catalyzed by platinum complex and their adsorption behavior towards Cu^{2+}, Cd^{2+}, Cr^{3+}, Ni^{2+} and Co^{2+} ions was investigated. The polymers were fully characterized by chemical and spectroscopic methods. The uptake capacities of the polymers obtained varied between 0.24 mmol (for Co^{2+}) and 1.48 mmol (for Cu^{2+}) per 1 g of polymer. The process of Cu^{2+}, Cd^{2+}, Cr^{3+}, Ni^{2+} and Co^{2+} ions adsorption onto the polymers obtained generally followed the Langmuir adsorption isotherm. The polymer with the shorter linker was more selective towards Cu^{2+} ion, while the one with the longer linker was more versatile in removal of metal ions. The adsorption kinetics was found to follow the pseudo-second-order kinetic model. The positive ΔH° value indicated the endothermic nature of the adsorption. The negative ΔG° value indicated that adsorption of metal ions was a spontaneous process, whereas the positive ΔS° values showed that the adsorption was driven by entropy. The adsorption properties of the materials obtained were worse towards metal ions at lower pH. The polymers obtained were characterized by satisfactory thermal and chemical stability. The polymers studied can be applicable for removal of metal ions from wastewaters.

Acknowledgement

This work was supported by the Polish National Science Center (NCN; Decision No. DEC-2012/05/N/ST5/01274).

Appendix A. Supplementary data

Supplementary data associated with this article can be found, in the online version, at http://dx.doi.org/10.1016/j.cej.2014.08.058.

References

[1] F. Çeçen, N. Semerci, A.G. Geyik, Inhibition of respiration and distribution of Cd, Pb, Hg, Ag and Cr species in a nitrifying sludge, J. Hazard. Mater. 178 (2010) 619–627.
[2] R.A. Anderson, Chromium as an essential nutrient for humans, Regul. Toxicol. Pharm. 26 (1997) S35–S41.
[3] D.A. Eastmond, J.T. MacGregor, R.S. Slesinski, Trivalent chromium: assessing the genotoxic risk of an essential trace element and widely used human and animal nutritional supplement, Crit. Rev. Toxicol. 38 (2008) 173–190.
[4] E. Denkhaus, K. Salnikow, Nickel essentiality, toxicity, and carcinogenicity, Crit. Rev. Oncol. Hematol. 42 (2002) 35–56.
[5] P. Gikas, Kinetic responses of activated sludge to individual and joint nickel (Ni(II)) and cobalt (Co(II)): an isobolographic approach, J. Hazard. Mater. 143 (2007) 246–256.
[6] D.G. Barceloux, D. Barceloux, Cobalt, Clin. Toxicol. 37 (1999) 201–216.
[7] M. Chiban, A. Soudani, F. Sinan, M. Persin, Single, binary and multi-component adsorption of some anions and heavy metals on environmentally friendly *Carpobrotus edulis* plant, Colloids Surf. B 82 (2011) 267–276.
[8] W. Ngeontae, W. Aeungmaitrepirom, T. Tuntulani, A. Imyim, Highly selective preconcentration of Cu(II) from seawater and water samples using amidoamidoxime silica, Talanta 78 (2009) 1004–1010.
[9] Ş. Turan, Ş. Tokalıoğlu, A. Şahan, C. Soykan, Synthesis, characterization and application of a chelating resin for solid phase extraction of some trace metal ions from water, sediment and tea samples, React. Funct. Polym. 72 (2012) 722–728.
[10] A. Adamczyk-Woźniak, Z. Brzózka, M.K. Cyrański, A. Filipowicz-Szymańska, P. Klimentowska, A. Zubrowska, K. Żukowski, A. Sporzyński, Ortho-(aminomethyl)phenylboronic acids—synthesis, structure and sugar receptor activity, Appl. Organomet. Chem. 22 (2008) 427–432.
[11] P. Rogowska, M.K. Cyrański, A. Sporzyński, A. Ciesielski, Evidence for strong heterodimeric interactions of phenylboronic acids with amino acids, Tetrahedron Lett. 47 (2006) 1389–1393.
[12] B. Gierczyk, M. Kazmierczak, G. Schroeder, A. Sporzynski, ^{17}O NMR studies of boronic acids and their derivatives, New J. Chem. 37 (2013) 1056–1072.
[13] A. Adamczyk-Woźniak, M. Jakubczyk, P. Jankowski, A. Sporzyński, P.M. Urbański, Influence of the diol structure on the Lewis acidity of phenylboronates, J. Phys. Org. Chem. 26 (2013) 415–419.
[14] J. Kurczewska, G. Schroeder, Epoxy resin modified with amine as an effective complexing agent of metal cations, Cent. Eur. J. Chem. 11 (2013) 1723–1728.
[15] M. Faisal, A.A. Ismail, F.A. Harraz, H. Bouzid, S.A. Al-Sayari, A. Al-Hajry, Mesoporous TiO_2 based optical sensor for highly sensitive and selective detection and preconcentration of Bi(III) ions, Chem. Eng. J. 243 (2014) 509–516.
[16] W. Wang, M. Chen, X. Chen, J. Wang, Thiol-rich polyhedral oligomeric silsesquioxane as a novel adsorbent for mercury adsorption and speciation, Chem. Eng. J. 242 (2014) 62–68.
[17] K.M. Diniz, F.A. Gorla, E.S. Ribeiro, M.B.O.d. Nascimento, R.J. Corrêa, C.R.T. Tarley, M.G. Segatelli, Preparation of $SiO_2/Nb_2O_5/ZnO$ mixed oxide by sol–gel method and its application for adsorption studies and on-line

preconcentration of cobalt ions from aqueous medium, Chem. Eng. J. 239 (2014) 233–241.
[18] M. Gurung, B.B. Adhikari, S. Alam, H. Kawakita, K. Ohto, K. Inoue, Persimmon tannin-based new sorption material for resource recycling and recovery of precious metals, Chem. Eng. J. 228 (2013) 405–414.
[19] I.V. Soares, E.G. Vieira, N.L.D. Filho, A.C. Bastos, N.C. da Silva, E.F. Garcia, L.J.A. Lima, Adsorption of heavy metal ions and epoxidation catalysis using a new polyhedral oligomeric silsesquioxane, Chem. Eng. J. 218 (2013) 405–414.
[20] C. Xiong, X. Chen, X. Liu, Synthesis, characterization and application of ethylenediamine functionalized chelating resin for copper preconcentration in tea samples, Chem. Eng. J. 203 (2012) 115–122.
[21] J. Kurczewska, G. Schroeder, Synthesis of silica chemically bonded with poly(ethylene oxide) 4-arm, amine-terminated for copper cation removal, Water Environ. Res. 82 (2010) 2387–2392.
[22] P. Rudnicki, Z. Hubicki, D. Kołodyńska, Evaluation of heavy metal ions removal from acidic waste water streams, Chem. Eng. J. 252 (2014) 362–373.
[23] Y. Qi, X. Jin, C. Yu, Y. Wang, L. Yang, Y. Li, A novel chelating resin containing high levels of sulfamine group: preparation and its adsorption characteristics towards p-toluenesulfonic acid and Hg(II), Chem. Eng. J. 233 (2013) 315–322.
[24] J. Gao, F. Liu, P. Ling, J. Lei, L. Li, C. Li, A. Li, High efficient removal of Cu(II) by a chelating resin from strong acidic solutions: complex formation and DFT certification, Chem. Eng. J. 222 (2013) 240–247.
[25] D. Kołodyńska, M. Gęca, M. Siek, Z. Hubicki, Nitrilotris(methylenephosphonic) acid as a complexing agent in sorption of heavy metal ions on ion exchangers, Chem. Eng. J. 215–216 (2013) 948–958.
[26] Y. Wang, X. Ma, Y. Li, X. Li, L. Yang, L. Ji, Y. He, Preparation of a novel chelating resin containing amidoxime–guanidine group and its recovery properties for silver ions in aqueous solution, Chem. Eng. J. 209 (2012) 394–400.
[27] S.-Y. Choi, V.T. Nguyen, J.-C. Lee, H. Kang, B.D. Pandey, Liquid–liquid extraction of Cd(II) from pure and Ni/Cd acidic chloride media using Cyanex 921: a selective treatment of hazardous leachate of spent Ni–Cd batteries, J. Hazard. Mater. 278 (2014) 258–266.
[28] E. Stanisz, A. Zgoła-Grześkowiak, H. Matusiewicz, Generation of volatile copper species after in situ ionic liquid formation dispersive liquid–liquid microextraction prior to atomic absorption spectrometric detection, Talanta 129 (2014) 254–262.
[29] A.M. Albu, M. Mocioi, C.D. Mateescu, A. Iosif, Maleic anhydride copolymers with ability to bind metal ions. 1. Polydentate amine derivatives for Cr(III) ions' removal, J. Appl. Polym. Sci. 121 (2011) 1867–1874.
[30] N. Van Nguyen, J.-c. Lee, J. Jeong, B.D. Pandey, Enhancing the adsorption of chromium(VI) from the acidic chloride media using solvent impregnated resin (SIR), Chem. Eng. J. 219 (2013) 174–182.
[31] R. Navarro, I. Saucedo, C. Gonzalez, E. Guibal, Amberlite XAD-7 impregnated with Cyphos IL-101 (tetraalkylphosphonium ionic liquid) for Pd(II) recovery from HCl solutions, Chem. Eng. J. 185–186 (2012) 226–235.
[32] K. Wieszczycka, M. Krupa, A. Wojciechowska, A. Olszanowski, Recovery of nickel(II) ions from sulphate/chloride solutions using hydrophobic pyridylketoximes, Solvent Extr. Ion Exch. 32 (2013) 267–280.
[33] A. Hawari, M. Khraisheh, M.A. Al-Ghouti, Characteristics of olive mill solid residue and its application in remediation of Pb^{2+}, Cu^{2+} and Ni^{2+} from aqueous solution: mechanistic study, Chem. Eng. J. 251 (2014) 329–336.
[34] A. Vani, V. Vyas, U. Sharma, Liquid–liquid extraction and transport of biologically important metal ions Li^{+}, K^{+}, Ca^{2+} and Mg^{2+} across an artificial liquid membrane system, Main Group Met. Chem. 34 (1–2) (2011) 29–31, http://dx.doi.org/10.1515/mgmc.2011.003.
[35] S. Memon, E. Akceylan, B. Sap, M. Tabakci, D.M. Roundhill, M. Yilmaz, Polymer supported calix[4]arene derivatives for the extraction of metals and dichromate anions, J. Polym. Environ. 11 (2003) 67–74.
[36] G. Barassi, A. Valdés, C. Araneda, C. Basualto, J. Sapag, C. Tapia, F. Valenzuela, Cr(VI) sorption behavior from aqueous solutions onto polymeric microcapsules containing a long-chain quaternary ammonium salt: kinetics and thermodynamics analysis, J. Hazard. Mater. 172 (2009) 262–268.
[37] F. Abbasi, H. Mirzadeh, A.-A. Katbab, Modification of polysiloxane polymers for biomedical applications: a review, Polym. Int. 50 (2001) 1279–1287.
[38] N.M. El-Ashgar, I.M. El-Nahhal, M.M. Chehimi, M. Delamar, F. Babonneau, J. Livage, Synthesis and structural characterization of a new macrocyclic polysiloxane-immobilized ligand system, Monatsh. Chem. 137 (2006) 263–275.
[39] N.M. El-Ashgar, I.M. El-Nahhal, M.M. Chehimi, F. Babonneau, J. Livage, A new route synthesis of immobilized-polysiloxane iminodiacetic acid ligand system, its characterization and applications, Mater. Lett. 61 (2007) 4553–4558.
[40] N. El-Ashgar, I. El-Nahhal, M. Chehimi, M. Delamar, F. Babonneau, J. Livage, Extraction of metal ions (Fe^{3+}, Co^{2+}, Ni^{2+}, Cu^{2+} and Zn^{2+}) using immobilized-polysiloxane iminobis(n-2-aminophenylacetamide) ligand system, J. Sol–Gel Sci. Technol. 41 (2007) 3–10.
[41] A. Amarasekara, O. Owereh, S. Aghara, Synthesis of functionalized polysiloxane 4-acylpyrazolone Schiff base ligand system and its applications in the adsorption of lanthanide ions from aqueous solutions, J. Sol–Gel Sci. Technol. 52 (2009) 382–387.
[42] B. Gierczyk, G. Schroeder, M. Cegłowski, New polymeric metal ion scavengers with polyamine podand moieties, React. Funct. Polym. 71 (2011) 463–479.
[43] S. Radi, Y. Toubi, A. Attayibat, M. Bacquet, New polysiloxane-chemically immobilized C,C-bipyrazolic receptor for heavy metals adsorption, J. Appl. Polym. Sci. 121 (2011) 1393–1399.
[44] R. Coşkun, C. Soykan, M. Saçak, Removal of some heavy metal ions from aqueous solution by adsorption using poly(ethylene terephthalate)-g-itaconic acid/acrylamide fiber, React. Funct. Polym. 66 (2006) 599–608.
[45] S.A. Ali, O.C.S. Al Hamouz, N.M. Hassan, Novel cross-linked polymers having pH-responsive amino acid residues for the removal of Cu^{2+} from aqueous solution at low concentrations, J. Hazard. Mater. 248–249 (2013) 47–58.
[46] S. Radi, A. Attayibat, A. Ramdani, Y. Lekchiri, B. Hacht, M. Bacquet, M. Morcellet, C,N-pyridylpyrazole-based ligands: synthesis and preliminary use in metal ion extraction, Sep. Sci. Technol. 42 (2007) 3493–3501.
[47] I.A.W. Tan, B.H. Hameed, A.L. Ahmad, Equilibrium and kinetic studies on basic dye adsorption by oil palm fibre activated carbon, Chem. Eng. J. 127 (2007) 111–119.
[48] S. Lagergren, B.R. Svenska, Zur theorie der sogenannten adsorption geloester stoffe, Veternskapsakad Handlinger 24 (1898) 1–39.
[49] Y.S. Ho, G. McKay, Sorption of dye from aqueous solution by peat, Chem. Eng. J. 70 (1998) 115–124.
[50] H.K. Boparai, M. Joseph, D.M. O'Carroll, Kinetics and thermodynamics of cadmium ion removal by adsorption onto nano zerovalent iron particles, J. Hazard. Mater. 186 (2011) 458–465.

Chemical Engineering Journal 263 (2015) 402–411

Contents lists available at ScienceDirect

Chemical Engineering Journal

journal homepage: www.elsevier.com/locate/cej

Preparation of porous resin with Schiff base chelating groups for removal of heavy metal ions from aqueous solutions

Michał Cegłowski *, Grzegorz Schroeder

Faculty of Chemistry, Adam Mickiewicz University in Poznan, Umultowska 89b, 61-614 Poznań, Poland

HIGHLIGHTS

- A new porous resin with Schiff base chelating groups was synthesized.
- Extraction of Cu^{2+}, Cd^{2+}, Cr^{3+}, Ni^{2+} and Co^{2+} from aqueous solution was examined.
- The process of metal ions adsorption generally followed the Langmuir model.
- The adsorption kinetics follow the pseudo-second-order kinetic model.
- The resin was effective for removal of heavy metal ions from wastewater samples.

GRAPHICAL ABSTRACT

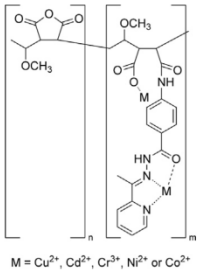

M = Cu^{2+}, Cd^{2+}, Cr^{3+}, Ni^{2+} or Co^{2+}

ARTICLE INFO

Article history:
Received 1 September 2014
Received in revised form 6 November 2014
Accepted 7 November 2014
Available online 15 November 2014

Keywords:
Chelating resin
Adsorption
Heavy metal ion
Schiff base
Functional polymer

ABSTRACT

A new chelating resin was synthesized in the reaction of poly(MVE-*alt*-MA) polymer with a Schiff base obtained in condensation of 2-acetylpyridine and 4-aminobenzoic hydrazide. Its composition, properties and morphology were characterized by Fourier transform infrared spectroscopy, elemental analysis, thermogravimetric analysis, derivative scanning calorimetry, scanning electron microscopy and N_2 sorptometry. The effects of several parameters that affect the adsorption of Cu^{2+}, Cd^{2+}, Cr^{3+}, Ni^{2+} and Co^{2+} including concentration, contact time, temperature and pH were examined. The adsorption capacity of the resin for the ions studied was found in the range 29.95–157.25 mg g^{-1}. The adsorption process of ions studied generally followed the Langmuir adsorption isotherm model. The kinetics of this process was found to follow the pseudo-second-order kinetic model. The changes in thermodynamic parameters, particularly in standard enthalpy ($\Delta H°$), standard entropy ($\Delta S°$) and Gibbs free energy ($\Delta G°$) were analyzed. The resin was found effective in removal of heavy metal ions from real wastewater samples that contained high concentrations of the above-mentioned ions.

1. Introduction

Removal of heavy metal ions from wastewater and contaminated soil is a matter of great importance because of their toxic effects on the human health and on the natural environment in general. Techniques such as adsorption, ion exchange, dialysis, precipitation and extraction have been widely used to purify water containing excessive amounts of heavy metal ions. Adsorption technique has received much attention because it allows the use of many materials that are environmental friendly and have low production cost [1–6]. Moreover, the adsorbents are easy to remove from a purified solution which considerably reduces the total cost of overall process. Recently, the design and synthesis of hybrid materials for removal and sensing of metal ions has become a subject of increasing interest. Particularly interesting is the synthesis of materials with magnetic properties that would allow their easy recollection and repeated use with low loss [7–12]. Carbon

* Corresponding author. Tel.: +48 618291486.
E-mail address: ceglowski.m@gmail.com (M. Cegłowski).

http://dx.doi.org/10.1016/j.cej.2014.11.047
1385-8947/

nanomaterials have been also used as an adsorbents, because of their high surface area for inorganic adsorption, excellent mechanical and thermal stability and exceptional water filtration capabilities. Interestingly, the weight loss of an adsorbent prepared from carbon nanotubes after many cycles of treatment is smaller when compared to that of the adsorbent made from activated carbon [13–15]. Zwitterionic hybrid polymers combine the advantages of organic and inorganic materials and also exhibit additional interesting properties, such as structural flexibility, thermal and mechanical stability. The pendant-side structure of ionic groups of the opposite signs on the polymer chains allows binding of heavy metal ions from solutions via electrostatic effect. This feature allows the use of materials of this type in the separation and recovery processes [16–18]. Chelating polymers possess functional groups that comprise one or more donor atoms acting as a ligands towards certain types of cations. These polymers usually show higher selectivity to metal cations than ionic polymers, therefore they have been used for transition metal ion separation [19–24].

Polymers that possess Schiff bases in their structure make an important group of chelating resins. Schiff bases that are built of nitrogen and oxygen donor atoms, are well known for their very good selectivity towards complexation of transition metals ions, and low affinity to alkali and alkaline earth metal ions. Moreover, many Schiff bases contain additional donor groups, which make them very good candidates for metal ion complexation. These Schiff bases can be obtained by simple self-condensation or even multiple self-condensation processes that take place in one synthetic step. Linking Schiff bases to polymers results in chelating resins that show well-defined molecular assemblies [25]. All these properties make Schiff base chelating resins very useful to removal of transition metal ions from solutions. Yan and Sun have prepared two novel chelating resins by anchoring diethylenetriamine bis- and mono-furaldehyde Schiff bases onto the macroporous GMA-DVB (glycidyl methacrylate-divinylbenzene) copolymer beads. These resins were used for the adsorption of Cu(II), Co(II), Ni(II) and Zn(II) ions [26]. Cross-linked magnetic chitosan-isatin Schiff's base resin was prepared and its usefulness in metal ion adsorption has been examined. The maximum adsorption capacities were 103.16, 53.51, and 40.15 mg/g for Cu^{2+}, Co^{2+} and Ni^{2+} ions, respectively. Cross-linked magnetic resin displayed higher adsorption capacity for Cu^{2+} in all pH ranges studied [27]. Duolite XAD 761 has been modified with 2-(2,4-dichlorobenzylideneamino) benzenethiol to produce a Schiff base containing a chelating resin. The material obtained was used for the sorption of Cr^{3+}, Co^{2+}, Cu^{2+}, Fe^{3+}, Ni^{2+}, and Zn^{2+} ions. A solid-phase extraction method based on the use of this new chelating resin has been applied to determine the contents of metals in real food samples [28]. Two chelating resins were synthesized by condensing Schiff bases derived from 2-aminophenol, 2-hydroxy-5-chloroaniline and terephthaldehyde with formaldehyde in an alkaline medium. The metal ion uptake of the resins was investigated by the batch method. The resins showed a preferential selectivity towards Cu(II) than Pb(II) metal ions [29]. Commercially available poly(vinyl chloride) has been synthetically modified to a polymer containing pendant primary amino groups. The amino polymer was reacted with salicylaldehyde to yield a Schiff-base chelating polymer. The polymer has been used to prepare polymer-supported copper complex which was a catalyst in the one-pot three-component Mannich reaction between aldehydes, ketones and anilines under mild and environmentally friendly conditions [30].

The aim of this study was to synthesize resin with Schiff base chelating groups and examine its effectiveness in heavy metal ion removal from aqueous solutions. To the best of our knowledge, this is the first study describing functionalization of poly(methyl vinyl ether-*alt*-maleic anhydride) with Schiff base and its use in adsorption of heavy metal ions. Moreover, the polymer obtained showed very interesting, porous structure, which can have additional impact on its adsorption properties. The influence of factors affecting the adsorption of Cu^{2+}, Cd^{2+}, Cr^{3+}, Ni^{2+} and Co^{2+} such as concentration, contact time, temperature and pH were investigated. The resin obtained was used to adsorb heavy metal ions from real wastewater samples.

2. Experimental

2.1. Materials and chemicals

All reagents used were commercial products. 2-Acetylpyridine, 4-aminobenzoic hydrazide, poly(methyl vinyl ether-*alt*-maleic anhydride) (poly(MVE-*alt*-MA)) of average M_w = 216,000 and metal perchlorates: $Cu(ClO_4)_2 \times 6H_2O$, $Cd(ClO_4)_2 \times 6H_2O$, $Cr(ClO_4)_3 \times 6H_2O$, $Ni(ClO_4)_2 \times 6H_2O$ and $Co(ClO_4)_2 \times 6H_2O$ obtained from Sigma–Aldrich (St. Louis, MO, USA). Anhydrous ethyl alcohol and all other solvents of the purity grade p.a., were purchased from POCH (Gliwice, Poland) and were used without further purification. Wastewater samples were obtained from PRESSEKO (Bolechowo near/Poznan, Poland) company.

2.2. Instruments

A Shimadzu AA-7000 atomic absorption spectrophotometer (Shimadzu, Japan) was used for determination of Cu^{2+}, Cd^{2+}, Cr^{3+}, Ni^{2+} and Co^{2+} concentrations. The measurement was performed in 3 replications, and the % RSD did not exceed 5%. The FTIR spectrum of the resin was recorded on a Bruker IFS 66s spectrometer (Billerica, MA, USA) using KBr pellets (about 1.5 mg of sample in 200 mg of KBr). NMR spectra were recorded on Agilent DD2 800 MHz (Santa Clara, California, USA). Elemental analyses were carried out on a Vario EL III Element Analyzer (Hanau, Germany). Thermal data were obtained by using a Setaram Setsys 1200 (Caluire, France). The thermal stability of the resin was investigated by thermogravimetric analysis and derivative scanning calorimetry in air stream at a heating rate of 5 °C min^{-1}. The pore structure of the resin obtained was characterized on the basis of low-temperature nitrogen adsorption–desorption isotherms measured on a sorptometer Quantachrome Autosorb iQ (Boynton Beach, Florida, USA). Surface area and pore size distribution were calculated by Brunauer–Emmett–Teller (BET) and Barrett–Joyner–Halenda (BJH) methods, respectively. Electron impact spectra were recorded using Bruker 320-MS spectrometer. The pH measurements were performed using Elmetron CP-505 apparatus (Zabrze, Poland) equipped with a combined pH electrode. Scanning electron microscopy images were obtained on a Hitachi Scanning Electron Microscope SU3500 (Tokyo, Japan).

2.3. Synthesis of acylhydrazone ligand (**1**)

Acylhydrazone ligand (**1**) was synthesized according to a literature method that was used to synthesize similar acylhydrazone ligands [31]. 2-Acetylpyridine (1.603 g, 13.23 mmol) was added to a solution of 4-aminobenzoic hydrazide (2.00 g, 13.23 mmol) in anhydrous ethanol (120 mL) and a few drops of concentrated hydrochloric acid were added. The solution was heated under reflux for 12 h. Upon overnight cooling, a bright yellow precipitate was recovered. The solid was filtered off, washed with cold ethanol and dried.

^{1}H NMR (DMSO-d6) δ: 2.42 (s, 3H); 5.86 (s, 2H); 6.66 (d, 2H); 7.59 (m, 1H); 7.62 (d, 2H); 7.81 (d, 1H); 8.11 (t, 1H); 8.91 (d, 1H). ^{13}C NMR (DMSO-d6) δ: 25.0; 116.3; 122.6; 123.3; 127.6; 131.9; 141,7; 144.5; 150.9; 155.8; 158.5; 165.8. EI-MS *m/z* (%):

65.0 (45.4); 77.9 (23.7); 91.9 (29.9); 105.9 (48.9); 119.9 (100); 133.9 (51.2); 254.1 (46.0).

2.4. Synthesis of poly(MVE-alt-MA-**1**)

Poly(methyl vinyl ether-*alt*-maleic anhydride) (0.8 g) was dissolved in toluene (15 mL) and added dropwise to a solution of ligand **1** (0.65 g, 2.56 mmol) in 40 mL of dimethylformamide (DMF). The mixture was subsequently stirred at 140 °C for 8 h in anhydrous atmosphere. Solvent was removed under reduced pressure and the residue obtained was washed with DMF, toluene, diethyl ether and dried at 80 °C yielding poly(MVE-*alt*-MA-**1**) as a pale brown powder.

2.5. Adsorption experiments

Adsorption studies were performed for $Cu(ClO_4)_2$, $Cd(ClO_4)_2$, $Cr(ClO_4)_3$, $Ni(ClO_4)_2$ and $Co(ClO_4)_2$. To prepare each isotherm, a series of samples containing 10 mg of poly(MVE-*alt*-MA-**1**) and 5 mL of metal perchlorate solution were used. The adsorption capacities were measured for seven different concentrations (0.1, 0.5, 1, 2.5, 5, 10 and 20 mM). The water solutions of metal ions were buffered to pH 5 (acetic acid/sodium acetate buffer). The solutions were stirred for 24 h at 298 ± 1 K. The starting (C_0; mg L^{-1}) and post-equilibration (C_{eq}; mg L^{-1}) concentrations of metal ions were measured by atomic absorption spectrophotometry. The amount of metal adsorbed (q_{eq}; mg g^{-1}) after equilibration was calculated from the difference between C_0 and C_{eq}:

$$q_{eq} = \frac{(C_0 - C_{eq})V}{m} \quad (1)$$

where m is the mass of resin (0.01 g) and V is the volume of aqueous solution (L).

For the adsorption kinetic studies, 20 mg of poly(MVE-*alt*-MA-**1**) and 20 mL of buffered (pH 5, acetic acid/sodium acetate buffer) metal perchlorate solution with the initial concentration of 5 mM were stirred at 298 ± 1 K. The aqueous samples were taken at preset time intervals and the concentrations of metal ions were measured by atomic absorption spectrophotometry. The amount of adsorbed metal ions at time t, q_t (mg g^{-1}), was calculated from:

$$q_t = \frac{(C_0 - C_t)V}{m} \quad (2)$$

where m is the mass of resin (0.01 g), C_0 (mg L^{-1}) is the initial metal ion concentration, C_t (mg L^{-1}) is the metal ion concentration at time t, V is the volume of aqueous solution (L).

Thermodynamic studies were performed for other sets of samples containing 10 mg of poly(MVE-*alt*-MA-**1**) and 5 mL of buffered (pH 5, acetic acid/sodium acetate buffer) metal perchlorate solution with the initial concentration of 5 mM; they were stirred at 298 ± 1 K, 308 ± 1 K and 323 ± 1 K for 24 h. Other experimental details were as for isotherms determination.

The relations between the sorption properties of poly(MVE-*alt*-MA-**1**) and the pH of the solution were studied in the pH range from 2 to 6. The pH of the solutions was adjusted with the buffers containing KCl/HCl (pH 2) and acetic acid/sodium acetate (pH 3–6). The measurements were made for 5 mM metal concentration, which guaranteed large excess of ions over ligand groups. Other experimental details were as for isotherms determination.

Sorption/desorption experiments were performed in 12 h intervals for the sets of samples containing 10 mg of poly(MVE-*alt*-MA-**1**) and 5 mL of buffered (pH 5, acetic acid/sodium acetate buffer) metal perchlorate solution at the initial concentration of 5 mM. Afterwards, the water phase was collected, the resin was washed with water and immersed in 0.1 M HCl or 0.1 M EDTA water solution. The starting and final concentrations of metal ions in aqueous phases were measured by atomic absorption spectrophotometry. To test the reusability of the polymers, this adsorption/desorption cycle was repeated five times with using the same adsorbent.

Experiments with real wastewater samples were performed by adding 2.5 mL of wastewater sample to 20 mg of poly(MVE-*alt*-MA-**1**). After stirring for 24 h the starting and final concentrations of metal ions in aqueous phases were measured by atomic absorption spectrophotometry.

3. Results and discussion

3.1. Synthesis and characterization of the resin obtained

The new chelating polymer was synthesized in two steps. In the first step, appropriate Schiff base ligand **1** was obtained in a simple condensation between 2-acetylpyridine and 4-aminobenzoic hydrazide. The second step consisted of reaction of ligand **1** with poly(MVE-*alt*-MA) polymer, resulting in formation of poly(MVE-*alt*-MA-**1**) chelating resin (reaction scheme is presented in Fig. 1). It is worth noting that not all maleic anhydride groups undergo amidation reaction [32]. The symbols m and n represent the numbers of modified and unmodified repeating unites of the polymer backbone, respectively. The values of m and n were estimated on the basis of elemental analysis. The following results were obtained (%): C, 58.82; H, 5.44; N, 8.90. The closest theoretical values were obtained using the model in which there are 7 unmodified maleic anhydride groups per 5 modified groups (n/m = 7/5). For this model, the calculated contents of elements were (in %): C, 58.81; H, 5.32; N, 8.91 which was in very good agreement with experimental data.

The FT-IR absorbance spectrum of poly(MVE-*alt*-MA-**1**) is presented in Fig. 2. The spectrum shows the absorption bands at 3379 cm^{-1} (ν O–H and ν COO–H, broad band), 2940 cm^{-1} (ν C–H), 1782 cm^{-1} (ν C=O of MA unit), 1730 cm^{-1} (ν C=O of carboxylic group), 1664 cm^{-1} (ν C=O of Schiff base), 1645 cm^{-1} (δ N–H), 1534 cm^{-1} (ν C=N), 1280 cm^{-1} (ν OC=OH of carboxylic group), 1104 cm^{-1} (ν C–O–C of MA unit) [33,34].

The results of thermogravimetric and differential scanning calorimetry (DSC) analysis of poly(MVE-*alt*-MA-**1**) are presented in Fig. 3. For the resin obtained, two decomposition steps can be observed. The first one gives a very broad signal, because it starts at around 150 °C and ends at 480 °C. This step is probably connected with continuous decomposition of the ligands by their slow oxidation. The second step is more rapid, it starts at 480 °C and ends at around 630 °C. During this step all organic residue is oxidized, because the initial mass of the resin is reduced to almost 0%. The DSC curve shows two exothermic effects with maxima at 330 °C and 535 °C. The first one corresponds to the broad decomposition step of poly(MVE-*alt*-MA-**1**). The second exothermic effect, which is significantly higher in amplitude than the first one, is related to the final decomposition step of the resin obtained.

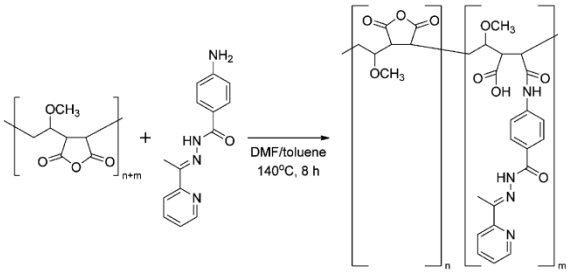

Fig. 1. Scheme of synthesis of poly(MVE-*alt*-MA-**1**) resin.

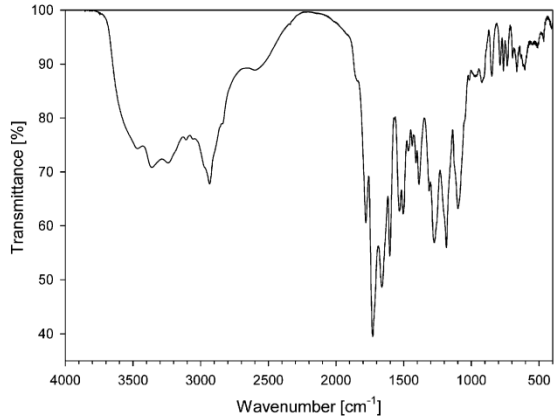

Fig. 2. FT-IR spectrum of poly(MVE-*alt*-MA-**1**) resin.

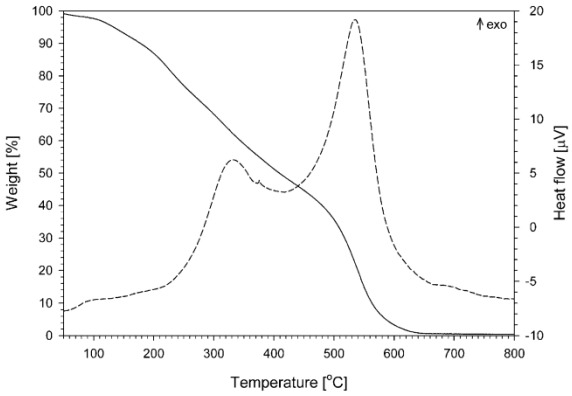

Fig. 3. TG (solid line) and DSC (dashed line) results of poly(MVE-*alt*-MA-**1**).

Fig. 4 shows the SEM images of poly(MVE-*alt*-MA-**1**). Many pores with a very wide distribution of diameters were found in the structure of the resin. The presence of these pores led to some increase in the surface area and porous structure of poly(MVE-*alt*-MA-**1**). To establish the porosity parameters a N_2 sorptometer was used. The BET surface area of the resin obtained was found to be 2.051 $m^2\ g^{-1}$, with total pore volume of 0.008 $cm^3\ g^{-1}$. The average pore diameter was found to be 4.45 nm. The surface area was relatively lower than for inorganic or hybrid adsorbents, but it was similar to that of other chelating polymers [35]. This indicates that adsorption of heavy metal ions is a result of strong chemical interactions between resins functional groups and these ions.

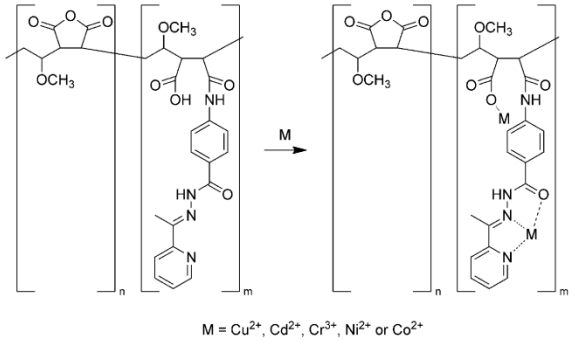

Fig. 5. The adsorption of metal ions on the poly(MVE-*alt*-MA-**1**) resin.

3.2. Adsorption isotherms

Adsorption isotherms are used to describe the adsorption process at the equilibrium state. The resin obtained may form complexes with heavy metal ions using Schiff base groups and free carboxyl groups (presented in Fig. 5). For metal ions adsorption studies, perchlorate salts were used because perchlorates are widely known to be very poor complexing agents which makes them useful as counter ions in the studies of metal cation chemistry. Moreover, perchlorates show also low reactivity as oxidants.

To fully understand the adsorption process, several different isotherm models were considered. Fitting experimental data to appropriate isotherm model is a very important step, because the results give information about the interactions of solutes with the adsorbent. Fig. 6 shows relationships between the equilibrium concentration of metal ions and the amount of metal adsorbed on poly(MVE-*alt*-MA-**1**). The adsorption rapidly increases at low concentrations of metal ions and starting from a certain concentration value it reaches a plateau. The Langmuir, Freundlich and Temkin isotherm models were used to interpret and evaluate the adsorption data from the experiments.

The Langmuir adsorption isotherm is mathematically expressed as:

$$\frac{C_{eq}}{q_{eq}} = \frac{C_{eq}}{q_m} + \frac{1}{Kq_m} \tag{3}$$

where K (L mg^{-1}) is the binding equilibrium constant, q_m (mg g^{-1}) is the maximum amount of ions bonded, C_{eq} (mg L^{-1}) is the equilibrium concentration of ions, and q_{eq} (mg g^{-1}) is the amount of ions bonded at the concentration C_{eq}. The calculated K, q_m and correlation coefficients (R^2) values are given in Table 1. The R^2 values for Cu^{2+}, Cd^{2+}, Ni^{2+} and Co^{2+} above 0.99 indicate that the data describing the adsorption of these cations on the resin obtained well fit the

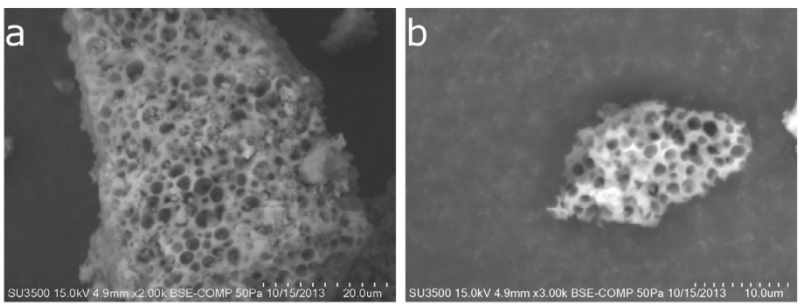

Fig. 4. SEM image of poly(MVE-*alt*-MA-**1**) magnified 2000× (a) and 3000× (b).

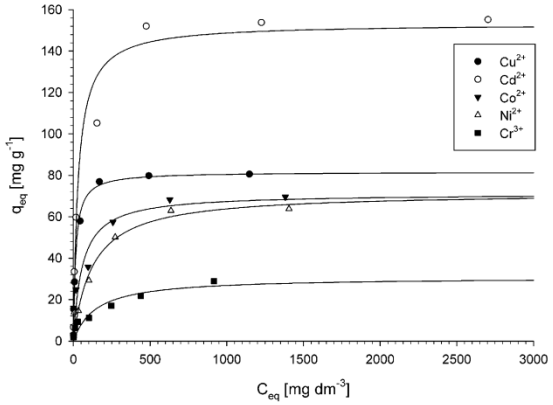

Fig. 6. Adsorption isotherms of metal ions onto poly(MVE-*alt*-MA-**1**).

Langmuir isotherm. The R^2 value for Cr^{3+} is above 0.95 indicating that the adsorption process partially follows the Langmuir model. The chelating polymer shows very good complexation properties towards Cu^{2+}, Cd^{2+}, Ni^{2+} and Co^{2+}, but relatively low towards Cr^{3+}. Low complexation properties towards chromium ions are probably a result of weak interactions between Cr^{3+} and ligands' donor atoms but the origin of this effect has not been established yet. The q_m values for Cu^{2+}, Cd^{2+}, Ni^{2+} and Co^{2+} after recalculation into mmol g^{-1} units for these ions are comparable. This indicates that the adsorption process is similar for Cu^{2+}, Cd^{2+}, Ni^{2+} and Co^{2+}, which is probably a result of the fact that binding efficiency of resins adsorption sites for these ions is similar. The selectivity of poly(MVE-*alt*-MA-**1**) towards heavy metal ions examined was investigated on the basis of the binding equilibrium constant (K parameter) [36]. The highest K value was obtained for Cu^{2+} ion, which means that poly(MVE-*alt*-MA-**1**) exhibits the highest selectivity towards this ion. K values for Cd^{2+} and Co^{2+} are similar and more than twice smaller than the value obtained for Cu^{2+} ion. This results indicates that the selectivity of poly(MVE-*alt*-MA-**1**) for Cd^{2+} and Co^{2+} adsorption is similar, but much lower than for Cu^{2+} ion. The lowest K values were obtained for Ni^{2+} and Cr^{3+} ions indicating, that the adsorption of these ions is the least favorable from among all ions examined.

The Freundlich adsorption isotherm is mathematically expressed as:

$$q_{eq} = K_f C_{eq}^{1/n} \tag{4}$$

$$\log q_{eq} = \log K_f + \frac{1}{n} \log C_{eq} \tag{5}$$

where K_f and n represent the Freundlich constants, C_{eq} (mg L^{-1}) is the equilibrium concentration of the ions, and q_{eq} (mg g^{-1}) is the amount of ions bonded at the concentration C_{eq}. The value of $1/n$ ranging between 0 and 1 is a measure of adsorption intensity or surface heterogeneity. The surface is more heterogeneous when the value of $1/n$ gets closer to zero [37]. A value of $1/n$ lower than one indicates a normal Langmuir isotherm, whereas a value above one is indicative of cooperative adsorption [38]. For all ions adsorbed on poly(MVE-*alt*-MA-**1**), the values if $1/n$ are very similar and lower than one. All values calculated from Freundlich isotherm are given in Table 1.

The Temkin adsorption isotherm is described by equations:

$$q_{eq} = \frac{RT}{b} \ln (K_t C_{eq}) \tag{6}$$

$$q_{eq} = B \ln K_t + B \ln C_{eq} \tag{7}$$

where R is a gas constant, T is temperature, K_t is the equilibrium constant (L g^{-1}) related to the maximum binding energy and B is related to the heat of adsorption. The Temkin adsorption model assumes that the heat of adsorption of the adsorbate molecules in a layer decreases linearly with increasing coverage which is caused by adsorbent–adsorbate interactions [39]. All values calculated from Temkin isotherm are given in Table 1.

3.3. Adsorption kinetics

To evaluate the kinetics of the adsorption process, the experimental results were compared to those predicted by three kinetic models, the pseudo-first-order, pseudo-second-order and the intraparticle diffusion. The pseudo-first-order model given by Langergren and Svenska [40] which can be expressed as:

$$\log (q_e - q_t) = \log q_e - \frac{k_1}{2.303} t \tag{8}$$

where q_e and q_t are the amounts of metal ions adsorbed (mg g^{-1}) at equilibrium and at time t (h), respectively, and k_1 (h^{-1}) is the pseudo-first-order rate constant. Values of k_1 were calculated from the plots of $\log(q_e - q_t)$ versus t (Fig. 7). The R^2 values are relatively high, however close inspection of the model fit and definitely higher values of R^2 obtained for pseudo-second-order kinetics suggest that the adsorption of metal ions on the resin obtained did not follow pseudo-first-order model kinetics. The k_1 and R^2 values are given in Table 2.

The pseudo-second-order equation based on the equilibrium adsorption [41] which can be expressed as:

$$\frac{t}{q_t} = \frac{1}{k_2 q_e^2} + \frac{1}{q_e} t \tag{9}$$

where k_2 (g mmol^{-1} h^{-1}) is the rate constant of second-order adsorption. The linear plot of t/q_t versus t is shown in Fig. 8. The correlation coefficients for all cations for the pseudo-second-order kinetic model were greater than 0.99 indicating the applicability of the pseudo-second-order kinetic model to describe the adsorption of metal ions onto poly(MVE-*alt*-MA-**1**). The k_2 and R^2 values are given in Table 2.

The intraparticle diffusion model is based on the theory proposed by Weber and Morris can be expressed as:

$$q_t = k_p t^{1/2} + x_i \tag{10}$$

Table 1
Parameters of metal ions adsorption by poly(MVE-*alt*-MA-**1**).

Metal ion	Langmuir			Freundlich			Temkin		
	q_m (mg g^{-1})	K (L mg^{-1})	R^2	K_f (mg g^{-1} (L mg^{-1})$^{1/n}$)	$1/n$	R^2	K_t (L g^{-1})	B	R^2
Cu^{2+}	81.72 ± 0.37	0.068 ± 0.010	0.999	7.79 ± 2.98	0.40 ± 0.09	0.813	1.89 ± 0.70	11.68 ± 0.99	0.965
Cd^{2+}	157.25 ± 1.41	0.031 ± 0.010	0.999	13.01 ± 4.37	0.37 ± 0.06	0.868	1.17 ± 0.47	20.87 ± 1.58	0.972
Cr^{3+}	29.97 ± 2.95	0.010 ± 0.004	0.953	2.05 ± 0.26	0.39 ± 0.03	0.976	0.57 ± 0.35	3.83 ± 0.61	0.885
Ni^{2+}	67.45 ± 2.55	0.013 ± 0.004	0.992	3.71 ± 1.03	0.43 ± 0.06	0.920	0.54 ± 0.22	9.41 ± 1.36	0.905
Co^{2+}	71.29 ± 1.98	0.026 ± 0.011	0.996	7.57 ± 1.68	0.34 ± 0.05	0.916	2.85 ± 1.39	8.21 ± 0.91	0.942

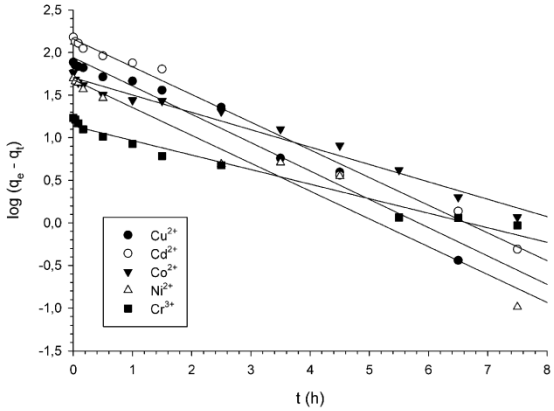

Fig. 7. Pseudo-first-order kinetic model for metal ion adsorption onto poly(MVE-*alt*-MA-**1**).

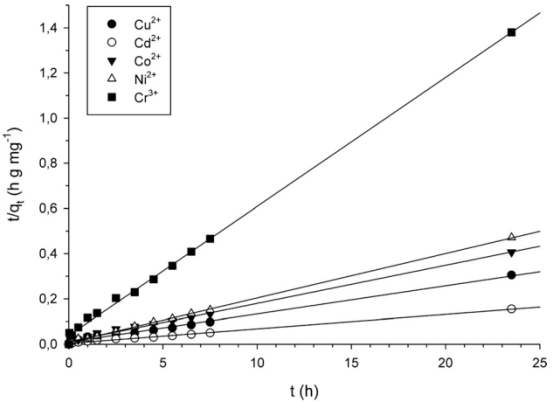

Fig. 8. Pseudo-second-order kinetic model for metal ion adsorption onto poly(-MVE-*alt*-MA-**1**).

where k_p (mg g^{-1} h$^{1/2}$) is the intraparticle diffusion rate constant and x_i is the intercept. This model assumes that the metal ions are transported from the solution through the interface between the solution and the adsorbent followed by a rate-limiting intraparticle diffusion step which brings them into the pores of the particles in the adsorbent [17]. If a straight line is obtained by plotting q_t versus $t^{1/2}$ than the intraparticle diffusion is considered as the rate-limiting step [42]. Usually a multilinear plot is obtained which suggests that two or more steps are involved in the adsorption process [43]. The plots presented in Fig. 9 suggest that the adsorption occurred in three phases. The initial steep section represents surface or film diffusion, the second one is connected with a gradual adsorption stage, where the rate-limiting step is intraparticle or pore diffusion, whereas the third section is the final equilibrium stage [44]. The plots do not pass through the origin of the system of coordinates, which means that the intraparticle diffusion within the pores of the resin is not the only rate-limiting step. This implies that adsorption kinetics may be limited simultaneously by the intraparticle diffusion and film diffusion. The value of intercept x_i gives the information about the boundary layer, that is the larger the intercept, the greater the boundary layer effect [45]. The k_p and x_i values are given in Table 2.

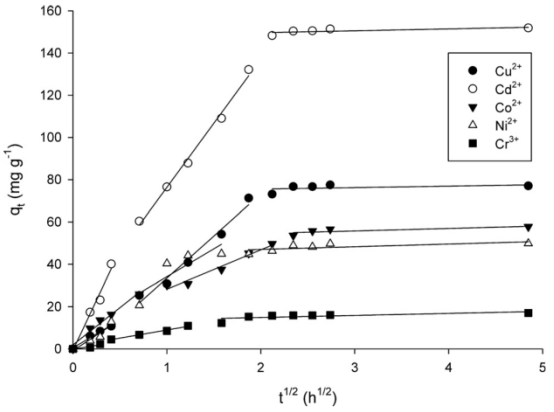

Fig. 9. Intraparticle diffusion plots for metal ion adsorption onto poly(MVE-*alt*-MA-**1**).

3.4. Adsorption thermodynamics

The heat of adsorption can provide information about the nature of the surface and the adsorbed phase. The thermodynamic parameters that must be considered are the changes in standard enthalpy ($\Delta H°$), standard entropy ($\Delta S°$) and Gibbs free energy ($\Delta G°$). The values of $\Delta H°$ and $\Delta S°$ were computed using the equation:

$$\ln K_d = \frac{\Delta S^\circ}{R} - \frac{\Delta H^\circ}{RT} \quad (11)$$

where R (8.314 J mol^{-1} K^{-1}) is the universal gas constant, T (K) is the solution temperature and K_d is the distribution coefficient which can be defined as:

$$K_d = \frac{C_{Ae}}{C_e} \quad (12)$$

where C_{Ae} is the amount adsorbed on solid (mg g^{-1}) and C_e is the equilibrium concentration (mg mL^{-1}). The values of $\Delta H°$ and $\Delta S°$ were calculated from the slope and intercept of the plot of $\ln K_d$ versus $1/T$ presented in Fig. 10. The value of $\Delta G°$ was calculated from Eq. (13):

$$\Delta G^{circ} = -RT \ln K_d \quad (13)$$

Table 2
Kinetic parameters calculated for pseudo-first-order, pseudo-second-order and intraparticle diffusion models.

Metal ion	Pseudo-first-order kinetic model		Pseudo-second-order kinetic model		Intraparticle diffusion model	
	k_1 (h^{-1})	R^2	k_2 (g mg^{-1} h^{-1})	R^2	k_p (mg g^{-1} h$^{1/2}$)	x_i
Cu^{2+}	0.766 ± 0.046	0.968	0.017 ± 0.003	0.993	19.21 ± 3.54	16.04 ± 7.40
Cd^{2+}	0.749 ± 0.022	0.993	0.012 ± 0.002	0.996	34.48 ± 6.28	41.94 ± 13.13
Cr^{3+}	0.393 ± 0.022	0.973	0.087 ± 0.012	0.998	3.82 ± 0.70	4.49 ± 1.47
Ni^{2+}	0.753 ± 0.055	0.963	0.053 ± 0.009	0.999	10.55 ± 2.64	17.69 ± 5.52
Co^{2+}	0.470 ± 0.021	0.977	0.026 ± 0.005	0.994	11.95 ± 1.84	17.03 ± 3.84

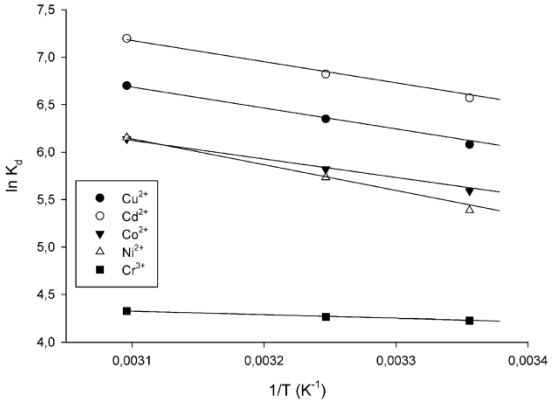

Fig. 10. Plot of $\ln K_d$ versus $1/T$ for adsorption of metal ions onto poly(MVE-*alt*-MA-**1**).

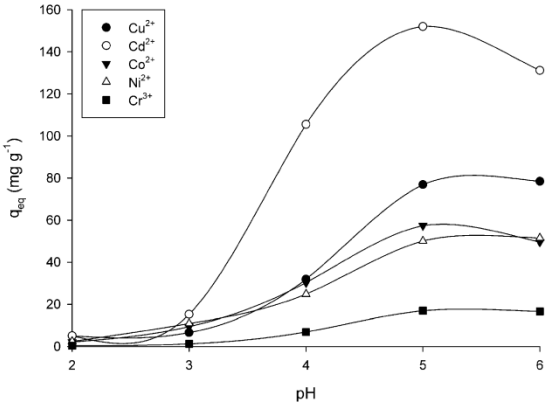

Fig. 11. The pH influence on the sorption ability of poly(MVE-*alt*-MA-**1**).

The calculated values of $\Delta H°$, $\Delta S°$ and $\Delta G°$ are listed in Table 3. The positive values of enthalpy changes $\Delta H°$ indicate that the adsorption is an endothermic process. The negative values of $\Delta G°$ prove that the adsorption of metal ions is a spontaneous process and the degree of spontaneity increases along with increasing temperature. The positive values of $\Delta S°$ suggest that randomness is increased at solid–liquid interface during the adsorption, which is probably a result of releasing water molecules from the hydration shell [17]. Thus, it can be concluded that the adsorption of metal ions onto poly(MVE-*alt*-MA-**1**) is driven by entropy.

3.5. Influence of pH on adsorption

The pH of aqueous solution is a very important factor that has a great impact on sorption of heavy metal ions. The influence of pH on q_{eq} of the resin studied is illustrated in Fig. 11. The structure of chelating groups can be changed by protonation at different pH values. In the pH range 5–6 there are only relatively small differences in sorption properties of the resin obtained. The protonation of chelating group below pH 5, which causes the repulsion of groups with positive charge, is the reason for poorer sorption properties of poly(MVE-*alt*-MA-**1**). At pH 2 the adsorption of metal ions is reduced to a minimum, which is probably caused by complete protonation of chelating groups.

3.6. Sorption/desorption experiments

The resin used for adsorption of metal ions must be capable of desorbing these ions in order to be reused. Moreover, it should not heavily lose adsorption properties after adsorption/desorption cycles. The results of adsorption capacity for five sorption/desorption cycles using 0.1 M HCl or 0.1 M EDTA as desorption agents are summarized in Table 5. In the sorption/desorption cycles of Cu^{2+}, Cd^{2+} and Co^{2+} using 0.1 M HCl as desorption agent, the adsorption capacity after first desorption with HCl rises by less than 20%. This phenomenon was explained by the fact that highly acidic environment causes hydrolysis of anhydride groups that remained in the polymer structure leading to formation of carboxylic groups. The additional presence of these groups after first desorption cycle leads to increased adsorption capacity of the poly(MVE-*alt*-MA-**1**) resin. The confirmation of this fact was that this phenomenon was not observed when 0.1 M EDTA solution was used as a desorption agent. For Cr^{3+} and Ni^{2+} ions, the increased capacity after

Table 4
The metal ion concentration in wastewater sample before and after the resin addition.

Metal ion	Wastewater sample (mg L^{-1})	Poly(MVE-*alt*-MA-**1**) (after treatment) (mg L^{-1})
Cu^{2+}	40.16	10.12
Cr^{3+}	13.60	9.95
Ni^{2+}	154.83	72.85

Table 5
Values of q_{eq} for five cycles of sorption/desorption of metal ions using 0.1 M HCl or 0.1 M EDTA as desorption agents.

Desorption agent	Cycle	q_{eq} (mg g^{-1})				
		Cu^{2+}	Cd^{2+}	Cr^{3+}	Ni^{2+}	Co^{2+}
HCl	1	72.08	120.17	17.61	46.14	51.05
	2	84.01	140.70	16.93	44.90	62.15
	3	82.97	135.57	16.65	44.65	59.27
	4	80.55	132.92	16.50	43.74	56.51
	5	78.56	132.30	15.99	42.50	55.96
EDTA	1	72.45	119.29	17.56	46.47	51.05
	2	71.16	115.96	16.65	44.40	50.59
	3	72.36	115.00	16.13	43.38	45.43
	4	67.38	110.04	15.72	42.63	44.72
	5	65.24	107.08	15.66	42.63	44.52

Table 3
Thermodynamic parameters obtained for process of metal ion adsorption.

Metal ion	$\Delta H°$ (kJ mol^{-1})	$\Delta S°$ (J mol^{-1} K^{-1})	$\Delta G°$ (kJ mol^{-1})		
			298 K	308 K	323 K
Cu^{2+}	19.84 ± 0.37	117.15 ± 1.20	−15.06 ± 0.51	−16.26 ± 0.52	−17.99 ± 0.54
Cd^{2+}	20.11 ± 0.47	122.07 ± 1.51	−16.28 ± 0.65	−17.47 ± 0.66	−19.33 ± 0.68
Cr^{3+}	3.28 ± 0.10	46.13 ± 0.33	−10.47 ± 0.14	−10.92 ± 0.14	−11.62 ± 0.15
Ni^{2+}	24.44 ± 0.96	126.89 ± 3.10	−13.35 ± 1.30	−14.68 ± 1.40	−16.52 ± 1.46
Co^{2+}	17.55 ± 0.05	105.39 ± 0.16	−13.85 ± 0.07	−14.90 ± 0.07	−16.49 ± 0.07

Table 6
Comparison of maximum sorption capacities with results of recent studies.

M^{n+}	Adsorbent	Sorption capacity (mg g^{-1})	References
Cu^{2+}	Silica gel functionalized with ditopic zwitterionic Schiff base ligand	41.31	[46]
	Dowex M-4195	50.77	[47]
	CS-zeolite composite cross-linked with ECH	51.32	[48]
	Poly(MVE-*alt*-MA-**1**)	81.72	Present study
Cd^{2+}	SiO_2/lignin	84.66	[49]
	Fe_3O_4-poly(L-cysteine/2-hydroxyethyl acrylate)	19.59	[50]
	Steel-making slag	10.16	[51]
	Poly(MVE-*alt*-MA-**1**)	157.25	Present study
Cr^{3+}	Mn_3O_4 nanomaterial	41.7	[52]
	Laminaria seaweed biosorbent	41	[53]
	Algal biomass *spirogyra* spp.	28.16	[54]
	Poly(MVE-*alt*-MA-**1**)	29.97	Present study
Ni^{2+}	Cellulose acetate/zeolite composite fiber	16.95	[55]
	NaA/xanthan gum–alginate composite	45.87	[56]
	Poly(styrene-*co*-maleic anhydride) microspheres	47.9	[57]
	Poly(MVE-*alt*-MA-**1**)	67.45	Present study
Co^{2+}	Activated carbons	65.79	[58]
	Magnetic multiwalled carbon nanotube/iron oxide composites	8.84	[59]
	Ammonium molybdophosphate–polyacrylonitrile	9.43	[60]
	Poly(MVE-*alt*-MA-**1**)	71.29	Present study

desorption with HCl was not observed, which is probably caused by weaker interactions of carboxyl groups that were formed in the polymer structure with these ions. After five cycles, the poly(MVE-*alt*-MA-**1**) resin still retained above 87% of its initial adsorption capacity for all ions examined. This proves that the resin can be efficiently used in continuous sorption/desorption processes.

3.7. Treatment of real wastewater samples

Wastewater samples were obtained from PRESSEKO Company, which neutralizes hazardous wastes. The samples obtained contained very high concentrations of heavy metal ions because they came from wastes produced during electrochemical processes. Most of the heavy metal ions were introduced into this wastewater by dissolving simple inorganic salts like chlorides, sulfates or nitrates. Chromium was present in the mixture as Cr^{3+} ions, because the wastewater with these ions was produced during trivalent chromium plating. It is essential to decrease the concentration of heavy metal ions to acceptable levels before returning the water into the ecosystem. Table 4 shows the concentration of heavy metal ions in the wastewater samples before and after the sorption process using poly(MVE-*alt*-MA-**1**). The results clearly show that the resin obtained can be successfully used to absorb heavy metal ions from wastewaters.

3.8. Comparison of the maximum sorption capacities with other adsorbents

A comparison of the maximum sorption capacities with some recent results obtained using different types of adsorbent, is presented in Table 6. The maximum sorption capacities of the present chelating resin are greater for Cu^{2+}, Cd^{2+}, Ni^{2+} and Co^{2+} ions than for other materials listed in Table 6. This clearly illustrates that the chelating resin obtained can be used as a very efficient adsorbent of these ions. For Cr^{3+} ions the resin obtained has generally lower maximum sorption capacity than the other materials listed in Table 6. This is in accordance with the general adsorption properties of the resin obtained, because it shows very good complexation properties towards Cu^{2+}, Cd^{2+}, Ni^{2+} and Co^{2+}, but relatively low towards Cr^{3+}. The poly(MVE-*alt*-MA-**1**) resin is therefore a poor adsorbent of Cr^{3+} ions.

4. Conclusions

New chelating resin poly(MVE-*alt*-MA-**1**) was prepared in the reaction of poly(MVE-*alt*-MA) polymer with an appropriate Schiff base obtained in condensation of 2-acetylpyridine and 4-aminobenzoic hydrazide. The resin obtained was characterized by chemical and spectroscopic methods and showed satisfactory thermal and chemical stabilities. The resins adsorption behavior towards Cu^{2+}, Cd^{2+}, Cr^{3+}, Ni^{2+} and Co^{2+} ions was investigated. The process of Cu^{2+}, Cd^{2+}, Cr^{3+}, Ni^{2+} and Co^{2+} ions adsorption generally followed the Langmuir adsorption isotherm model. The adsorption kinetics was found to follow the pseudo-second-order kinetic model and to be controlled both by intraparticle diffusion and film diffusion. The negative $\Delta G°$ values but positive $\Delta H°$ and $\Delta S°$ values indicated that the adsorption of metal ions was a spontaneous process driven by entropy. The adsorption properties of the resin were worse at lower pH. The poly(MVE-*alt*-MA-**1**) was effective for removal of heavy metal ions from real wastewater samples that contained high concentrations of these ions. This clearly indicates that the resin obtained may be successfully used for purification of wastewaters highly contaminated with heavy metal ions.

Acknowledgements

This work was supported by the Polish National Science Center (NCN; decision no. DEC-2012/05/N/ST5/01274).

Scanning electron microscope surface analysis was carried out thanks to the laboratory of Adam Mickiewicz University Foundation in Poznań, established within the project WND-POIG.05.01.00-00-058/2011 "Waste Cluster – raising the standards of waste management using new technologies". The project is co-financed by the European Union from the European Regional Development Fund.

The authors thank PRESSEKO Company for providing samples of hazardous wastes.

References

[1] M. Chiban, A. Soudani, F. Sinan, M. Persin, Single, binary and multi-component adsorption of some anions and heavy metals on environmentally friendly *Carpobrotus edulis* plant, Colloids Surf. B 82 (2011) 267–276.
[2] G.Z. Kyzas, M. Kostoglou, N.K. Lazaridis, D.A. Lambropoulou, D.N. Bikiaris, Environmental friendly technology for the removal of pharmaceutical

contaminants from wastewaters using modified chitosan adsorbents, Chem. Eng. J. 222 (2013) 248–258.
[3] V.K. Gupta, M.R. Ganjali, A. Nayak, B. Bhushan, S. Agarwal, Enhanced heavy metals removal and recovery by mesoporous adsorbent prepared from waste rubber tire, Chem. Eng. J. 197 (2012) 330–342.
[4] F. Ciesielczyk, P. Bartczak, K. Wieszczycka, K. Siwińska-Stefańska, M. Nowacka, T. Jesionowski, Adsorption of Ni(II) from model solutions using co-precipitated inorganic oxides, Adsorption 19 (2013) 423–434.
[5] P. Rudnicki, Z. Hubicki, D. Kołodyńska, Evaluation of heavy metal ions removal from acidic waste water streams, Chem. Eng. J. 252 (2014) 362–373.
[6] D. Kołodyńska, M. Kowalczyk, Z. Hubicki, Evaluation of iron-based hybrid materials for heavy metal ions removal, J. Mater. Sci. 49 (2014) 2483–2495.
[7] J. Gómez-Pastora, E. Bringas, I. Ortiz, Recent progress and future challenges on the use of high performance magnetic nano-adsorbents in environmental applications, Chem. Eng. J. 256 (2014) 187–204.
[8] L. Zhou, S. Pan, X. Chen, Y. Zhao, B. Zou, M. Jin, Kinetics and thermodynamics studies of pentachlorophenol adsorption on covalently functionalized Fe_3O_4@SiO_2–MWCNTs core–shell magnetic microspheres, Chem. Eng. J. 257 (2014) 10–19.
[9] C. Zhang, C. Shan, Y. Jin, M. Tong, Enhanced removal of trace arsenate by magnetic nanoparticles modified with arginine and lysine, Chem. Eng. J. 254 (2014) 340–348.
[10] H. Alijani, M.H. Beyki, Z. Shariatinia, M. Bayat, F. Shemirani, A new approach for one step synthesis of magnetic carbon nanotubes/diatomite earth composite by chemical vapor deposition method: application for removal of lead ions, Chem. Eng. J. 253 (2014) 456–463.
[11] J. Kurczewska, G. Schroeder, U. Narkiewicz, Copper removal by carbon nanomaterials bearing cyclam-functionalized silica, Cent. Eur. J. Chem. 8 (2010) 341–346.
[12] J. Kurczewska, G. Schroeder, U. Narkiewicz, Adsorption of metal ions on magnetic carbon nanomaterials bearing chitosan-functionalized silica, Int. J. Mater. Res. 101 (2010) 1543–1547.
[13] W.-L. Sun, J. Xia, Y.-C. Shan, Comparison kinetics studies of Cu(II) adsorption by multi-walled carbon nanotubes in homo and heterogeneous systems: effect of nano-SiO_2, Chem. Eng. J. 250 (2014) 119–127.
[14] M. Hadavifar, N. Bahramifar, H. Younesi, Q. Li, Adsorption of mercury ions from synthetic and real wastewater aqueous solution by functionalized multi-walled carbon nanotube with both amino and thiolated groups, Chem. Eng. J. 237 (2014) 217–228.
[15] C. Luo, R. Wei, D. Guo, S. Zhang, S. Yan, Adsorption behavior of MnO_2 functionalized multi-walled carbon nanotubes for the removal of cadmium from aqueous solutions, Chem. Eng. J. 225 (2013) 406–415.
[16] J. Liu, Y. Ma, T. Xu, G. Shao, Preparation of zwitterionic hybrid polymer and its application for the removal of heavy metal ions from water, J. Hazard. Mater. 178 (2010) 1021–1029.
[17] S.A. Ali, O.C.S. Al Hamouz, N.M. Hassan, Novel cross-linked polymers having pH-responsive amino acid residues for the removal of Cu^{2+} from aqueous solution at low concentrations, J. Hazard. Mater. 248–249 (2013) 47–58.
[18] J. Liu, Y. Ma, Y. Zhang, G. Shao, Novel negatively charged hybrids. 3. Removal of Pb^{2+} from aqueous solution using zwitterionic hybrid polymers as adsorbent, J. Hazard. Mater. 173 (2010) 438–444.
[19] C. Sun, G. Zhang, R. Qu, Y. Yu, Removal of transition metal ions from aqueous solution by crosslinked polystyrene-supported bis-8-oxyquinoline-terminated open-chain crown ethers, Chem. Eng. J. 170 (2011) 250–257.
[20] H. Bessbousse, J.-F. Verchère, L. Lebrun, Characterisation of metal-complexing membranes prepared by the semi-interpenetrating polymer networks technique. Application to the removal of heavy metal ions from aqueous solutions, Chem. Eng. J. 187 (2012) 16–28.
[21] L. Yang, Y. Li, X. Jin, Z. Ye, X. Ma, L. Wang, Y. Liu, Synthesis and characterization of a series of chelating resins containing amino/imino-carboxyl groups and their adsorption behavior for lead in aqueous phase, Chem. Eng. J. 168 (2011) 115–124.
[22] H. Bessbousse, T. Rhlalou, J.F. Verchère, L. Lebrun, Mercury removal from wastewater using a poly(vinylalcohol)/poly(vinylimidazole) complexing membrane, Chem. Eng. J. 164 (2010) 37–48.
[23] C. Xiong, C. Yao, Synthesis, characterization and application of triethylenetetramine modified polystyrene resin in removal of mercury, cadmium and lead from aqueous solutions, Chem. Eng. J. 155 (2009) 844–850.
[24] H.-T. Fan, J.-X. Liu, H. Yao, Z.-G. Zhang, F. Yan, W.-X. Li, Ionic imprinted silica-supported hybrid sorbent with an anchored chelating schiff base for selective removal of cadmium(II) ions from aqueous media, Ind. Eng. Chem. Res. 53 (2013) 369–378.
[25] P.A. Vigato, S. Tamburini, The challenge of cyclic and acyclic schiff bases and related derivatives, Coord. Chem. Rev. 248 (2004) 1717–2128.
[26] X. Yan, W. Sun, Synthesis and metal ion adsorption studies of chelating resins derived from macroporous glycidyl methacrylate-divinylbenzene copolymer beads anchored schiff bases, J. Appl. Polym. Sci. 117 (2010) 953–959.
[27] M. Monier, D.M. Ayad, Y. Wei, A.A. Sarhan, Adsorption of Cu(II), Co(II), and Ni(II) ions by modified magnetic chitosan chelating resin, J. Hazard. Mater. 177 (2010) 962–970.
[28] F. Marahel, M. Ghaedi, M. Montazerozohori, M. Nejati Biyareh, S. Nasiri Kokhdan, M. Soylak, Solid-phase extraction and determination of trace amount of some metal ions on Duolite XAD 761 modified with a new Schiff base as chelating agent in some food samples, Food Chem. Toxicol. 49 (2011) 208–214.
[29] M.K. Othman, F.A. Al-Qadri, F.A. Al-Yusufy, Synthesis, physical studies and uptake behavior of: copper(II) and lead(II) by Schiff base chelating resins, Spectrochim. Acta A 78 (2011) 1342–1348.
[30] G.R. Krishnan, M.K. Sreeraj, K. Sreekumar, Modification of poly(vinyl chloride) with pendant metal complex for catalytic applications, C. R. Chim. 16 (2013) 736–741.
[31] S. Choudhary, J.R. Morrow, Dynamic acylhydrazone metal ion complex libraries: a mixed-ligand approach to increased selectivity in extraction, Angew. Chem. Int. Ed. 41 (2002) 4096–4098.
[32] V.K. Sachan, A. Devi, R.S. Katiyar, R.K. Nagarale, P.K. Bhattacharya, Proton transport properties of sulphanilic acid tethered poly(methyl vinyl ether-alt-maleic anhydride)-PVA blend membranes, Eur. Polym. J. 56 (2014) 45–58.
[33] M.M. Andrade, M.T. Barros, Fast synthesis of N-acylhydrazones employing a microwave assisted neat protocol, J. Comb. Chem. 12 (2010) 245–247.
[34] H. Mazi, A.L.I. Gulpinar, Cu(II), Zn(II) and Mn(II) complexes of poly(methyl vinyl ether-alt-maleic anhydride). Synthesis, characterization and thermodynamic parameters, J. Chem. Sci. (Bangalore, India) 126 (2014) 239–245.
[35] M. Monier, D.A. Abdel-Latif, Modification and characterization of PET fibers for fast removal of Hg(II), Cu(II) and Co(II) metal ions from aqueous solutions, J. Hazard. Mater. 250–251 (2013) 122–130.
[36] M.A. Hussein, H.M. Marwani, K.A. Alamry, A.M. Asiri, S.A. El-Daly, Surface selectivity competition of newly synthesized polyarylidene(keto amine) polymers toward different metal ions, J. Appl. Polym. Sci. 131 (2014). n/a-n/a.
[37] F. Haghseresht, G.Q. Lu, Adsorption characteristics of phenolic compounds onto coal-reject-derived adsorbents, Energy Fuels 12 (1998) 1100–1107.
[38] K. Fytianos, E. Voudrias, E. Kokkalis, Sorption–desorption behaviour of 2,4-dichlorophenol by marine sediments, Chemosphere 40 (2000) 3–6.
[39] M. Hosseini, S.F.L. Mertens, M. Ghorbani, M.R. Arshadi, Asymmetrical Schiff bases as inhibitors of mild steel corrosion in sulphuric acid media, Mater. Chem. Phys. 78 (2003) 800–808.
[40] S. Lagergren, B.R. Svenska, Zur theorie der sogenannten adsorption geloester stoffe, Veternskapsakad Handlinger 24 (1898) 1–39.
[41] Y.S. Ho, G. McKay, Sorption of dye from aqueous solution by peat, Chem. Eng. J. 70 (1998) 115–124.
[42] S.I.H. Taqvi, S.M. Hasany, M.I. Bhanger, Sorption profile of Cd(II) ions onto beach sand from aqueous solutions, J. Hazard. Mater. 141 (2007) 37–44.
[43] F.-C. Wu, R.-L. Tseng, R.-S. Juang, Initial behavior of intraparticle diffusion model used in the description of adsorption kinetics, Chem. Eng. J. 153 (2009) 1–8.
[44] H.K. Boparai, M. Joseph, D.M. O'Carroll, Kinetics and thermodynamics of cadmium ion removal by adsorption onto nano zerovalent iron particles, J. Hazard. Mater. 186 (2011) 458–465.
[45] D. Kavitha, C. Namasivayam, Experimental and kinetic studies on methylene blue adsorption by coir pith carbon, Bioresour. Technol. 98 (2007) 14–21.
[46] Q. Wang, W. Gao, Y. Liu, J. Yuan, Z. Xu, Q. Zeng, Y. Li, M. Schröder, Simultaneous adsorption of Cu(II) and SO_4^{2-} ions by a novel silica gel functionalized with a ditopic zwitterionic Schiff base ligand, Chem. Eng. J. 250 (2014) 55–65.
[47] J. Gao, F. Liu, P. Ling, J. Lei, L. Li, C. Li, A. Li, High efficient removal of Cu(II) by a chelating resin from strong acidic solutions: complex formation and DFT certification, Chem. Eng. J. 222 (2013) 240–247.
[48] W.S. Wan Ngah, L.C. Teong, R.H. Toh, M.A.K.M. Hanafiah, Comparative study on adsorption and desorption of Cu(II) ions by three types of chitosan–zeolite composites, Chem. Eng. J. 223 (2013) 231–238.
[49] Ł. Klapiszewski, P. Bartczak, M. Wysokowski, M. Jankowska, K. Kabat, T. Jesionowski, Silica conjugated with kraft lignin and its use as a novel 'green' sorbent for hazardous metal ions removal, Chem. Eng. J. 260 (2015) 684–693.
[50] R. Hua, Z. Li, Sulfhydryl functionalized hydrogel with magnetism: synthesis, characterization, and adsorption behavior study for heavy metal removal, Chem. Eng. J. 249 (2014) 189–200.
[51] J. Duan, B. Su, Removal characteristics of Cd(II) from acidic aqueous solution by modified steel-making slag, Chem. Eng. J. 246 (2014) 160–167.
[52] Y. Cantu, A. Remes, A. Reyna, D. Martinez, J. Villarreal, H. Ramos, S. Trevino, C. Tamez, A. Martinez, T. Eubanks, J.G. Parsons, Thermodynamics, kinetics, and activation energy studies of the sorption of chromium(III) and chromium(VI) to a Mn_3O_4 nanomaterial, Chem. Eng. J. 254 (2014) 374–383.
[53] I.M. Dittert, V.J.P. Vilar, E.A.B. da Silva, S.M.A.G.U. de Souza, A.A.U. de Souza, C.M.S. Botelho, R.A.R. Boaventura, Adding value to marine macro-algae Laminaria digitata through its use in the separation and recovery of trivalent chromium ions from aqueous solution, Chem. Eng. J. 193-194 (2012) 348–357.
[54] N.R. Bishnoi, R. Kumar, S. Kumar, S. Rani, Biosorption of Cr(III) from aqueous solution using algal biomass spirogyra spp, J. Hazard. Mater. 145 (2007) 142–147.
[55] F. Ji, C. Li, B. Tang, J. Xu, G. Lu, P. Liu, Preparation of cellulose acetate/zeolite composite fiber and its adsorption behavior for heavy metal ions in aqueous solution, Chem. Eng. J. 209 (2012) 325–333.
[56] W. Zhang, F. Xu, Y. Wang, M. Luo, D. Wang, Facile control of zeolite NaA dispersion into xanthan gum–alginate binary biopolymer network in improving hybrid composites for adsorptive removal of Co^{2+} and Ni^{2+}, Chem. Eng. J. 255 (2014) 316–326.
[57] Z. Zhu, F. Sun, L. Yang, K. Gu, W. Li, Poly (styrene-co-maleic anhydride) microspheres prepared in ethanol/water using a photochemical method and their application in Ni^{2+} adsorption, Chem. Eng. J. 223 (2013) 395–401.

[58] W. Liu, J. Zhang, C. Cheng, G. Tian, C. Zhang, Ultrasonic-assisted sodium hypochlorite oxidation of activated carbons for enhanced removal of Co(II) from aqueous solutions, Chem. Eng. J. 175 (2011) 24–32.
[59] Q. Wang, J. Li, C. Chen, X. Ren, J. Hu, X. Wang, Removal of cobalt from aqueous solution by magnetic multiwalled carbon nanotube/iron oxide composites, Chem. Eng. J. 174 (2011) 126–133.
[60] Y. Park, Y.-C. Lee, W.S. Shin, S.-J. Choi, Removal of cobalt, strontium and cesium from radioactive laundry wastewater by ammonium molybdophosphate–polyacrylonitrile (AMP–PAN), Chem. Eng. J. 162 (2010) 685–695.

„From molecules to functional architecture. Supramolecular interactions"
Edited by V.I. Rybachenko
Donetsk 2012, East Publisher House, ISBN 978-966-317-155-5

Chapter 10

Synthesis of pyrazole-based bidentate and tridentate supramolecular ligands

Michał Cegłowski and Grzegorz Schroeder
Adam Mickiewicz University in Poznań, Department of Chemistry, Umultowska 89b, 61-614 Poznań

1. Introduction

Self-assembly is one of the most interesting process in modern supramolecular chemistry. Although its nature and complexity have been known from biochemical research, the ability to fully control it and construct "supermolecules" has stemmed from the developments made in supramolecular chemistry. It is now possible to design and construct molecules whose complexity and size can match those observed in biological assemblies. The self-assembly process of metal complexes formation is determined by two factors: the type, geometry and number of ligand active sites and the geometric preferences of the metal cation. While the second factor is usually known or easy to predict (for example Pt(II) is usually square planar) the first factor can be altered by synthesis of appropriate ligand. That is why of key importance for a successful self-assembly process leading to target supermolecules with metal complexes is to design and synthesise the right type of ligand.

The most extensively used ligands in metal coordination chemistry are π-electron deficient heterocyclic compounds such as 2,2'-bipyridine, 2,2':6',2"-terpyridine and 1,10-phenanthroline. Because they are π-electron deficient they act as a π-acceptors and are considered to be soft sites. Pyrazole is an aromatic compound which is classified as a π-excessive compound [1] and therefore acts as a hard donor site [2]. That is why it is possible to directly attach pyrazole to common π-electron deficient heterocycles (for example pyridine) in order to obtain ligands with interesting electronic properties. Moreover, it is possible to attach pyrazole to a desired heterocycle with incorporation of an appropriate linker that will provide additional space and therefore flexibility to the ligand obtained (for example alkil chain). Such a linker can also be another

binding site (for example amine, ether or thioether group) that will improve coordination properties of the final ligand.

Pyrazoles act as a monodentate ligands if they coordinate metal with nitrogen lone pair in the sp^2 orbital or as bidentate ligands after deprotonation of the N-H group. Moreover, after deprotonation the corresponding anion can be an *endo* (η^2) or *exo*-bidentate (η^1-η^1) bridging ligand (Figure 1) [3]. Substituents at positions 3-, 4-, 5- and on N atom (instead of the N-H group) can modify the steric properties and change the electronic properties of a pyrazole-based ligand.

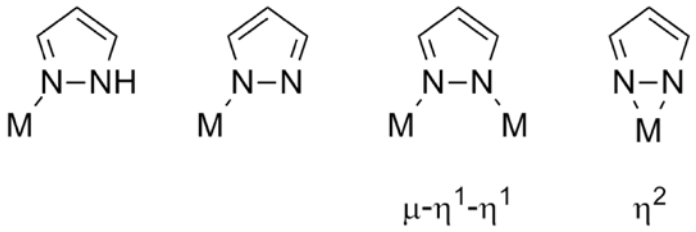

Figure 1. Coordination modes of pyrazole ligand and the corresponding anion [3].

2. Bidentate ligands

Ligands described in this section have two binding sites, which are pyrazole ring and another donor atom or two pyrazole rings linked through a spacer.

Synthesis of ligand **1**, obtained by attaching pyrazole ring to pyridine, has been reported. The highest yield of the reaction was observed when it was carried out in DMF with the use of pyrazole and 2-bromopyridine as reagents, copper(I) chloride with 6-(1*H*-pyrazol-yl) nicotinic acid as a catalyst and K_3PO_4 as a base (Figure 2) [4]. A simple method for the synthesis of ligand **1** with a similar yield and requires refluxing a mixture of 2-hydroxypyridine and pyrazole in trichlorophosphate without any metal catalyst has been reported recently [5]. Complexes of ruthenium of the stoichiometry of $RuCl_2$(cod) (**1**) (cod – 1,5-cyclooctadien) have been prepared and characterized by NMR and IR spectroscopy [6]. It has been concluded that three isomers are possible depending on the relative disposition of the ligands (Figure 3). The *cis*-chloro isomers had C_1 symmetry, whereas the *trans*-chloro isomers had C_s symmetry. Ligand **1** was also used to prepare $[Ru(bipy)_2\mathbf{1}]^{2+}$ (bipy – 2,2′bipyridyl) complex [7]. Electrochemical data indicated that ligand **1** is weaker π-acceptor than bipy but the complex obtained has similar excited-state properties to $[Ru(bipy)_3]^{2+}$.

Ligand **2**, which has a methylene group between pyrazole and pyridine ring in comparison to ligand **1**, has been synthesized from pyrazole and 2-(chloromethyl)pyridine hydrochloride in the presence of sodium hydroxide and tetrabutylammonium hydroxide with benzene as a solvent (Figure 4) [8].

It has been used to prepare complexes with cobalt(II) ($[Co(\mathbf{2})_2Cl_2]\cdot 4H_2O$) [9], nickel(II) ($[Ni(\mathbf{2})_2Cl_2]\cdot 4H_2O$) [9], palladium(II) ([PdIMe(**2**)]) [10] and ruthenium(II) ($[Ru(\eta^6C_6H_6)(\mathbf{2})Cl][PF_6]$) [11]. The crystallographic data of complex $[Co(\mathbf{2})_2Cl_2]\cdot 4H_2O$) reveal that the coordination of cobalt(II) is *trans* octahedral. An interesting feature to note is that the Co-N (pyridine) bond is longer than the Co-N (pyrazole) bond by about 0.1 Å. What is more, the four positions around cobalt(II) occupied by nitrogen atoms of pyrazole and pyridine rings have coordination angles ranging from 85.7° to 94.3°. Because the theoretical value is exactly 90°, this results indicates that the structure is distorted [9].

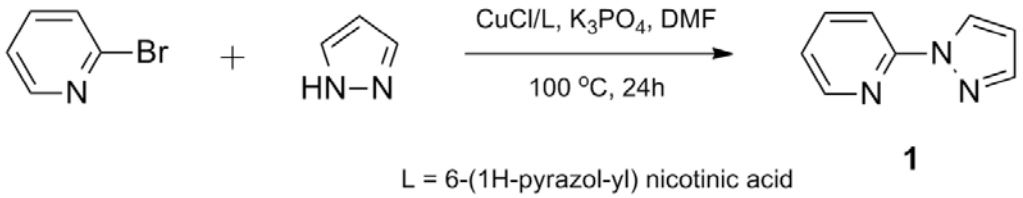

Figure 2. Synthetic route to N-arylated pyrazole ligand **1**.

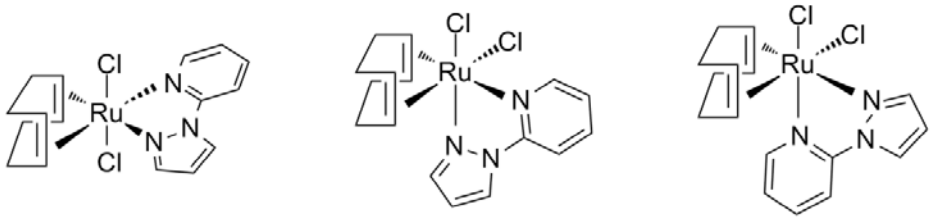

*Figure 3. Isomers of $RuCl_2(cod)$(**1**) depending on the relative disposition of the ligands [6].*

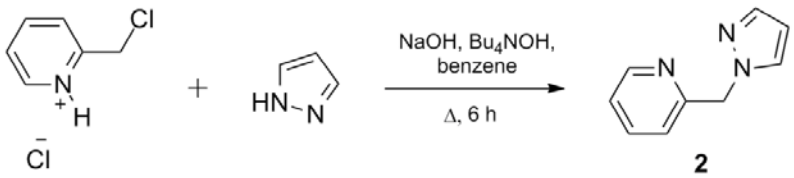

Figure 4. Synthetic route to ligand **2**.

Ligand **3** has been synthesized by the same method as that used for the synthesis of ligand **2**. Pyrazole and 2(chloromethyl)thiophene were heated in benzene in the presence of sodium hydroxide and tetrabutylammonium hydroxide (Figure 5) [12]. What is interesting, ligand **3** appeared to be monodentate when

coordinating to palladium (it gave $Pd(\mathbf{3})_2Cl_2$ as a resulting complex). It has been suggested that the nitrogen of pyrazole is the donor atom and sulphur from the thiophene ring is not coordinated [12].

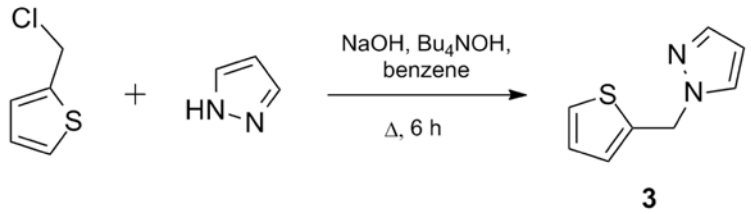

3

Figure 5. Synthetic route to ligand **3**.

Many interesting properties can be observed if the heterocycle-like pyridine or thiophene is replaced by another pyrazole ring to give a bis(pyrazolyl) ligand. Such a synthesis involves the reaction of pyrazole with methylene chloride (as a reagent and solvent) with the use of tetrabutylammonium hydrogensulfate and water solution of sodium hydroxide (Figure 6) [13]. Crystal structure of thus obtained ligand **4** (Figure 7 **A**) reveals that the crystal is additionally stabilized be weak N-H intermolecular hydrogen bonds [13]. Moreover, the bond lengths in both pyrazole rings are in excellent agreement. The greatest difference in their lengths is visible on C(1) atom that binds two pyrazole rings, because the length of C(1)-N(11) bond is 1.446(2) Å, while that of C(1)-N(21) bond is 1.436(2) Å.

Ligand **4** forms complexes with rhenium(V) $[ReCl_2(NNPh)(\mathbf{4})(PPh_3)]$ and $[ReOCl_3(\mathbf{4})]$. The latter slowly creates dimeric species and forms $[Re_2O_3Cl_4(\mathbf{4})_2]$ (Figure 7 **B**) that were isolable by evaporation of acetonitrile from the solution of $[ReOCl_3(\mathbf{4})]$[14]. The first of the above complexes was characterized by NMR and IR spectroscopy, whereas the next two complexes (mono- and dimeric) were characterized by X-ray diffractometry. $[ReOCl_3(\mathbf{4})]$ could be hydrogenated to polyhydride $Re(\mathbf{4})H_7$ with the use of $LiAlH_4$ and further hydrolysis [15]. Ligand **4** was also used to prepare complexes with molybdenum(II) $(Mo(CO)_2(\mathbf{4})Br_2)$ [16], tungsten(II) $(W(\mathbf{4})(CO)_3Br_2)$ [16] and rhodium(III) $([(\eta^5C_5Me_5)Rh(\mathbf{4})Cl][CF_3SO_3])$ [17].

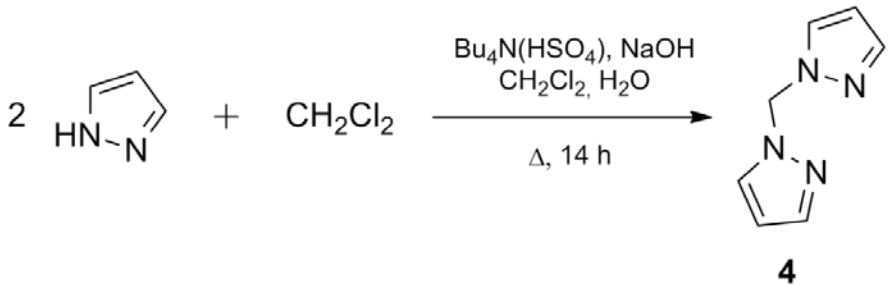

4

Figure 6. Synthetic route to ligand **4**.

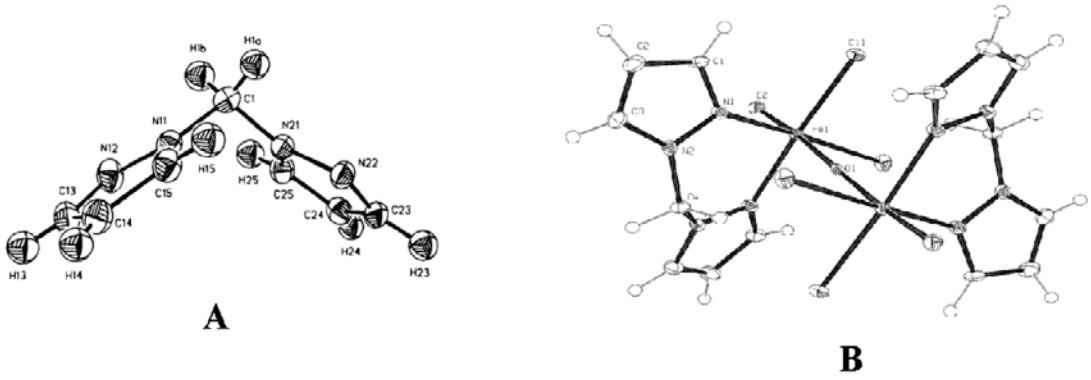

A **B**

*Figure 7. (***A***) Structure and labelling of atoms in the ligand* **4***;[13] (***B***) Structure of the complex [$Re_2O_3Cl_4$(**4**)$_2$] [14]..*

Besides binding pyrazole ring to other heterocyclic compounds it can be attached to aliphatic amine that could also be a donor binding site in the ligand obtained. A simple procedure involving condensation of 6-aminohexan-1-ol with benzaldehyde (or other aldehydes) was used to produce imine intermediate. After reduction with $NaBH_4$ the compound obtained was condensed with 1-hydroxymethylpyrazole at 70 °C without a solvent to form ligand **5** (Figure 8) [18]. Complex of ligand **5** with copper(II) was used toward catalytic oxidation of 3,5-di-*tert*-butylcatechol. It appeared that the complex formed with **5** had a higher catalytic rate for this reaction than its analogues bearing pyridine or pyrazine residues instead of phenyl group. The authors explained this results by a lower stability of the copper(II) complex with **5** due to poor electronic density and higher accessibility of 3,5-di-*tert*-butylcatechol to the metallic centre thanks to the absence of the coordination arm [18].

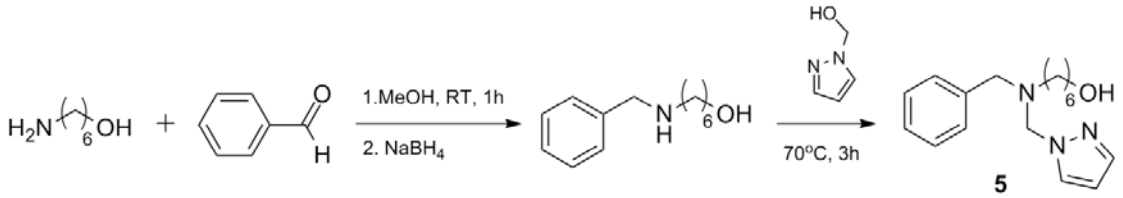

Figure 8. Synthetic route to ligand **5** *[18].*

3. Tridentate ligands

Tridentate pyrazole ligands make a wide group of ligands including tris(pyrazolyl)borate (first introduced by Trofimenko [19]) and substituted tris(pyrazolyl)borate. Coordination chemistry of this class of ligands has been extensively developed because of abundant possibilities to modify steric and electronic environment around the metal centre by different substitutions of pyrazole ring. The research work of Trofimenko and his followers has been extended over tris(pyrazolyl)alkanes that are isoelectronic and isosteric with poly(pyrazolyl)borates [20].

Tris(pyrazolyl)borate can be synthesized by the reaction of alkali metal borohydride with pyrazole. The number of attached pyrazole rings strongly depends on the reaction temperature (Figure 9) [21]. The products are stable compounds isolable after acidification, and can be converted into organic-soluble quaternary ammonium salts after neutralization with NR_4OH. B-substituted ligands are accessible by starting with $(BR_nH_{4-n})^-$ and C-substituted ligands are prepared by using appropriate pyrazole derivatives.

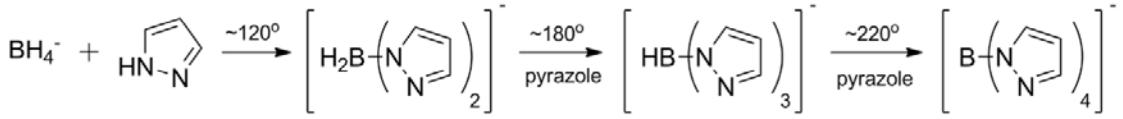

Figure 9. Synthesis of poly(pyrazolyl)borates [21].

Structure of octahedral coordination compounds formed by $RB(pyrazole)_3^-$ with divalent transition metals is presented in Figure 10. If the R group is another 1-pyrazolyl group the whole ligand still remains tridentate. $[HB(pyrazole)_3]_2M$ compounds are stable to light, air, water, dilute bases and acids, they can be sublimated *in vacuo* and can be dissolved in organic solvents [21].

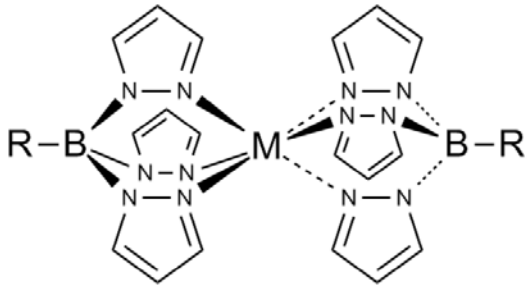

Figure 10. Structure of coordination compounds formed by $RB(pyrazole)_3^-$ with divalent transition metals.

Reaction of 3-(2-pyridyl)pyrazole with KBH_4 in melt gives tris(3-(2-pyridyl)pyrazole)borate (ligand **6**). Combination of ligand **6** with $[Cu(MeCN)_4][PF_6]$ affords $[Cu_3(\mathbf{6})_2][PF_6]$ (structure presented in Figure 11) [22]. In $[Cu_3(\mathbf{6})_2]^+$ each bidentate arm of each ligands is bonded to a different metal ion. Pseudo-tetrahedral coordination environment around Cu(I) ion is therefore formed by two bidentate arms that belong to different ligand molecules. The distances between Cu(I) ions are not equivalent, because there is one short Cu-Cu separation (2.915 Å) and two longer ones (3.500 Å and 3.614 Å). The length of the shortest Cu-Cu separation is the result of π-stacking interactions between ligands attached to the two metal ions.

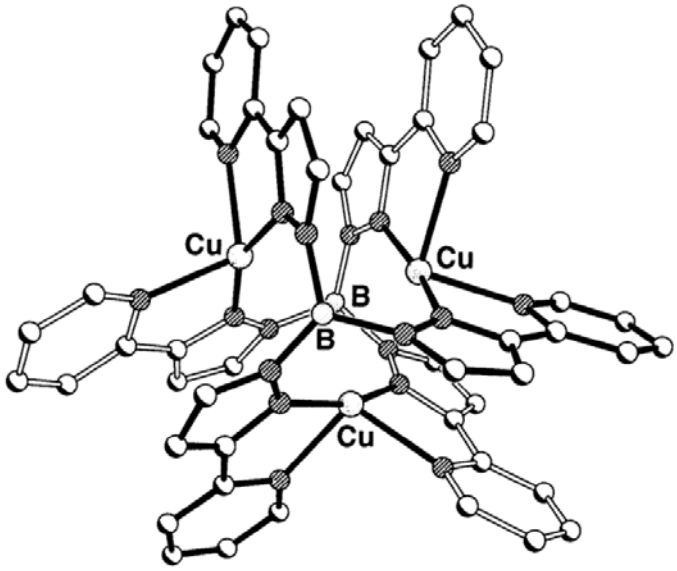

Figure 11. Structure of $[Cu_3(\mathbf{6})_2]^+$ [22].

Tris(pyrazolyl)alkanes are ligands isoelectronic and isosteric with poly(pyrazolyl)borates that can be easily prepared with many different substituents that will modify the electronic and steric effects up to desired values. The azole rings are usually very chemically resistant against both oxidizing and reducing reagents or other chemical attacks. The simples member of this class of ligands, tris(pyrazolyl)methane (ligand **7**), can be prepared by the phase transfer procedure involving heating at reflux of a mixture of pyrazole, potassium carbonate, chloroform and tetrabutylammonium hydrogensulfate (Figure 12) [23]. Complexes of tris(pyrazolyl)alkanes with titanium(III) ([Ti(**7**)Cl_3]) have been reported as catalysts for polymerization of olefins. Other compounds of the formula RE(pyrazolyl)$_3$MX_3 (R = H, alkyl, aryl, halide, amino group; E = C, Si, Ge, Pb, Sn; M = Ti, Zr, Hf) have been reported as catalysts of this process [24]. What is more, compounds of the formula RC(pyrazolyl)$_3$Cr(R)$_n$ (R = halide, chain or branched alkyl, n = 1-3) have been used as catalysts to produce 1-hexene by ethylene trimerization [25].

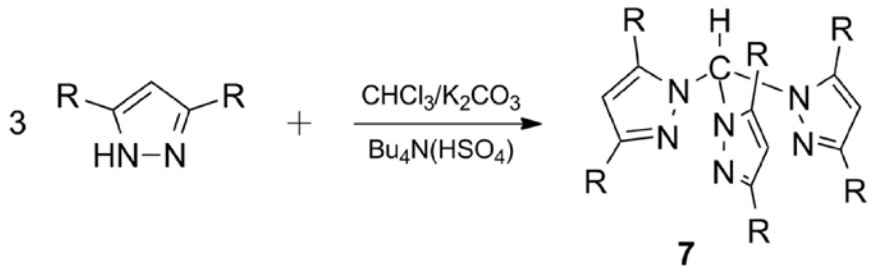

Figure 12. Synthesis of tris(pyrazolyl)methane.

Tridentate pyrazole ligands can be also prepared by attaching pyrazole ring to already existing donor sites. Ligand **8** was prepared by a simple mixing of *N*-hydroxymethylpyrazole with ethylamine in acetonitrile (Figure 13) [26]. With the use of ligand **8** compounds of the formula [M(**8**)$_2$]X_2 (M = Mn, Fe, Co, Ni, Cu, Zn, Cd, X = BF_4 or M = Ni, Cu; X = NO_3) were prepared [26]. The X-ray structure of a similar complex compound [Cu(**8**)$_2$][CF_3SO_3] has revealed that the copper cation is surrounded by four nitrogen atoms from pyrazol rings of two ligand molecules. The geometry of the copper atom coordination is slightly distorted tetrahedral. The tertiary amine group is 3.91 Å away from the copper atom so it is too far away to create even medium strength bond [27].

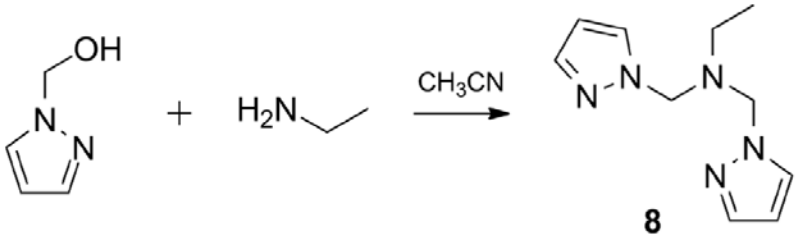

Figure 13. Synthetic route to ligand **8**.

Ligand **9**, which has a hydrogen atom instead of an ethyl group on the nitrogen atom and one methylene group more between the tertiary amine and pyrazole ring than ligand **8**, has very different coordination chemistry than ligand **8**. It was synthesized in the reaction of sodium 3,5-dimethylpyrazolate with bis(2-chloroethyl)amine hydrochloride in DMF (Figure 14) [28]. X-ray structure of copper(II) complexes of Cu(**9**)·2NO_3 and Cu(**9**)·NO_3·H_2O showed that two symmetrically independent complexes were formed: [Cu(**9**)$(NO_3)_2$] and [Cu(**9**)$(NO_3)(H_2O)$][NO_3]. The coordination of copper(II) is an intermediate between distorted trigonal bipyramid and an octahedron. Nitrogen atoms of the two pyrazole rings and amino nitrogen form T-shaped arrangement around the copper(II) ion. In both complexes there is a nitrate group that is involved in coordination through one short and one long bond. The second nitrate group (or a water molecule in the second complex) coordinates monodentately [28].

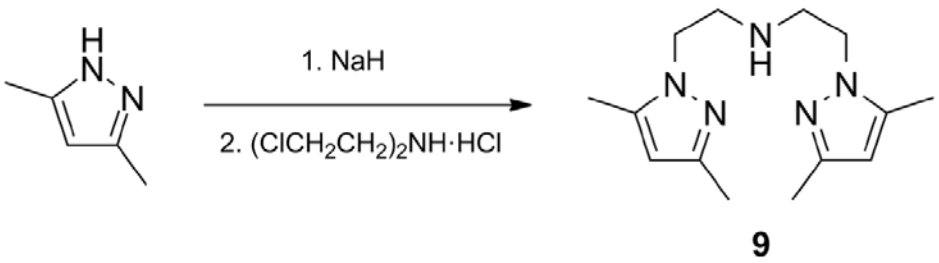

Figure 14. Synthetic route to ligand **9**.

Instead of a simple amine group, a pyridine ring was introduced into the ligand system. Ligand **10** was obtained in the reaction between sodium 3,5-dimethylpyrazolate with 2,6-bis(chloromethyl)pyridine in DMF (Figure 15) [29]. Copper(I) complexes with ligand **10** were prepared: [Cu(**10**)$OClO_3$]·CH_2Cl_2 and [Cu(**10**)(PPh_3)]. In the first complex, copper is coordinated with pyridine, two pyrazole nitrogen and oxygen from the perchlorate group. The coordination around copper(I) is distorted tetrahedron with weakly coordinated perchlorate group that makes the coordination of the whole ligand to be similar to distorted

trigonal-planar. In [Cu(**10**)(PPh_3)] copper is coordinated with pyridine, two pyrazole nitrogen and phosphorus from triphenylphosphine group and the chelation ring has a boat-like structure [29].

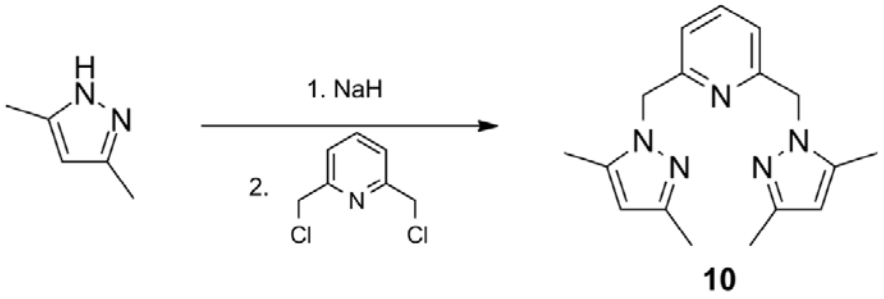

Figure 15. Synthetic route to ligand **10**.

Unsymmetrical ligand **11**, which also consists of two pyrazole rings and a pyridine ring, was prepared by mixing pyrazole and sodium hydride in freshly distilled THF. After that thionyl chloride and subsequently 2-pyridinecarboxaldehyde with a catalytic amount of cobalt(II) chloride were added (Figure 16) [30]. Ligand **11** was used to prepare metal(II) complexes [M(**11**)$_2$][NO_3] (M = Fe, Co, Ni, Cu, Zn). X-ray crystallography studies revealed that metal(II) complexes have octahedral geometry with a small trigonal distortion. Moreover, the ligand-metal bonds are significantly shorter than those in monodentate complexes of pyridine or pyrazole ligands with metals. The high energies of the 'd-d' transitions indicated that ligand **11** produces a relatively strong ligand field, stronger than monodentate pyridine or pyrazole groups [31].

Ligand **12** which is a combination of pyrazole ring and 1,10-phenanthroline has been prepared in a multistep reaction. 2,9-Dimethyl-1,10-phenanthroline was oxidized with selenium dioxide to produce aldehyde groups that were subsequently reduced with sodium borohydride. Further bromination with HBr and reaction with 3,5-dimethylpyrazole in the presence of NaOH solution and tetrabutylammonium hydroxide (TBAH) solution results in a desired product (Figure 17) [32].

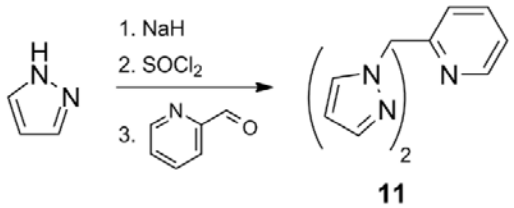

Figure 16. Synthetic route to ligand **11**.

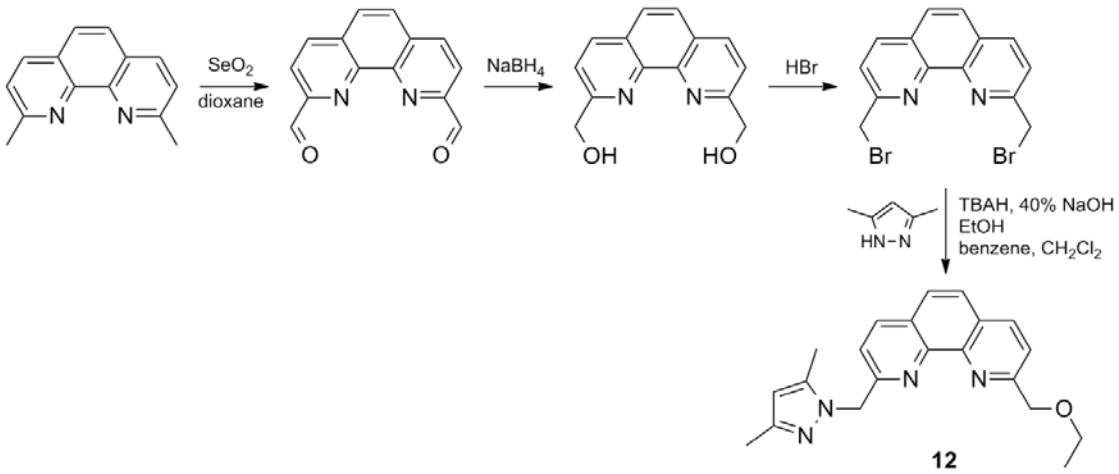

Figure 17. Synthetic route to ligand **12**.

Ligand **12** was used to prepare nickel(II) complex [Ni(**12**)Cl_2]·CH_3CN. This complex has a five-coordinate geometry provided by two 1,10-phenanthroline nitrogen atoms, the nitrogen atom from pyrazolyl ring and two chloride atoms (structure presented in Figure 18). The geometry of the complex is described as distorted trigonal bipyramid with one of 1,10-phenanthroline nitrogen atoms being equatorial, while the chloride atoms and the second 1,10-phenanthroline nitrogen and nitrogen from pyrazolyl ring being axial. In this type of complex, nickel and three equatorial ligands should be coplanar, while the axial ligands should be disposed above and below the plane. The mean deviation from this four-atoms least-square plane through nickel and axial ligand atoms is only 0.039 Å so they can be considered as coplanar [32].

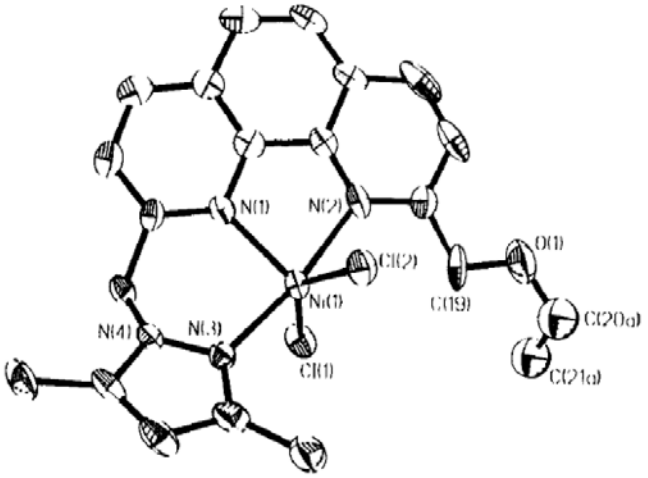

*Figure 18. View of the structure of the neutral complex [Ni(***12***)Cl_2] [32].*

Sulphur-containing ligand **13** was prepared in a sequence of chemical reactions. 2-Hydroxyethylhydrazine was condensed with acetylacetone to yield *N*-(2-hydroxyethyl)-3,5-dimethylpyrazole that was further tosylated with p-toluenesulfonyl chloride in water/acetone mixture and NaOH as a base [33]. The tosylated *N*-(2-hydroxyethyl)-3,5-dimethylpyrazole was reacted with $Na_2S{\cdot}7H_2O$ and NaOH in water to yield ligand **13** (Figure 19) [34]. It was used to prepare complexes [M(**13**)$(NCS)_2$] (M = Co or Zn), Cu(**13**)(F)(BF_4), [Ni(**13**)$(NCS)_2(H_2O)$], M(**13**)Cl_2 (M = Co or Cu), Zn(**13**)$Cl_2{\cdot}0.5$EtOH, M(**13**)$(NO_3)_2$ (M = Co or Cu), Cu(**13**)X (X = Br or Cl), [Cu(**13**)]$BF_4{\cdot}H_2O$ and Ag(**13**)(NO_3). The coordination geometry in [Co(**13**)$(NO_3)_2$] is distorted octahedral and cobalt ion is coordinated by two pyrazole nitrogen atoms, thioether sulphur and two nitrate anions of which one is bidentate. In Cu(**13**)Br copper(I) atom is coordinated by two pyrazole nitrogens, one thioether and one bromide. The two nitrogen donors are not part of one ligand molecule, which results in a polymeric nature of Cu(**13**)Br [34].

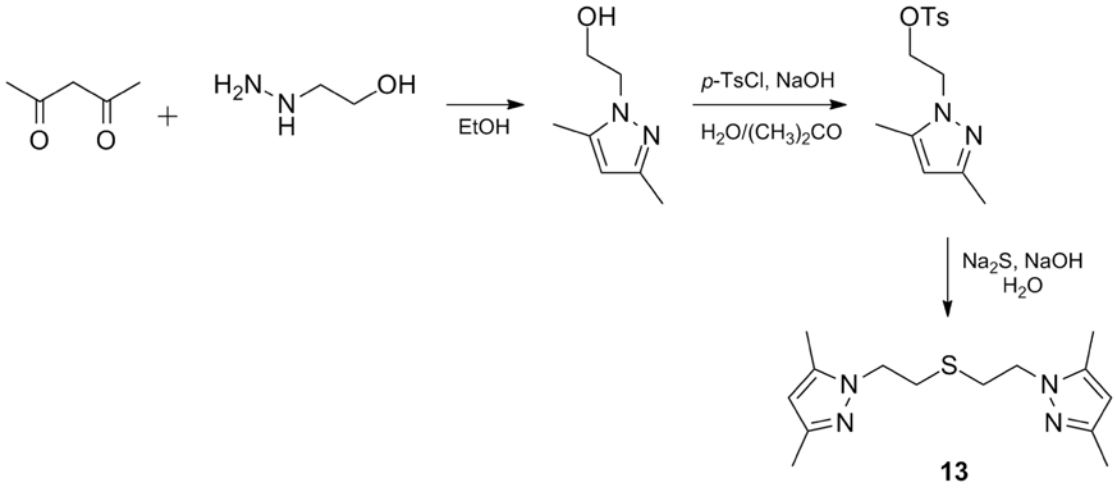

Figure 19. Synthetic route to ligand **13**.

4. Conclusions

Synthesis and coordination properties of various pyrazole based bidentate and tridentate ligands have been presented. It is worth noting that in all cases synthesis of appropriate ligand is limited to only few steps and a target product can be isolated with satisfying yields. It has been demonstrated that geometries and binding properties of chelating ligands can be varied by changing substituent groups near the donor site of the ligand. In future the design of new pyrazole-based ligands will depend on the creativity of researcher and requirements imposed by a particular scientific problem. What is more, the ligands of this

type can be used as building blocks that construct complex supramolecular architectures, such as supramolecular polymers or other sophisticated products.

Acknowledgements
This work was partially supported from the funds of National Science Centre (grant no. 2012/05/N/ST5/01274).

References

1. Albert, A., *Heterocyclic Chemistry*. London, 1968; ISBN: 048511092X
2. Mukherjee, R., Coordination chemistry with pyrazole-based chelating ligands: molecular structural aspects. *Coord. Chem. Rev.* **2000**, *203* (1), 151-218.
3. Viciano-Chumillas, M.; Tanase, S.; de Jongh, L. J.; Reedijk, J., Coordination Versatility of Pyrazole-Based Ligands towards High-Nuclearity Transition-Metal and Rare-Earth Clusters. *Eur. J. Inorg. Chem.* **2010**, *2010* (22), 3403-3418.
4. Liu, H.-Y.; Yu, Z.-T.; Yuan, Y.-J.; Yu, T.; Zou, Z.-G., Efficient N-arylation catalyzed by a copper(I) pyrazolyl-nicotinic acid system. *Tetrahedron* **2010**, *66* (47), 9141-9144.
5. Deng, X.; Roessler, A.; Brdar, I.; Faessler, R.; Wu, J.; Sales, Z. S.; Mani, N. S., Direct, Metal-Free Amination of Heterocyclic Amides/Ureas with NH-Heterocycles and N-Substituted Anilines in $POCl_3$. *J. Org. Chem.* **2011**, *76* (20), 8262-8269.
6. Elguero, J.; Guerrero, A.; de la Torre, F. G.; de la Hoz, A.; Jalon, F. A.; Manzano, B. R.; Rodriguez, A., New complexes with pyrazole-containing ligands and different metallic centres. Comparative study of their fluxional behaviour involving M-N bond rupture. *New J. Chem.* **2001**, *25* (8), 1050-1060.
7. Hage, R.; Prins, R.; Haasnoot, J. G.; Reedijk, J.; Vos, J. G., Synthesis, spectroscopic, and electrochemical properties of bis(2,2[prime or minute]-bipyridyl)-ruthenium compounds of some pyridyl-1,2,4-triazoles. *J. Chem. Soc., Dalton Trans.* **1987**, (6), 1389-1395.
8. House, D.; Steel, P.; Watson, A., Chiral Heterocyclic Ligands. II. Synthesis and Palladium(II) Complexes of Chiral Pyrazolylmethyl-Pyridines and Pyrazolylmethyl-Pyrazoles. *Aust. J. Chem.* **1986**, *39* (10), 1525-1536.
9. Kumar Lal, T.; Mukherjee, R., New cobalt(II) and nickel(II) complexes with 2-(pyrazol-1-ylmethyl)pyridine. Stereochemical variations in

cobalt(II) complexes and X-ray crystal structure of bis[2-(pyrazol-1-ylmethyl) pyridine]dichlorocobalt(II) tetrahydrate. *Polyhedron* **1997**, *16* (20), 3577-3583.

10. Byers, P. K.; Canty, A. J., Synthetic routes to methylpalladium(II) and dimethylpalladium(II) chemistry and the synthesis of new nitrogen donor ligand systems. *Organometallics* **1990**, *9* (1), 210-220.
11. Shirin, Z.; Mukherjee, R.; Richardson, J. F.; Buchanan, R. M., New piano-stool ruthenium(II) complexes of benzene and bidentate/tridentate nitrogen-donor ligands: synthesis and characterization. *J. Chem. Soc., Dalton Trans.* **1994**, (4), 465-469.
12. Watson, A.; House, D.; Steel, P., Chiral Heterocyclic Ligands. VIII. Syntheses and Complexes of New Chelating Ligands Derived From Camphor. *Aust. J. Chem.* **1995**, *48* (9), 1549-1572.
13. Churchill, M.; Churchill, D.; Huynh, M.; Takeuchi, K.; Castellano, R.; Jameson, D., Crystal and molecular structure of di(1-pyrazolyl) methane, $CH_2(C_3N_2H_3)_2$. *J. Chem. Crystallogr.* **1996**, *26* (2), 93-97.
14. Cowley, A. R.; Dilworth, J. R.; Salichou, M., Syntheses and structures of pyrazolylmethane complexes of rhenium(III), (IV) and (V). *Dalton Trans.* **2007**, (16), 1621-1629.
15. Hamilton, D. G.; Luo, X. L.; Crabtree, R. H., The first polyhydrides stabilized only by N-donor ligands, hexahydro[hydrotris(pyrazolyl) borato]rhenium and heptahydro[dipyrazolylmethane]rhenium. *Inorg. Chem.* **1989**, *28* (16), 3198-3203.
16. Shiu, K. B.; Liou, K. S.; Wang, S. L.; Wei, S. C., Organotransition-metal complexes of multidentate ligands. 10. Steric vs. electronic control on formation of six- and seven-coordinate carbonyl halides of molybdenum(II) and tungsten(II). *Organometallics* **1990**, *9* (3), 669-675.
17. Pettinari, C.; Pettinari, R.; Marchetti, F.; Macchioni, A.; Zuccaccia, D.; Skelton, B. W.; White, A. H., Synthesis, Reactivity, Spectroscopic Characterization, X-ray Structures, PGSE, and NOE NMR Studies of (η^5-C_5Me_5)-Rhodium and -Iridium Derivatives Containing Bis(pyrazolyl)alkane Ligands. *Inorg. Chem.* **2007**, *46* (3), 896-906.
18. Marion, R.; Saleh, N. M.; Le Poul, N.; Floner, D.; Lavastre, O.; Geneste, F., Rate enhancement of the catechol oxidase activity of a series of biomimetic monocopper(ii) complexes by introduction of non-coordinating groups in N-tripodal ligands. *New J. Chem.* **2012**, *36* (9), 1828-1835.
19. Trofimenko, S., Boron-pyrazole chemistry. II. Poly(1-pyrazolyl)-

borates. *J. Am. Chem. Soc.* **1967**, *89* (13), 3170-3177.
20. Pettinari, C.; Pettinari, R., Metal derivatives of poly(pyrazolyl)alkanes: I. Tris(pyrazolyl)alkanes and related systems. *Coord. Chem. Rev.* **2005**, *249* (5–6), 525-543.
21. Trofimenko, S., Coordination chemistry of pyrazole-derived ligands. *Chem. Rev. (Washington, DC, U. S.)* **1972**, *72* (5), 497-509.
22. Jones, P. L.; Jeffery, J. C.; Maher, J. P.; McCleverty, J. A.; Rieger, P. H.; Ward, M. D., A Triangular Copper(I) Complex Displaying Allosteric Cooperativity in Its Electrochemical Behavior and a Mixed-Valence Cu(I)−Cu(I)−Cu(II) State with Unusual Temperature-Dependent Behavior. *Inorg. Chem.* **1997**, *36* (14), 3088-3095.
23. Juliá, S.; del Mazo, J. M.; Avila, L.; Elguero, J., Improved synthesis of polyazolylmethanes under solid-liquid phase-transfer catalysis. *Org. Prep. Proced. Int.* **1984**, *16* (5), 299-307.
24. Nakazawa, H.; Igai, S.; Kai, Y. JP 10338698, 1998.
25. Yoshida, O.; Okada, H.; Yamamoto, T.; Murakita, H. JP 2002205960, 2002.
26. Veldhuis, J. B. J.; Driessen, W. L.; Reedijk, J., A pyrazole derivative of aminoethane as a tridentate chelating ligand towards transition metals. The X-ray structure of [N,N-bis(pyrazol-1-ylmethyl)aminoethane] dibromocopper(II). *J. Chem. Soc., Dalton Trans.* **1986**, (3), 537-541.
27. Pennings, Y. C. M.; Driessen, W. L.; Reedijk, J., Copper(I) coordination compounds with two bidentate chelating pyrazole ligands. X-ray crystal structures of DI-μ-chloro-bis[[N,N-bis(1- pyrazolylmethyl) aminoethane]copper(I)] and [bis(N,N-bis(1-pyrazolylmethyl) aminoethane]copper(I) triflate. *Polyhedron* **1988**, *7* (24), 2583-2589.
28. Martens, C. F.; Schenning, A. P. H. J.; Feiters, M. C.; Berens, H. W.; van der Linden, J. G. M.; Admiraal, G.; Beurskens, P. T.; Kooijman, H.; Spek, A. L.; Nolte, R. J. M., X-ray Structures and Redox Properties of Copper(II) Bis(pyrazole) Complexes. *Inorg. Chem.* **1995**, *34* (19), 4735-4744.
29. Manikandan, P.; Varghese, B.; Manoharan, P. T., Structure, characterisation and dynamics of copper(I) complexes of 2,6-bis(3,5-dimethylpyrazol-1-ylmethyl)pyridine. *J. Chem. Soc., Dalton Trans.* **1996**, (3), 371-376.
30. Hoffmann, A.; Flörke, U.; Schürmann, M.; Herres-Pawlis, S., Novel Synthetic Strategy towards the Efficient Synthesis of Substituted Bis(pyrazolyl)(2-pyridyl)methane Ligands. *Eur. J. Org. Chem.* **2010**, *2010* (21), 4136-4144.

31. Astley, T.; Canty, A. J.; Hitchman, M. A.; Rowbottom, G. L.; Skelton, B. W.; White, A. H., Structural, spectroscopic and angular-overlap studies of the nature of metal-ligand bonding for tripod ligands. *J. Chem. Soc., Dalton Trans.* **1991**, (8), 1981-1990.
32. Masood, M. A.; Hodgson, D. J., Five- and Six-Coordinate Nickel(II) Complexes of New Multidentate Ligands Containing 2,9-Disubstituted-1,10-Phenanthroline and Pyrazolyl Units. *Inorg. Chem.* **1994**, *33* (14), 3038-3042.
33. Haanstra, W. G.; Driessen, W. L.; Reedijk, J.; Turpeinen, U.; Hamalainenn, R., Unusual chelating properties of the ligand 1,8-bis(3,5-dimethyl-1-pyrazolyl)-3,6-dithiaoctane (bddo). Crystal structures of $Ni(bddo)(NCS)_2$, $Zn(bddo)(NCS)_2$ and $Cd_2(bddo)(NCS)_4$. *J. Chem. Soc., Dalton Trans.* **1989**, (11), 2309-2314.
34. Haanstra, W. G.; Driessen, W. L.; van Roon, M.; Stoffels, A. L. E.; Reedijk, J., Co-ordination compounds with the N2S-donor ligand 1,5-bis(3,5-dimethylpyrazol-1-yl)-3-thiapentane. *J. Chem. Soc., Dalton Trans.* **1992**, (3), 481-486.

„New trends in supramolecular chemistry"
Edited by Volodymyr I. Rybachenko
Donetsk 2014, East Publisher House, ISBN 978-966-317-208-8

Chapter 9

Functional polymers forming complexes with metal ions

Michał Cegłowski and Grzegorz Schroeder
Adam Mickiewicz University in Poznań, Faculty of Chemistry, Umultowska 89b, 61-614 Poznań, Poland

1. Introduction

Polymer chemistry is among the most important disciplines of material science. Innovative monomer design and a wide range of synthetic strategies allow production of polymers of unique properties. Also over the last two decades, a variety of methods allowing performance of chemical reactions on already polymerized macromolecules have been developed. Many industrially important polymers that possess catalytically active or other functional groups are obtained by the reaction of a polymer chain with an appropriate functionalizing agent [1].

Functional polymers show specific properties such as adhesion, repellence, pH-stability, anti-corrosion etc. Their quality and advanced attributes make them materials with almost unlimited potential of application. The term functional polymer has two meanings:

- a polymer that includes in its structure a functional organic group that is ready to be involved in chemical reactions,
- a polymer showing specific properties and thus be able to be used for a particular purpose for which it has been designed [2].

Coordination compound consists of an central atom or ion that is surrounded by anions or molecules with which it is joined by chemical bonds. The groups that are bonded to the central metal or ion are known as ligands. The chemical bonds that connect central atom or ion with ligands are coordinate or coordinate-covalent in character. The coordination compounds include e.g. biological substances such as vitamin B_{12} or hemoglobin and synthetic compounds such as dyes, pigments and catalysts [3].

A polymer-metal complex is composed of a polymer and a metal atom or ion, which forms a coordinate bond with a polymer donor site. Such donor sites, which usually contain atoms such as nitrogen, sulfur or oxygen, are introduced by polymerization of appropriate monomer or by chemical functionalization

of a polymer chain with a molecule that is capable of forming coordination compounds. Polymer-metal complexes have found application as heterogeneous catalysts [4, 5], chelating resins for water treatment [6-8] or recovery of trace metal ions [9, 10], hydrometallurgy [11, 12] and polymeric carries of diagnostic agents [13].

2. Structure and synthesis of polymer-metal complexes

The functional polymers that form complexes with metal ions can be classified in many ways based on method of synthesis, structure or their principal use. The methods of synthesis include making a complex between a polymeric ligand and a metal ion and polymerization of a monomer that already contains a metal ion.

2.1. Reaction of polymeric ligand with metal ion

In water a metal ion forms hydrated ions or complex compounds with different molecules. To bind a metal ion from a solution, a polymer ligand must make more stable complex than the ions or neutral molecules. The nature of the ligand and the strength of bond formed with the metal ion is therefore the fundamental issue in every extraction system. The ligands may be classified according to the characteristic functional groups and/or donor atoms incorporated in their structure. The most commonly used ligands are presented in Table 1. It is worth noticing that some polymers may contain a mixed ligand system to improve their chelating properties or enhance selectivity towards a particular ion.

Table 1. Commonly used polymer ligands.

Coordinating group	Structure of polymer ligand unit
Alcohols	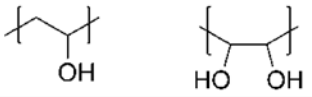
Carbocylic acids	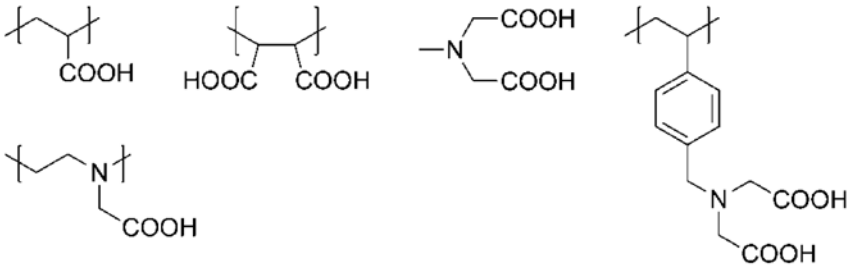

Coordinating group	Structure of polymer ligand unit
Ketones, ester, amides	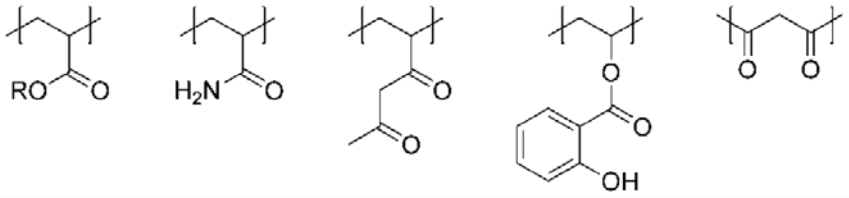
Thiols	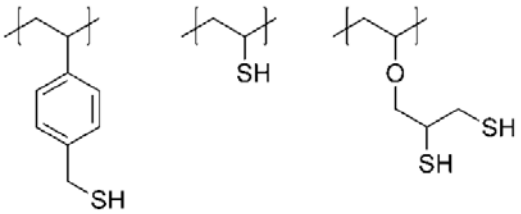
Amines	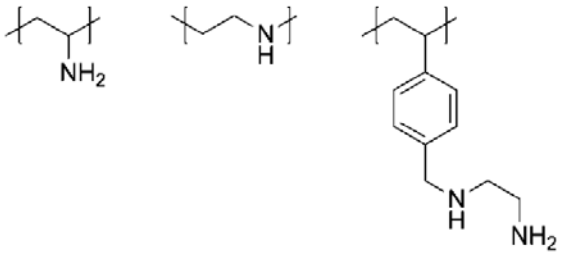
Pyridines	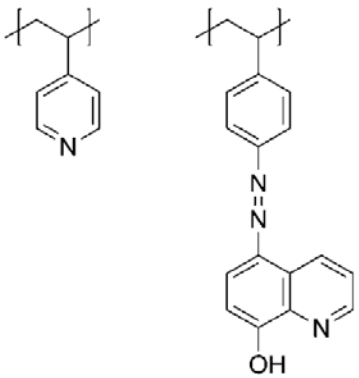
Bipyridines	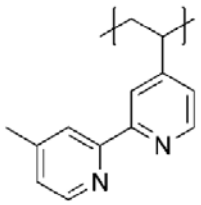

Coordinating group	Structure of polymer ligand unit
Terpyridines	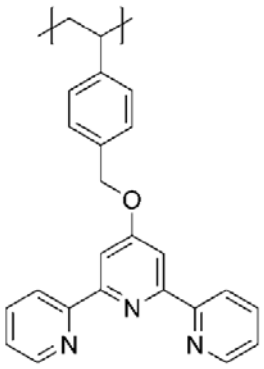
Pyrazoles, imidazoles	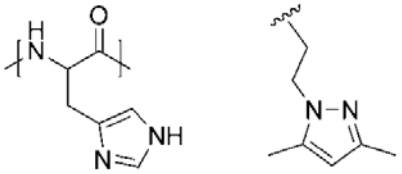
Schiff bases	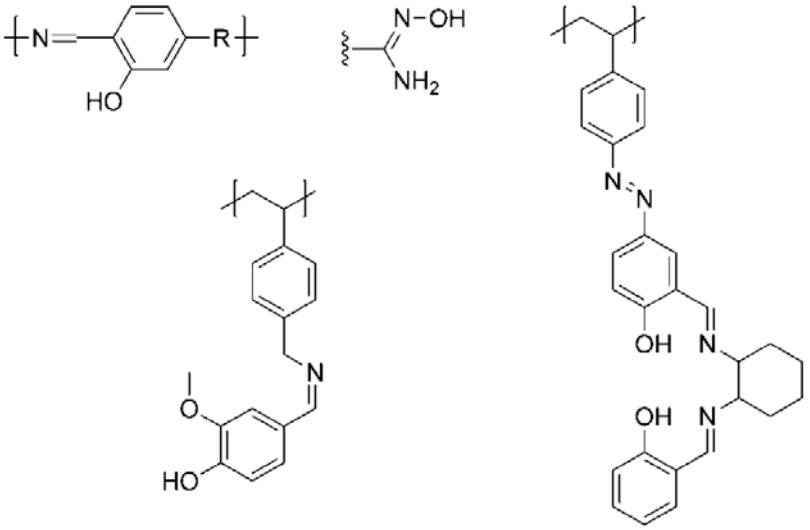
Phosphoric acids	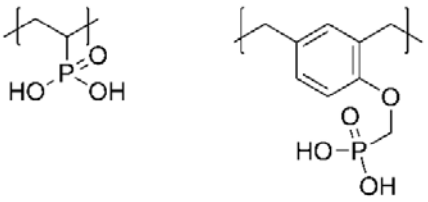
Sulfonic acids	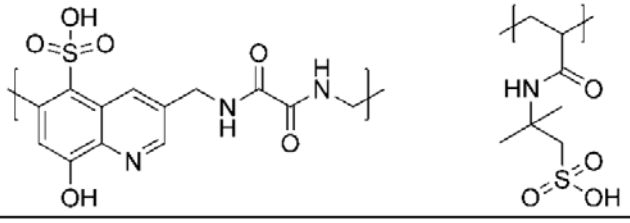

The reactions between a polymeric ligand and a metal ion can be divided into two groups depending on the structure obtained. The first group are pendant metal complexes, whereas the second groups are inter/intra-molecular complexes [14].

Pendant metal complexes can be classified as monodentate or polydentate complexes depending on the kind of ligand attached to the polymer chain. If the ligand has one donor site it can form monodentate complexes, if it has multiple donor sites it can form polydentate complexes with metal ions.

In the monodentate polymer-metal complexes the ligand donor site occupies one coordinate site of the metal ion, whereas other coordination sites are usually occupied by low-molecular weight anions. If a ligand has several coordination sites it is possible to obtain monodentate complex by appropriate tuning the polymer/metal ratio. If a large excess of metal ion is used, it is highly probable that all donor sites form coordination compounds with only one metal ion, resulting in a monodentate polymer-metal complexes. An example of a monodentate polymer-metal complex is presented in Figure 1.

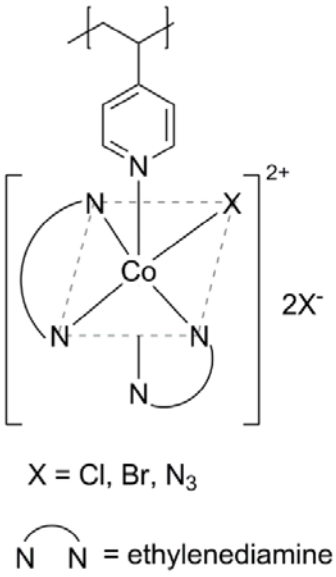

Figure 1. An example of a monodentate polymer-metal complex.

Polydentate ligands are more widespread in polymer-metal complexes. These complexes are usually more stable than those formed by monodentate ligands and have well-defined coordination structure. This is the reason why most of chelating resins possess in their structure a polydentate ligand. An exemplary polydentate polymer-metal complex is presented in Figure 2 [15].

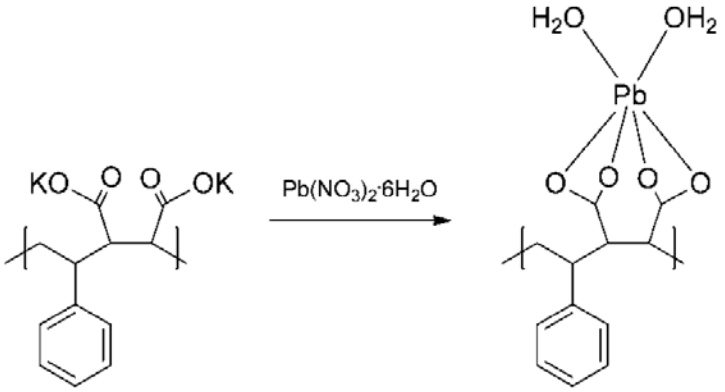

Figure 2. An example of a polydentate polymer-metal complex.

When a metal ion has four or six coordination binding sites, it can create bonds with different ligands that are attached to the main polymer chain or even ligands that are connected to different polymer chains. The first complex type is called intra-polymer chelate, whereas the second one is called inter-polymer chelate. A schematic presentation of these two types of polymer-metal complexes is given in Figure 3.

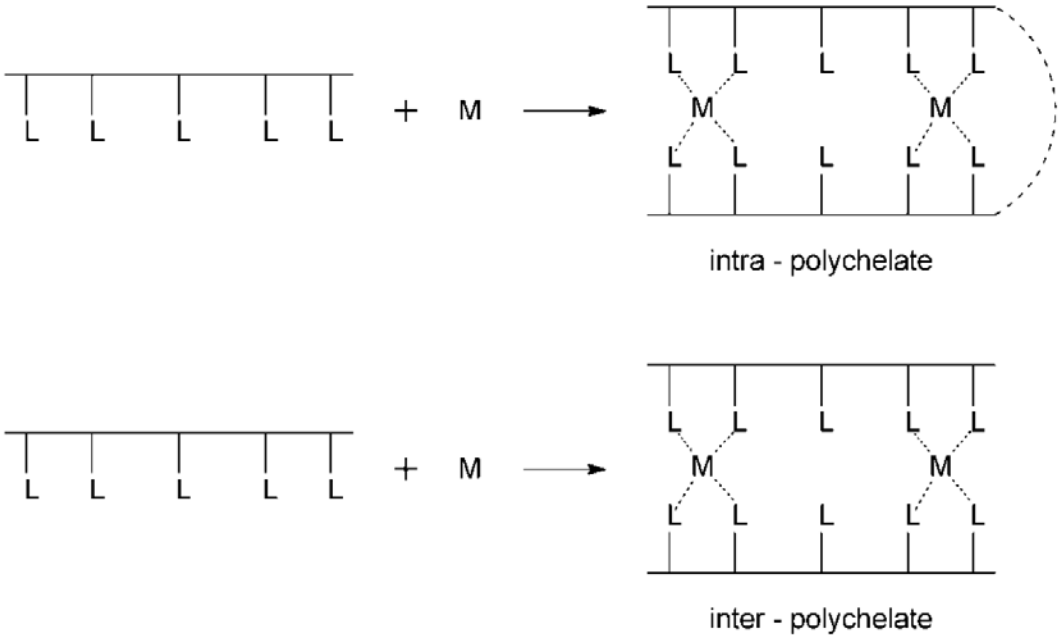

Figure 3. Schematic representation of intra- and inter-polychelates.

From the experimental point of view it is very difficult to distinguish whether a particular polymer-metal complex has an inter- or intra-molecular bridging. In

many examples the product obtained is a mixture of inter and intra-chelates. If the intra-chelate complex, predominates in the overall structure, the product of the reaction is usually insoluble and precipitate from the reaction mixture.

2.2. Polymerization of monomer-metal complexes

This method of synthesis is used to prepare polymer-metal complexes with well-defined coordination structure. The materials obtained are frequently used as heterogeneous catalysts or redox centres. The polymers are usually prepared by radical or ionic polymerization.

Figure 4 presents an exemplary monomer and polymer obtained by the method of polymerization. The polymer was prepared using controlled polymerization by employing the reversible addition–fragmentation chain transfer polymerization (RAFT) with cumyl dithiobenzoate as a chain transfer agent. The obtained side-chain cobaltocenium containing polymer was a metal-containing polyelectrolyte that showed characteristic redox behaviour of cobaltocenium [16].

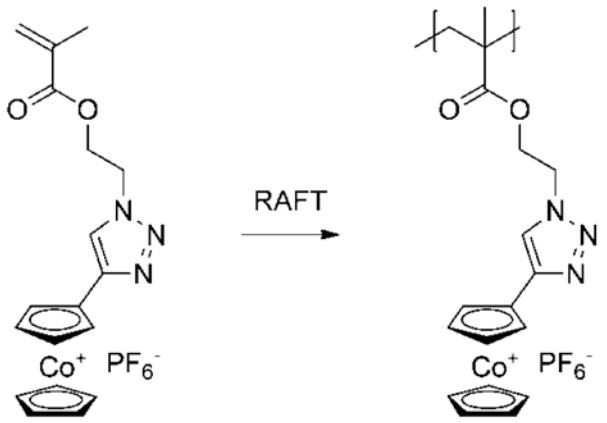

Figure 4. Synthesis of side-chain cobaltocenium-containing polymer.

3. Applications of polymeric ligand systems

3.1. Ion removal

Chelating polymers are used for removal or selective adsorption of heavy metal ions. In many industries, such as mining, hydrometallurgical processes and processes of removal of pollutants it is essential to recover specifically a particular ion. By using appropriate chelating polymer it is possible to reduce overall consumption of energy and materials in this process. Chelating resins are used on a very large scale in water-softening to replace calcium and magnesium ions with monovalent ions.

Removal of Ca, Mg, Pb, Zn metals present as pollutants in Ag-NaCl

solution was conducted on a Lewatit TP-260 ion exchange resin. This resin is an amphoteric aminomethylphosphonic polymer, capable of forming high-affinity complexes with divalent metal ions. Successful separation was achieved in both counter-current and cross-current configurations. Silver was collected in over 99% purity with practically 100% yield. Column efficiency and the liquid to solid flow rate ratio were found to have strong influence on the process performance. It was shown that counter-current simulated moving-bed process can be used for purification of precious metal solutions with overall high yield [17].

Purolite S930 chelating resin, a macroporous polystyrene based chelating resin with iminodiacetic groups, was used for adsorption of copper and nickel, from the pulps being side products of the leaching of low-grade sulfide ores. At the solution pH of around 3, the copper, nickel, and cobalt recovery for a long contact time exceeded 99%. Unfortunately it was established that in the presence of silicic acid in the pulp the rate of recovery of the metals decreased. To ensure high recovery, sorption was carried out at a temperature increased to around 50°C [18].

Uranium mining and hydrometallurgical processes produce a large number of uranium waste water, which can be a serious threat to the environment. Polyamidoamine modified poly(styrene-co-divinylbenzene) absorbents carrying phosphorus functional groups were prepared and used as adsorbents for adsorption of uranium(VI) from aqueous solution. The maximum adsorption capacity of 99.89 mg/g was observed at pH 5 and the initial uranium concentration of 100 mg/L. The adsorbent obtained has been used repeatedly and adsorption and desorption percentage did not show any noticeable decline after 27 cycles [19].

The adsorption properties of chelating polymer obtained by modification of commercially available ammoniated polystyrene beads with *P*,*P*-dichlorophenylphosphine oxide toward U(VI) were evaluated using the batch adsorption method. The maximum adsorption rate of U(VI) of 99.72% was noted at 318 K and pH 5. The U(VI) adsorption capacity increased with contact time and attained equilibrium within 4 h [20].

An ion exchange polymer was obtained by immobilization of Kemp's triacid derivatives onto a TentaGel resin. The chelating module was shown to form a 1 : 1 complex with the uranyl ion in solution. The new polymer was completely recyclable with no detectable aging and showed unusual activity for a carboxylate ligand in solutions of high ionic strength. The resins uranyl extraction efficiency was maintained even in the seawater [21].

The concentration of thorium isotopes in seawater is a key parameter in investigation of marine biogeochemical cycles, because they are important tracers for collecting information on the suspended particulate matter dynamics

in the ocean. Their concentration in seawater is extremely low (few fg per kg), therefore co-precipitation methods have been widely used for preconcentration of its radioisotopes. DIAION CR-20 chelating resin, which has a polyamine group as a chelating ligand bonded onto a highly porous crosslinked polystyrene matrix, was used to recover thorium isotopes that co-precipitate with iron hydroxide. Using the proposed method, the time of preconcentration for 5 L seawater samples was markedly reduced from a few days to 3–4 h [22].

The adsorption of Th(IV) and U(VI) was studied on chelating resin synthesized through copolymerization of glycidyl methacrylate in the presence of divinylbenzene followed by further immobilization with 3,4,5-trihydroxybenzoic acid. The novel chelating resin showed a high capacity for Th(IV) and U(VI), maximum adsorption of Th(IV) and U(VI) was 56 and 83.6 mg/g, respectively. The adsorption of Th(IV) and U(VI) was found to proceed according to pseudo second order kinetics, indicating the influence of textural properties of resin on the rate of adsorption [23].

Poly(amido)amine dendron was grown on the surface of styrene divinylbenzene by the divergent polymerization method. This new polymer has been investigated in liquid–solid extraction of thorium. The maximum adsorption capacity of thorium ions was determined to be 36.2 mg/g at 298 K [24].

A chelating ion resin, prepared by functionalization of Merrifield resin with 2,2′-pyridylimidazole, was used to selectively adsorb and separate nickel from other metal ions from their solutions. Even in highly acidic sulfate solution, this adsorbent's efficiency was pretty high with loading capacities in the range 56–79 mg Ni/g resin [25].

Separation of cobalt from mixed-waste mobile phone batteries containing $LiCoO_2$ cathodic active material was investigated using selective precipitation and chelating resin. Chelating resin was synthesized by polymerization of acrylonitrile followed by amidoximation reaction. Physically cross-linked gel of polyacrylonitrile was obtained by a cooling technique. Cobalt was recovered from the active powder materials containing 47% Co oxide together with Mn, Cu, Li, Al, Fe, and Ni oxides [26].

Poly(1,3-thiazol-2-yl methacrylamide-*co*-4-vinylpyridine-*co*-divinylbenzene) was prepared and used as a sorbent for the solid-phase extraction of Cr(VI). The adsorption capacity and binding equilibrium constant were calculated to be 80.0 mg/g and 0.018 L/mg, respectively. The polymer was applied as a sorbent for chromium from stream water and waste water samples [27].

Sorption properties of Presep® PolyChelate resin, which is chelate resin modified with carboxymethylated polyethylenimine were examined. This material showed excellent sorption potential for the solid-phase extraction of the Cd, Co,

Cu, Fe, Mo, Ni, Pb, V and Zn elements. The resin's performance was superior to other commercially available aminocarboxylic acid-type chelating resins [28].

A solid phase preconcentration method has been developed using a new chelating resin prepared by immobilization of 4-(2-thiazolylazo)resorcinol on Chromosorb 106 polymer. The method was optimized for determination of rare earth elements in seawater and estuarine water samples by inductively coupled plasma mass spectrometry. The resin shows large sorption capacity for lanthanides ranging from 81.1 μmol/g for Lu and 108 μmol/g for Nd [29].

Chelating terpolymer resin was synthesized from anthranilic acid, 2-amino pyridine and formaldehyde. The chelating properties of the terpolymer resin were evaluated by the batch equilibrium method for Fe^{3+}, Co^{2+}, Ni^{2+}, Cu^{2+}, Zn^{2+} and Pb^{2+}. It was established that the resin acted as an excellent cation-exchanger. Compared to the commercially available phenolic and polystyrene resins, the resin obtained showed an excellent ion-exchange capacity with the selected metal ions [30].

Polyacrylonitrile fiber with a chelating ligand was obtained by grafting fibers with iminodiacetic acid. The material obtained showed good potential for enrichment of trace amount of Nd(III) from large sample volumes. The sorption capacity of functionalized resin was 8.9 mg/g. The profile of Nd(III) uptake on the sorbent proved good accessibility of the chelating sites in the modified fibers [31].

Polyacrylonitrile-2-aminothiazole resin was synthesized by simple reaction of polyacrylonitrile beads with 2-aminothiazole. The functional group capacity and the percentage conversion of the functional group of the polymeric material prepared under the optimum conditions were 3.94 mmol/g and 41.10%, respectively. The resin shows much better adsorption capacity of 454.9 mg/g towards Hg(II) than towards other metal ions. This chelating polymer could be regenerated through the desorption of Hg(II) anions using nitric acid solution to be reused [32].

3.2. Catalytic properties

The role of catalysts is to increase the rate of chemical reaction without being consumed. Catalyst are divided into homogenous or heterogeneous ones. The former are used as solutions, whereas the latter are usually used in solid state. The advantage of heterogeneous catalysts is the ease of their separation from the products.

Catalytic activity of a heterogeneous catalyst, obtained by adsorption of Cu(II) ions onto a macroporous chelating polymer, functionalized with diethylenetriamine, was examined in decolorization and mineralization of Orange G dye in aqueous solutions with hydrogen peroxide. The catalyst obtained

showed good stability and was efficient for the decolorization and mineralization of Orange G dye under mild reaction conditions. Complete color removal for the dye concentration of 50 mg/L was achieved in 30 min at 24°C and in 15 min at 50°C. The heterogeneous catalyst tested is a cost effective alternative for the treatment of wastewaters containing Orange G dye [33].

A tetradentate Schiff base, obtained from triethylenetetramine and salicylaldehyde, has been covalently bonded to divinylbenzene cross-linked chloromethylated polystyrene. After the reaction with $CuCl_2$, $CoCl_2$ and $NiCl_2$, appropriate polymer-bound transition metal complexes have been obtained. The catalytic activities of these polymeric complexes were tested for the liquid-phase oxidation of olefins using hydrogen peroxide as the oxidant. Excellent yield and selectivity of these catalysts toward the oxidation of olefins were observed. The catalysts were found to exhibit higher catalytic activity than those of the corresponding neat complexes. Figure 5 presents the structure of catalysts obtained [34].

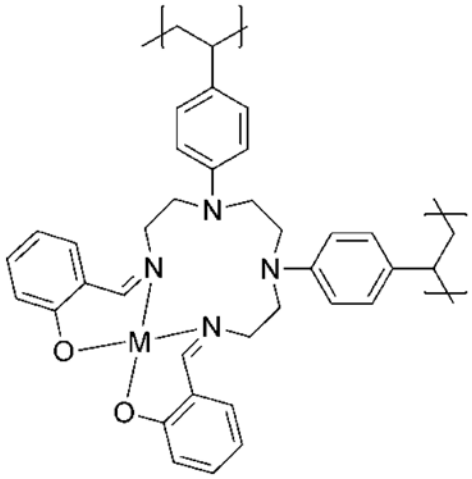

M = Cu^{2+}, Ni^{2+}, Co^{2+}

Figure 5. Structure of polymer-anchored Schiff base complex [34].

Catalyst for the Huisgen's [3+2] azide-alkyne cycloaddition have been prepared by immobilization of copper(I) on commercially available polymers functionalized with 1,5,7-triazabicyclo[4.4.0]dec-5-ene. The new catalytic systems enabled development of regioselective, convergent, operationally simple and efficient three-component transformations that allow rapid assembly of 1,2,3-triazoles from simple and readily available starting materials. Figure 6 presents the structure of the functional polymer obtained [35].

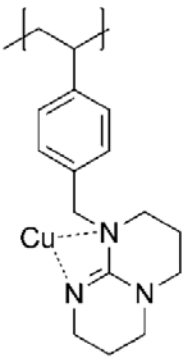

Figure 6. The polymeric catalysts for the Huisgen's [3+2] azide-alkyne cycloaddition [35].

An amphiphilic block copolymer (Figure 7) bearing a chelating *N*,*N*-dipyrid-2-ylamide-based ligand was prepared via ROMP using a Mo-based Schrock initiator. Functionalization with Rh(I) yielded a polymer catalyst that was used for the hydroformylation of 1-octene under micellar conditions. The use of a micellar catalyst was found to favor the formation of *n*-aldehyde by suppressing the isomerization propensity of a catalyst. The use of the micellar setup allows to reuse the polymeric catalyst and reduce the metal contamination of the products [36].

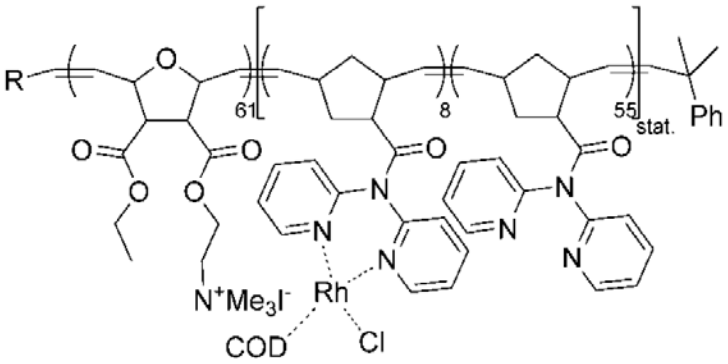

COD = 1,5-cyclooctadiene
R = ferrocen-1-yl

Figure 7. Structure of polymer-rhodium hydroformylation catalyst [36].

Molecularly imprinted polymer beads have been prepared by polymerization of methacryloylhistidine complexes with Co^{2+}, Ni^{2+} or Zn^{2+} (Figure 8) and applied as catalyst in the hydrolysis of paraoxon which is an organophosphate ester that is used as a pesticide. The catalytic performance of polymers having Co^{2+}, Ni^{2+}

or Zn^{2+} ions was evaluated according to the enzyme kinetic model of Michaelis–Menten and their activities were compared to each other. The use of polymers of methacryloylhistidine complexes with Co^{2+}, Ni^{2+}, or Zn^{2+} ions provided an increase in the hydrolysis rate by a factor of 356, 241, and 95, respectively, with respect to that in non-catalyzed media that contained only buffer [37].

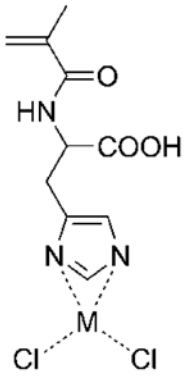

M = Co^{2+}, Zn^{2+}, Ni^{2+}

Figure 8. The structure of monomeric methacryloylhistidine complexes with Co^{2+}, Ni^{2+}, or Zn^{2+} [37].

3.3. Biocide properties

The advantages offered by antimicrobal polymers over their low molecular weight analogues include a reduction of agents residual toxicity, increased efficiency and selectivity and prolonged lifetime. Moreover, these materials are non-volatile, chemically stable and do not permeate through skin [1].

Polymer-bound Schiff bases and Cr(III) complexes have been synthesized by the reaction of 4-benzyloxybenzaldehyde, polymer-bound with 2-aminophenol, 2-amino-4-chlorophenol and 2-amino-4-methylphenol. The structures of polymer-metal complexes are presented in Figure 9. All these compounds have also been investigated for antibacterial activity by the well-diffusion method against *Staphylococcus aureus (RSKK-07035), Shigella dysenteria type 10 (RSKK 1036), Listeria monocytogenes 4b(ATCC 19115, Escherichia coli (ATCC 1230), Salmonella typhi H (NCTC 901.8394), Staphylococcus epidermis (ATCC 12228), Brucella abortus (RSKK-03026), Micrococcs luteus (ATCC 93419, Bacillus cereus sp., Pseudomonas putida sp.* and for antifungal activity against *Candida albicans (Y-1200-NIH)*. Polymer-bound Schiff bases and their Cr(III) complexes have proven to possess moderate or high activity against examined germs except *S. dysenteria type 10*. According to the results of biological activity, the polymers obtained may be used in various applications as antimicrobial agents [38].

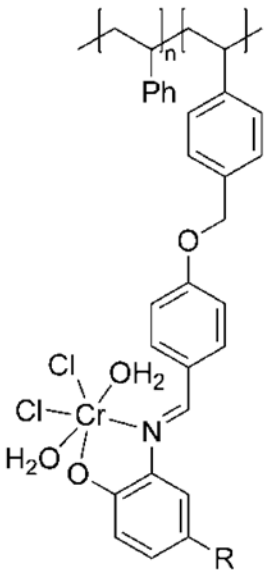

Figure 9. Structure of polymer-bound Schiff bases Cr(III) complexes [38].

A terpolymer involving 2-amino-6-nitrobenzothiazole, melamine, and formaldehyde has been synthesized in the presence of dimethyl formamide medium. The polymer obtained was used to prepare complexes with Cu^{2+}, Ni^{2+} and Zn^{2+} ions, whose structure is presented in Figure 10. The antibacterial activity of the terpolymer and its Cu(II), Ni(II), and Zn(II) complexes was determined by the disc diffusion method with Amoxicillin as the standard antibiotic. The prepared compounds were tested against *S. sonnei, E. coli, Klebsiella species, S. aureus, B. subtilis, and S. typhimurium* microbes. The studies showed that the ligand and its metal chelates stronger inhibit the growth of *E. coli, Klebsiella* species, and *B. subtilis*, whereas the inhibition of the growth of *S. sonnei, S. aureus*, and *S. typhimurium* was at a reasonable level [39].

Phenylthiourea–formaldehyde polymer has been synthesized via polycondensation of phenylthiourea and formaldehyde in basic medium. The corresponding metal complexes were prepared with Mn(II), Co(II), Ni(II), Cu(II) and Zn(II) ions (Figure 11). The antibacterial activity of the polymer-metal complexes obtained was tested against *Bacillus subtiis, B. megaterium, S. aureus, E. coli, P. aeruginosa and S. typhi* using agar well diffusion method, whereas their antifungal activity was examined against *C. albicans, T. species, A. flavus, A. niger, F. species*, and *M. species*. All synthesized polymers showed excellent antimicrobial activity against several bacteria and fungi. The polymer-

Cu(II) complex showed the highest antibacterial as well as antifungal activity, interpreted as related to a higher stability constant of Cu(II) ions [40].

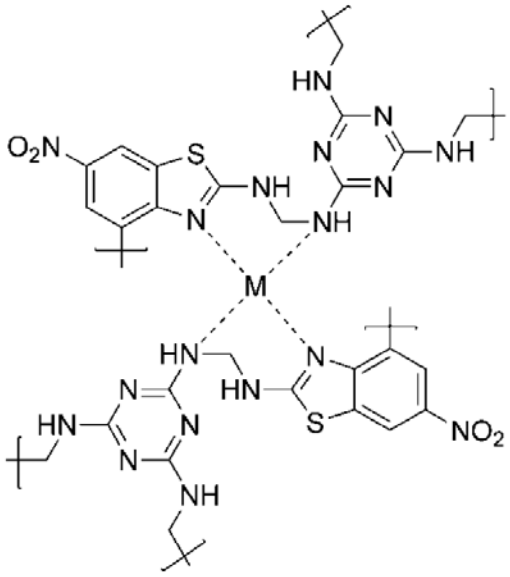

Figure 10. Proposed structure of terpolymer-metal complexes [39].

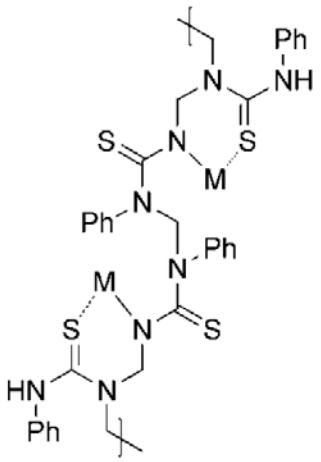

Figure 11. Structure of phenylthiourea–formaldehyde polymer complexes with metal ions [40].

4. Conclusions

Complexes of polymers with metal ions have been widely investigated to understand the relationship between the structure of polymer-metal complex and its chemical properties. The progress in such investigation has been possible thanks to the fact that much information about the structure and properties of polymer-metal complexes can be obtained by analytical methods such as UV-VIS, EPR, NMR, IR or CD spectroscopy and measuring redox potentials. For further development more detailed studies of polymer-metal complexes should be undertaken, including examination of higher-order structure of polymer and dynamic changers in the structure of polymer ligand, determination of configuration within the coordination sphere and stability of the complex formed.

Acknowledgements

This work was supported by the Polish National Science Center (NCN; decision no. DEC-2012/05/N/ST5/01274).

References

1. B.L. Rivas, E. Pereira, A. Maureira, Functional water-soluble polymers: polymer–metal ion removal and biocide properties, Polym. Int., 58 (2009) 1093-1114.
2. K. Horie, M. Barón, R.B. Fox, J. He, M. Hess, J. Kahovec, T. Kitayama, P. Kubisa, E. Maréchal, W. Mormann, R.F.T. Stepto, D. Tabak, J. Vohlídal, E.S. Wilks, W.J. Work, Definitions of terms relating to reactions of polymers and to functional polymeric materials (IUPAC Recommendations 2003), Pure Appl. Chem., 76 (2004) 889-906.
3. T. Kaliyappan, P. Kannan, Co-ordination polymers, Prog. Polym. Sci., 25 (2000) 343-370.
4. S.B. Kim, R.D. Pike, D.A. Sweigart, Multifunctionality of Organometallic Quinonoid Metal Complexes: Surface Chemistry, Coordination Polymers, and Catalysts, Acc. Chem. Res., 46 (2013) 2485-2497.
5. H. Jiang, J. Jiang, H. Wei, C. Cai, Heterogeneous Cyanation Reaction of Aryl Halides Catalyzed by a Reusable Palladium Schiff Base Complex in Water, Catal. Lett., 143 (2013) 1195-1199.
6. X. Ma, Y. Li, Z. Ye, L. Yang, L. Zhou, L. Wang, Novel chelating resin with cyanoguanidine group: Useful recyclable materials for Hg(II) removal in aqueous environment, J. Hazard. Mater., 185 (2011) 1348-1354.

7. P.K. Neghlani, M. Rafizadeh, F.A. Taromi, Preparation of aminated-polyacrylonitrile nanofiber membranes for the adsorption of metal ions: Comparison with microfibers, J. Hazard. Mater., 186 (2011) 182-189.
8. C. Sun, G. Zhang, R. Qu, Y. Yu, Removal of transition metal ions from aqueous solution by crosslinked polystyrene-supported bis-8-oxyquinoline-terminated open-chain crown ethers, Chem. Eng. J. (Lausanne), 170 (2011) 250-257.
9. E. Moazzen, H. Ebrahimzadeh, M.M. Amini, O. Sadeghi, A high selective ion-imprinted polymer grafted on a novel nanoporous material for efficient gold extraction, J. Sep. Sci., 36 (2013) 1826-1833.
10. K.R. Desai, Z.V.P. Murthy, Removal of silver from aqueous solutions by complexation–ultrafiltration using anionic polyacrylamide, Chem. Eng. J. (Lausanne), 185–186 (2012) 187-192.
11. M.J. Hudson, M.J. Shepherd, Selective extraction and separation of metals especially silver (and copper) using poly(2-S-vinyl-1,3,4-thiadiazole-5-thiol), Hydrometallurgy, 9 (1983) 223-234.
12. C.O. Giwa, M.J. Hudson, Extraction of metals using poly[N-(dithiocarboxylato)-iminoethenehydrogenoiminioethene], Hydrometallurgy, 8 (1982) 65-75.
13. T.K. Bronich, S. Bontha, L.S. Shlyakhtenko, L. Bromberg, T. Alan Hatton, A.V. Kabanov, Template-assisted synthesis of nanogels from Pluronic-modified poly(acrylic acid), J. Drug Targeting, 14 (2006) 357-366.
14. E. Tsuchida, H. Nishide, Polymer-metal complexes and their catalytic activity, in: Molecular Properties, Springer Berlin Heidelberg, 1977, pp. 1-87.
15. X. Liang, Y. Su, Y. Yang, W. Qin, Separation and recovery of lead from a low concentration solution of lead(II) and zinc(II) using the hydrolysis production of poly styrene-co-maleic anhydride, J. Hazard. Mater., 203–204 (2012) 183-187.
16. Y. Yan, J. Zhang, Y. Qiao, C. Tang, Facile Preparation of Cobaltocenium-Containing Polyelectrolyte via Click Chemistry and RAFT Polymerization, Macromol. Rapid Commun., 35 (2014) 254-259.
17. S. Virolainen, I. Suppula, T. Sainio, Continuous ion exchange for hydrometallurgy: Purification of Ag(I)–NaCl from divalent metals with aminomethylphosphonic resin using counter-current and cross-current operation, Hydrometallurgy, 142 (2014) 84-93.
18. V.I. Kuz'min, D.V. Kuz'min, Sorption of nickel and copper from leach pulps of low-grade sulfide ores using Purolite S930 chelating resin,

Hydrometallurgy, 141 (2014) 76-81.
19. Q. Cao, Y. Liu, C. Wang, J. Cheng, Phosphorus-modified poly(styrene-co-divinylbenzene)–PAMAM chelating resin for the adsorption of uranium(VI) in aqueous, J. Hazard. Mater., 263, Part 2 (2013) 311-321.
20. Q. Cao, Y. Liu, X. Kong, L. Zhou, H. Guo, Synthesis of phosphorus-modified poly(styrene-co-divinylbenzene) chelating resin and its adsorption properties of uranium(VI), J. Radioanal. Nucl. Chem., 298 (2013) 1137-1147.
21. A.C. Sather, O.B. Berryman, J. Rebek, Selective recognition and extraction of the uranyl ion from aqueous solutions with a recyclable chelating resin, Chemical Science, 4 (2013) 3601-3605.
22. A. Okubo, H. Obata, M. Magara, T. Kimura, H. Ogawa, Rapid collection of iron hydroxide for determination of Th isotopes in seawater, Anal. Chim. Acta, 804 (2013) 120-125.
23. S. Sadeek, M. El-Sayed, M. Amine, M. Abd El-Magied, A chelating resin containing trihydroxybenzoic acid as the functional group: synthesis and adsorption behavior for Th(IV) and U(VI) ions, J. Radioanal. Nucl. Chem., (2013) 1-8.
24. [P. Ilaiyaraja, A. Deb, K. Sivasubramanian, D. Ponraju, B. Venkatraman, Removal of thorium from aqueous solution by adsorption using PAMAM dendron-functionalized styrene divinyl benzene, J. Radioanal. Nucl. Chem., 297 (2013) 59-69.
25. A.I. Okewole, E. Antunes, T. Nyokong, Z.R. Tshentu, The development of novel nickel selective amine extractants: 2,2′-Pyridylimidazole functionalised chelating resin, Miner. Eng., 54 (2013) 88-93.
26. S. Badawy, A.A. Nayl, R.A. El Khashab, M.A. El-Khateeb, Cobalt separation from waste mobile phone batteries using selective precipitation and chelating resin, J Mater Cycles Waste Manag, (2013) 1-8.
27. [O. Hazer, D. Demir, Speciation of Chromium in Water Samples by Solid-Phase Extraction on a New Synthesized Adsorbent, Anal. Sci., 29 (2013) 729-734.
28. S. Kagaya, Y. Saeki, D. Morishima, R. Shirota, T. Kajiwara, T. Kato, M. Gemmei-Ide, Potential of Presep® PolyChelate as a Chelating Resin: Comparative Study with Some Aminocarboxylic Acid-type Resins, Anal. Sci., 29 (2013) 1107-1112.
29. F. Zereen, V. Yilmaz, Z. Arslan, Solid phase extraction of rare earth elements in seawater and estuarine water with 4-(2-thiazolylazo) resorcinol immobilized Chromosorb 106 for determination by

inductively coupled plasma mass spectrometry, Microchem. J., 110 (2013) 178-184.
30. R.S. Azarudeen, R. Subha, D. Jeyakumar, A.R. Burkanudeen, Batch separation studies for the removal of heavy metal ions using a chelating terpolymer: Synthesis, characterization and isotherm models, Sep. Purif. Technol., 116 (2013) 366-377.
31. H.B. Sadeghi, H.A. Panahi, M. Abdouss, B. Esmaiilpour, M.N. Nezhati, E. Moniri, Z. Azizi, Modification and characterization of polyacrylonitrile fiber by chelating ligand for preconcentration and determination of neodymium ion in biological and environmental samples, J. Appl. Polym. Sci., 128 (2013) 1125-1130.
32. C. Xiong, Q. Jia, X. Chen, G. Wang, C. Yao, Optimization of Polyacrylonitrile-2-aminothiazole Resin Synthesis, Characterization, and Its Adsorption Performance and Mechanism for Removal of Hg(II) from Aqueous Solutions, Ind. Eng. Chem. Res., 52 (2013) 4978-4986.
33. V. Dulman, S.M. Cucu-Man, R.I. Olariu, R. Buhaceanu, M. Dumitraş, I. Bunia, A new heterogeneous catalytic system for decolorization and mineralization of Orange G acid dye based on hydrogen peroxide and a macroporous chelating polymer, Dyes Pigm., 95 (2012) 79-88.
34. S. Islam, M. Mobarok, P. Mondal, A. Roy, N. Salam, D. Hossain, S. Mondal, Use of immobilized transition metal complexes as recyclable catalysts for oxidation reactions with hydrogen peroxide as oxidant, Transition Met. Chem. (London), 37 (2012) 97-107.
35. A. Coelho, P. Diz, O. Caamaño, E. Sotelo, Polymer-Supported 1,5,7-Triazabicyclo[4.4.0]dec-5-ene as Polyvalent Ligands in the Copper-Catalyzed Huisgen 1,3-Dipolar Cycloaddition, Adv. Synth. Catal., 352 (2010) 1179-1192.
36. G.M. Pawar, J. Weckesser, S. Blechert, M.R. Buchmeiser, Ring opening metathesis polymerization-derived block copolymers bearing chelating ligands: synthesis, metal immobilization and use in hydroformylation under micellar conditions, Beilstein J. Org. Chem., 6 (2010) 28.
37. M. Erdem, R. Say, A. Ersöz, A. Denizli, H. Türk, Biomimicking, metal-chelating and surface-imprinted polymers for the degradation of pesticides, React. Funct. Polym., 70 (2010) 238-243.
38. C. Selvi, D. Nartop, Novel polymer anchored Cr(III) Schiff base complexes: Synthesis, characterization and antimicrobial properties, Spectrochimica Acta Part A: Molecular and Biomolecular Spectroscopy, 95 (2012) 165-171.
39. M.A.R. Ahamed, A.R. Burkanudeen, Thiazole-Based Novel Terpolymer

Ligand and Its Transition Metal Complexes: Thermal and Biological Studies, Adv. Polym. Technol., 32 (2013) 21376.
40. T. Ahamad, S.M. Alshehri, Physiochemical characterization and antimicrobial evaluation of phenylthiourea–formaldehyde polymer (PTF) based polymeric ligand and its polymer metal complexes, Spectrochimica Acta Part A: Molecular and Biomolecular Spectroscopy, 108 (2013) 26-31.